

Copyright
by
Jeetain Mittal
2007

The Dissertation Committee for Jeetain Mittal
certifies that this is the approved version of the following dissertation:

**Structure, Thermodynamics and Dynamics of Confined
and Supercooled Liquids**

Committee:

Thomas M. Truskett, Supervisor

Roger T. Bonnecaze

David van den Bout

Venkat Ganesan

Isaac C. Sanchez

**Structure, Thermodynamics and Dynamics of Confined
and Supercooled Liquids**

by

Jeetain Mittal, B.Tech., M.Tech.

DISSERTATION

Presented to the Faculty of the Graduate School of

The University of Texas at Austin

in Partial Fulfillment

of the Requirements

for the Degree of

DOCTOR OF PHILOSOPHY

THE UNIVERSITY OF TEXAS AT AUSTIN

May 2007

Dedicated in loving memory of my grand father

Acknowledgments

First and foremost, I would like to thank my adviser Tom Truskett for providing both a wonderful environment for research and critical inputs in every aspect of this work. His knowledge of multitude of topics helped in the evolution of this dissertation by providing a cohesive framework for a very broad range of topics. Tom, Thanks for your enduring patience.

I am very grateful to Jeff Errington for an incredible collaboration over the course of this work. His promptness in providing the requested simulation data motivated me to work harder to be able to catch up with his speed. Jeff, Thanks for sharing your expertise on various simulation techniques.

A large fraction of the time during graduate studies is spent interacting with other people in the research group. I was very lucky to share my office with Jason (Dr.) and numerous discussions everyday with him on liquids, proteins, and football made the time pass quickly. Thanks Bill for insightful discussions on your favorite topic, how to write efficient scripts to make life easier. I am also thankful to Gaurav for several useful discussions.

I was fortunate to have several friends in Austin who made the stay here enjoyable. Jyoti, Thanks for your advice when I needed it. I am also grateful for your helpful feedback on my work which improved it. Scott: Our “running” / “discussions” really helped me identifying some of the important

aspects of my research problems. Bharani & Shilpa: Thanks for listening to my endless phone calls. Sridhar: I very much enjoyed the frequent trips to swad and claypit with you. Shruti (people), Thanks for listening to my new results and ideas even when you had no idea what I am talking about. I would also like to thank Gopal, Bijal, Nikhil & Reena (bhabhi), Puneet, Anurag, Chak, Ankur, Marghoob.

Finally, I would like to thank my family for their constant support and love.

Structure, Thermodynamics and Dynamics of Confined and Supercooled Liquids

Publication No. _____

Jeetain Mittal, Ph.D.

The University of Texas at Austin, 2007

Supervisor: Thomas M. Truskett

Static measures such as density and entropy, which are intimately connected to structure, have featured prominently in modern thinking about the dynamics of the liquid state. In this dissertation, we explore the connections between self-diffusivity, density, available space, and excess entropy in two non-trivial problems in liquid state theory, confined and supercooled liquids.

We present exact simulation data for the relationship between self-diffusivity and excess entropy for a wide range of simple fluids (i.e. hard-sphere, Lennard-Jones and square-well) confined to pores with a variety of different sizes and fluid-wall interactions. Our main finding is that, at a given temperature, self-diffusivity of the confined fluids collapses onto the bulk behavior when plotted versus excess entropy. In other words, the only information required to “predict” the implications of confinement for the single-particle dynamics is the bulk fluid behavior at a given temperature and the

excess entropy of the confined fluid. This should prove practically useful given that the bulk behavior is well known for these fluid systems, and the excess entropy of the confined fluids can be readily estimated from classical density functional theory.

We also show that the self-diffusivity of the confined fluids approximately collapses onto the data for the corresponding bulk fluid when plotted versus the average packing fraction (which is based on total, rather than center accessible volume). For continuous interaction potentials such as Lennard-Jones, calculation of effective packing fraction requires knowledge of both the number density of the fluid and a temperature-dependent Boltzmann diameter associated with the repulsive part of the interparticle interactions. We suggest a way to calculate this effective diameter, which to a very good approximation, collapse the temperature- and density-dependent data for the self-diffusivity of the bulk Lennard-Jones fluid onto hard-sphere fluid data plotted versus the fluid's effective packing fraction.

Finally, we found that the self-diffusivities of several model systems in their supercooled state also scale exponentially not only with the excess entropy, but also with the two-body contribution to the excess entropy obtained from the pair correlation function of the fluid. The latter observation is particularly interesting because it provides direct evidence of a quantitative link between the dynamics and the average structural order of supercooled liquids. Whether such a connection could indeed be discovered is part of a long-standing question in the study of liquids.

Table of Contents

Acknowledgments	v
Abstract	vii
List of Figures	xii
Chapter 1. Introduction	1
1.1 Confined Fluids	2
1.2 Supercooled Liquids	3
1.3 Background and Motivation	5
1.4 Thesis Organization	7
Chapter 2. Thermodynamics predicts the dynamics of the confined equilibrium hard-sphere fluid	11
2.1 Introduction	11
2.2 Simulation details	14
2.3 Results and discussion	17
2.3.1 Self-diffusivity versus excess entropy	17
2.3.2 Self-diffusivity versus average density	20
2.3.3 Local fluid structure versus diffusivity	24
2.4 Conclusions	24
Chapter 3. Average properties of the highly confined hard-sphere fluid	27
3.1 Introduction	27
3.2 Simulation Methods	31
3.3 Results and Discussion	34
3.3.1 Volume definition and the equation of state	34
3.3.2 Interfacial free energy and excess adsorption	37

3.3.3	Comparing bulk and pore fluid self-diffusivities	42
3.3.4	Diffusivity and excess entropy	50
3.4	Conclusions	54
Chapter 4.	Self-diffusivity, packing fraction and excess entropy of simple bulk and confined fluids	55
4.1	Introduction	55
4.2	Model Systems and Simulation Methods	57
4.3	Results and discussion	61
4.3.1	Effective packing fraction and self-diffusivity: Bulk fluids	61
4.3.2	Excess entropy and self-diffusivity: Bulk fluids	68
4.3.3	Effective packing fraction and self-diffusivity: Confined fluids	76
4.3.4	Excess entropy and self-diffusivity: Confined fluids	82
4.4	Conclusions	86
Chapter 5.	Fluid diffusivity in random porous media	87
5.1	Introduction	87
5.2	Model and simulation details	89
5.3	Simple diffusion equation from scaling	90
5.4	Calculating available space	92
5.5	Comparison between diffusion equation and exact results	94
5.6	Conclusions	100
Chapter 6.	Thermodynamics, static structure and dynamics of supercooled liquids	101
6.1	Introduction	101
6.2	Relationship between thermodynamics and dynamics	102
6.2.1	Core-softened water-like model	103
6.2.2	Binary Lennard-Jones mixture	104
6.3	Relationship between static structure and dynamics	108
6.3.1	SPC/E water model	110
6.3.2	Short-range attractive (SRA) colloid model	111
6.3.3	Monatomic glass former “Dzugutov” model	117
6.4	Conclusions	120

Bibliography	121
Vita	137

List of Figures

2.1	Self-diffusivity D versus the negative of excess entropy per particle $-s^{\text{ex}}/k_{\text{B}}$ for the bulk HS fluid (solid curve) and for the HS fluid in $2d$ channels (symbols). The symbols correspond to $h_z = 2.5$ (circle), 5 (square), 7.5 (plus), 10 (triangle up) and 15 (cross). The color codes are $\epsilon_w = 1$ (blue), 0.5 (cyan), 0 (red), -0.5 (yellow), and -1 (green).	18
2.2	Self-diffusivity D versus the negative of excess entropy per particle $-s^{\text{ex}}/k_{\text{B}}$ for the same data as shown in Fig. 2.1 with added points for the $1d$ channels: 5×5 , 7.5×7.5 , and 5×7.5 shown by red diamonds.	19
2.3	Self-diffusivity D vs average density $\rho = N/V$ based on the the total system volume V . Symbols are identical to those given in Fig. 2.2.	21
2.4	Self-diffusivity D versus average density $\rho_h = N/V_h$ based on the the total particle-center accessible volume V_h . Systems shown include the bulk HS fluid (solid curve) and the HS fluid confined to the $2d$ channels between hard walls.	23
2.5	Density profiles $\rho(z)$ for HS fluids confined to a $2d$ channel of width $h_z = 2.5$. Although each system has different particle-wall interaction strengths ϵ_w , they share a common average density ρ (dashed) and self-diffusivity D	25
3.1	Equation of state of a confined HS fluid between hard walls separated by center-accessible distance $H - 1$. Top panels show the negative of the grand potential density (average transverse pressure) versus average fluid density calculated using (a) the center-accessible volume V_h and (b) the total volume V . Bottom panels illustrate the normal pressure versus average density calculated using (c) the center-accessible volume V_h and (d) the total volume V	35
3.2	The quantity $(H/2) [\Omega/V + P_b]$ calculated from our GC-TMMC simulations for various H along with the $H \rightarrow \infty$ limit, γ^∞ , computed using Eq. 3.8. Data are plotted as a function of ϕ_b , the packing fraction of the bulk HS fluid that is in equilibrium with the pore fluid.	39

3.3	Pore fluid density ρ as a function of pore width H at different values of activity [$\ln \xi = 0.4, 4.4, \text{ and } 8.8$]. Filled and open symbols correspond to the GC-TMMC data and the predictions of Eq. 3.10, respectively. The dashed lines correspond to the bulk density ρ_b for a given activity ξ	41
3.4	Self-diffusivity D as a function of pore width H at different pore fluid packing fractions ϕ . For $\phi = 0.45$, crosses mark regions for which the confined system penetrates into the fluid-solid coexistence region or the solid phase region on its equilibrium phase diagram [40].	44
3.5	2D projections of typical instantaneous particle configurations of the confined HS fluid are shown (top) along with equilibrium density profiles $\rho(z)$ (bottom), where z represents the positional coordinate normal to the walls.	45
3.6	Average density ρ and self-diffusivity D as a function of pore size H for the confined HS fluid in equilibrium with the bulk HS fluid at a given activity ξ [$\ln \xi = 0.4, 4.4, \text{ and } 8.8$]. Dashed lines correspond to the density ρ_b and self-diffusivity D of the bulk HS fluid at the given activity ξ	49
3.7	(a) Self-diffusivity D and (b) excess entropy s^{ex} as a function of pore size H for the confined HS fluid at a given pore packing fraction $\phi = \pi\rho/6$. Data from top to bottom correspond to $\phi = 0.15, 0.3, \text{ and } 0.4$. (c) Self-diffusivity D and (d) excess entropy s^{ex} as a function of pore size H for the confined HS fluid at a given activity ξ . Data from top to bottom correspond to $\ln \xi = 0.4, 4.4, \text{ and } 8.8$	52
3.8	Self-diffusivity D vs negative excess entropy per particle $-s^{\text{ex}}$ for the bulk HS fluid (solid curve) and for the HS fluid confined between smooth hard walls (symbols). The filled symbols correspond to the confined system at a fixed pore packing fraction ϕ as shown on the legend and empty symbols are for system at a given activity ξ for which bulk packing fraction is given on the legend.	53
4.1	Scaled self diffusivity $DT^{-1/2}$ of the bulk LJ fluid versus effective packing fraction ϕ_{eff} defined using the Boltzmann factor criterion of Eq. 4.8 with parameter values, $a =$ (a) 1, (b) 1.5, and (c) 2. Symbols correspond to $T = 1$ (filled circle), 1.2 (filled square), 3 (filled diamond), and 10 (filled triangle left). The curve corresponds to data for the bulk HS fluid.	63

4.2	Scaled self diffusivity $DT^{-1/2}$ versus effective packing fraction ϕ_{eff} for the SW fluid (symbols) at the various temperatures T described in the legend. The black curve corresponds to the bulk HS data (or, equivalently, the data for the SW fluid in the $T \rightarrow \infty$ limit). Speedy <i>et al.</i> [106] proposed that the T -dependent SW self-diffusivity data might collapse onto the HS curve if divided by an empirical factor of the form $(1 - \alpha T^{-1})$, where α is a constant. The inset shows the scaled HS diffusivity $D_{\text{HS}}T^{-1/2}$ that is predicted by applying this type of normalization to the scaled SW diffusivity data, $D_{\text{SW}}T^{-1/2}$, in the main panel [i.e., $D_{\text{HS}} = D_{\text{SW}}/(1 - 0.68T^{-1})$].	66
4.3	Scaled self diffusivity data (symbols) versus negative excess entropy per particle for the bulk LJ fluid using the (top) Rosenfeld and (bottom) Dzugutov reduction parameters discussed in the text. In the top panel, the solid line represents the Rosenfeld scaling law, $0.58\exp(0.78s^{\text{ex}})$, for the dense fluid, and the dashed curve shows the low-density behavior expected for fluids with soft-sphere potentials, $0.37(-s^{\text{ex}})^{-2/3}$ [87]. In the bottom panel, the solid line represents the Dzugutov scaling law, $0.078\exp(s^{\text{ex}})$.	70
4.4	Scaled self diffusivity data (symbols) versus negative excess entropy per particle for the bulk SW fluid using the (top) Rosenfeld and (bottom) Dzugutov reduction parameters discussed in the text. In the top panel, the solid line represents the Rosenfeld scaling law, $0.58\exp(0.78s^{\text{ex}})$, for the dense fluid, and the dashed curve shows the low-density behavior expected for fluids with soft-sphere potentials, $0.37(-s^{\text{ex}})^{-2/3}$ [87]. In the bottom panel, the solid line represents the Dzugutov scaling law, $.078\exp(s^{\text{ex}})$.	72
4.5	Pair correlation function $g(r)$ for the SW fluid at density $\rho = 0.84$ and various T values presented in the legend (T increases from top to bottom for SW fluid). The bottom curve corresponds to $g(r)$ for the HS fluid with the same density. Curves for the SW fluid have been vertically shifted for clarity.	74
4.6	Schematic showing a paricle confined in a slit-pore geometry. The effective packing fraction of this system can be defined based either on the volume that the particle centers access ($V_h = Ah$) or the “total” volume that the particle surfaces access ($V = AH$), where A is the fluid contact area at a single wall.	76

4.7	Scaled self diffusivity $DT^{-1/2}$ for bulk and confined LJ fluids versus effective packing fraction $\phi_{\text{eff}}(T)$ based on the total (i.e., “particle surface” rather than “particle center”-accessible) volume, as discussed in the text. Temperatures for data points follow the color code shown in the legend. Various fluid-wall interactions used are effective “hard wall” (HW, $\epsilon_{\text{fw}} = .01$), and neutral wall (NW, $\epsilon_{\text{fw}} = 1$) both modeled by a 9-3 LJ interaction potential described in the text. The symbols correspond to bulk (filled circle), HW: $H_z = 5$ (filled square), NW: $H_z = 5$ (filled diamond), and NW: $H_z = 10$ (asterisk). The solid curve corresponds to the bulk HS fluid data.	79
4.8	Self diffusivity D of the confined SW fluid versus ϕ_{eff} based on the total (i.e., “particle surface” rather than “particle center”-accessible) volume, as discussed in the text. Temperatures for data points follow the color code shown in the legend. Various fluid-wall interactions used are hard wall (HW, $\epsilon_{\text{fw}} = 0$), repulsive wall (RW, $\epsilon_{\text{fw}} = -1$), attractive wall, (AW, $\epsilon_{\text{fw}} = 1$). The range of the fluid-wall potential is $\lambda_{\text{fw}} = 1.5$ except for a few data sets (SR) where it is $\lambda_{\text{fw}} = 1.1$. Symbols correspond to bulk (filled circle), HW: $H_z = 3.5$ (filled square), HW: $H_z = 8.5$ (filled triangle up), RW: $H_z = 3.5$ (filled diamond), RW: $H_z = 8.5$ (filled triangle left), AW: $H_z = 3.5$ (filled triangle down), AW: $H_z = 8.5$ (filled triangle right), AW-SR: $H_z = 3.5$ (plus), and AW-SR: $H_z = 8.5$ (times).	81
4.9	Scaled self diffusivity data (symbols) versus negative excess entropy per particle for the bulk and confined LJ fluids using the (top) Rosenfeld and (bottom) Dzугutov reduction parameters discussed in the text. Symbols are the same as those presented in Fig. 4.7.	83
4.10	Self diffusivity versus negative excess entropy per particle. (a) Bulk and confined LJ fluids at temperatures $T = 1$ and 3. Symbols and color code are the same as in Fig. 4.7. (b) Bulk and confined SW fluids at temperatures $T = 1.2$ and 2.5 from bottom to top curve. Various fluid-wall interactions used are hard wall (RW, $\epsilon_{\text{fw}} = -1$), repulsive wall (HW, $\epsilon_{\text{fw}} = 0$), attractive wall, (AW, $\epsilon_{\text{fw}} = +1$). The range of the fluid-wall potential is $\lambda_{\text{fw}} = 1.5$. Symbols correspond to bulk (line), RW: $H_z = 4$ (filled circle), HW: $H_z = 4$ (filled square), AW: $H_z = 4$ (filled triangle down).	85
5.1	Schematic of a QA system. Equi-sized filled and empty circles are matrix and fluid particles, respectively. The bigger circle is a window with radius equal to the one particle diameter. Π_i is the probability that it will be occupied by exactly i matrix or fluid particle centers.	93

5.2	The fractional available volume V_0/V in HS QA-FM matrices computed using the IT approach of Eq. 5.4 and 5.5 (curves) and “exact” results (filled circles) using the available space algorithm of Ref [97].	95
5.3	Fluid self-diffusivity D versus fluid density ρ_F for HS (a) QA-FM and (b) QA-M system with matrix densities $\rho_M = 0.0, 0.05, 0.15, 0.25, 0.30,$ and 0.35 . Curves are predictions of Eq. 5.1 and circles are molecular dynamics simulation results.	96
5.4	(a) Fluid self-diffusivity D versus fluid density ρ_F for HS QA-FM (circles) and LJ QA-FM (diamonds) systems obtained via molecular dynamics simulations. The LJ QA-FM system is at $T = \epsilon/k_B$. Matrix densities of $\rho_M = 0.05, 0.15, 0.25,$ and 0.35 are presented. (b) Results for the LJ QA-FM system at $T = 3\epsilon/k_B$: molecular dynamics simulations (circles) and Eq. 5.1 (curves). Matrix densities of $\rho_M = 0.043, 0.128, 0.214,$ and 0.3 are presented.	99
6.1	(a, b) Excess entropy and diffusivity versus density obtained from molecular dynamics simulations of 1000 particles interacting via a core-softened potential (i.e., a Lennard-Jones potential plus a Gaussian repulsion). Symbols are simulation data, and curves are guides to the eye.	105
6.2	Diffusivity versus excess entropy for the data shown in Fig 6.1 along paths of constant density (symbols). Symbols are simulation data, and lines reflect the form.	106
6.3	Diffusivity versus excess entropy for different density states of a binary Lennard-Jones alloy. Excess entropy has been obtained from the semi-empirical free energy expression reported in Ref. 18, and diffusivity has been extracted from the Figure 3 in Ref. 18. The lines reflect the form.	107
6.4	The plot shows the linear dependence between excess entropy and the inverse product of temperature and configurational entropy, the latter extracted from Figure 2 in Ref. 12 for the data used in Fig 6.3.	109
6.5	Diffusivity D and two-body entropy s_2 versus density ρ for SPC/E water. Symbols are simulation data, and curves are guides to the eye.	112
6.6	Diffusivity D versus two-body entropy s_2 for the data shown in Fig. 1 along paths of constant density ρ shown by symbols. Lines are fits to the data of the form $D \propto \exp[A(\rho)s_2]$	113

6.7	Diffusivity D and two-body entropy s_2 versus polymer fraction ϕ_p for the SRA model [80, 81]. Particle volume fractions of $\phi_c = 0.25, 0.30, 0.35, 0.40, 0.45, 0.50, 0.55$ from top to bottom are shown.	116
6.8	Diffusivity D versus two-body entropy s_2 for the data shown in Fig. 6.7 along paths of constant particle volume fraction ϕ_c for the “repulsive” (top panel, $\phi_p < 0.25$) and “attractive” fluid (bottom panel, $\phi_p \geq 0.25$). Lines are fits to the data of the form $D \propto \exp[A(\phi_c)s_2]$. The dashed line in the bottom panel shows the fit to “repulsive” fluid data ($\phi_p < 0.25$).	118
6.9	Diffusivity D versus two-body entropy s_2 along a constant particle density $\rho = 0.85$ for the “Dzugutov” fluid. Line is the fit to the data of the form $D \propto \exp[As_2]$. The inset also shows the diffusivity versus inverse temperature data for the same condition as the main plot.	119

Chapter 1

Introduction

In this thesis, we explore the fundamental connections between thermodynamics, structure and dynamics for two non-trivial problems of the liquid state. Specifically, we study the relationship between the excess entropy, pair-correlation function, available space and self-diffusivity of confined and supercooled fluids. On one hand, the relationships found between these quantities can be practically useful for predicting the kinetic properties of confined fluids since theories for predicting thermodynamics / structure in confinement (e.g., density functional theory) are already very well developed. On the other hand, recasting these connections in terms of well defined textbook quantities can help resolve some of the outstanding issues related to the dynamical behavior of supercooled liquids. In this chapter, first we briefly describe some the important aspects of confined and supercooled fluid states along with some of the interesting open questions that we have addressed in this work. we will then outline the motivation and related background information for the approach used here. Finally, we provide the organization of the rest of the chapters along with a summary of each chapter and important findings of the work described there.

1.1 Confined Fluids

Confined fluids play an important role in a host of scientific phenomena and technological applications. Examples range from the aqueous fluids that fill the cytostructures of biological cells to the solvents that facilitate the operation of nano- and micro-fluidic devices. More traditional chemical engineering applications include membranes for separations and porous catalytic materials. In many of these systems, confinement significantly modifies the thermodynamic and kinetic behavior of the fluid relative to the bulk phase. Such modifications are generally attributed to a collective effect of the size and shape of the confined space and the interactions of the fluid with the confining surface. However, isolating the individual contributions of these various factors for a systematic experimental study can be a daunting task.

Given this difficulty, one alternative approach has been to use simplified models that allow one to explore the effect of confinement in the absence of the complicating details that are present in experimental systems. By using simple systems, we can also determine the effect of each contribution separately. A commonly investigated model is one with fluid confined between smooth and parallel interacting walls (commonly referred to as “films” for walls in only one direction and “pores” for walls in two directions). This is arguably the most basic model that can capture the main entropic packing effects and also the effect of fluid-wall interactions associated with fluids in confined spaces. The characteristic inhomogeneous density profile for this model (normal to the confining walls), which has been the primary focus of previous investigations,

is now qualitatively understood. Unfortunately, despite progress in elucidating some of the other properties of this system, a comprehensive picture for precisely how confinement modifies the average thermodynamic and kinetic behavior of the equilibrium fluid is yet to emerge.

Another interesting confinement model which can capture the effect of the complicated geometry of real systems such as membranes and porous catalysts is the “quenched-annealed” system [66]. Here, a part of the system is dynamically frozen thus hindering the relaxation of the remaining moving particles and thereby providing a simple model for flow through complicated porous media. Although intuitively one would expect the flow behavior in these model systems to be related to the geometrical characteristics of the underlying quenched structure, even a qualitative relationship between these quantities has been lacking.

1.2 Supercooled Liquids

Predicting the dynamic behavior of deeply supercooled liquids has been a long-standing challenge in condensed matter theory [4, 23]. One of the main conceptual hurdles is in understanding why the rapid decrease of fluid mobility near the glass transition is not accompanied by an equally pronounced change in the static structure. On one hand, this lack of an identifiable structural precursor for vitrification seems to support the perspective, embodied in kinetically constrained models [41, 42], that relaxation processes of deeply supercooled liquids are purely kinetic phenomena; i.e., they do not reflect an

underlying static structural or thermodynamic singularity. On the other hand, a well-known prediction connecting thermodynamics to dynamics appeared in the seminal work of Adam and Gibbs (AG) [1], where semi-empirical arguments led to an exponential relationship between the measure of mobility (or its inverse, i.e. the relaxation time) and the molar configurational entropy. The AG relation has been shown empirically to describe the behavior of a variety of computer-simulated liquids in their supercooled states, including models for silica [93] and water [98], a binary Lennard-Jones alloy [96], and a monatomic model glass-former introduced by Dzugutov [43]. The AG relationship has also been validated through analysis of experimentally obtained thermodynamic and kinetic data of various supercooled liquids [85]. One of the major drawbacks of the AG approach is that there is no general agreement on the definition of the involved thermodynamic quantity, i.e. the configurational entropy. Moreover, the configurational entropy is not relevant at high temperature and does not generally correlate with dynamics far above the freezing transition. As a result, it cannot provide a comprehensive description of liquid-state dynamics.

Then there is, the Mode coupling theory (MCT) [44], which utilizes the static structure factor [or pair correlation function $g(r)$] as an input and successfully predicts many of the nontrivial dynamic properties of supercooled liquids. This suggests that mobility is, in fact, closely intertwined with the equilibrium structure. But still, the increases in structural order reflected by direct inspection of $g(r)$ appears relatively modest in comparison to the

pronounced increases in relaxation time upon supercooling. Therefore, a clear physical picture for how static structural properties such as $g(r)$ are connected to the self-diffusivity of supercooled liquids have been elusive.

1.3 Background and Motivation

The self-diffusivity of several equilibrium bulk fluids, when cast in an appropriately reduced form, show an approximate scaling with s^{ex} , the excess entropy per particle of the fluid (relative to an ideal gas with the same number density) [26, 86, 87]. This type of empirical scaling behavior has great practical value because it relates the diffusivity that can be difficult to predict, to an experimentally-accessible thermodynamic quantity, s^{ex} , which can also be calculated directly in a computer simulation [32, 71, 72] or estimated based on knowledge of the pair-correlation function [8, 77, 78].

Entropy scaling laws for the transport coefficients of fluids were first noticed by Rosenfeld [86] while studying the performance of a variational thermodynamic perturbation theory [68]. In particular, Rosenfeld observed that the reduced diffusion coefficient $D_{\text{R}} = D\rho^{1/3}\sqrt{m/(k_{\text{B}}T)}$ approximately obeyed the relationship $D_{\text{R}} \approx 0.58\exp(As^{\text{ex}}/k_{\text{B}})$ for several dense model fluids over a wide range of equilibrium conditions. Here, ρ is number density, k_{B} is the Boltzmann constant, T is temperature, m is particle mass and A is a parameter that depends weakly on the species investigated (e.g., $A = 0.65$ and 0.8 approximately describe behavior for the HS and LJ fluids, respectively [86]).

Later, Dzugasov used a different conceptual starting point [26–28] to

arrive at a similar scaling law. However, his proposed relationship provided a seemingly “universal” (i.e., species-independent) connection between the reduced diffusivity $D_D = D\rho^{2/3}\Gamma_E^{-1}$ and excess entropy s^{ex} for equilibrium liquids, $D_D \approx .078 \exp(s^{\text{ex}}/k_B)$ [28]. The parameter $\Gamma_E = 4\pi\sigma^2\rho g(\sigma)\sqrt{k_B T/\pi m}$ is an effective Enskog interparticle collision frequency, σ is the interparticle separation corresponding to the first peak in the radial distribution function, and $g(\sigma)$ is the magnitude of that first peak. Note that Γ_E in the Dzугutov scaling law is a microscopic quantity, whereas the reduction parameters in the Rosenfeld scaling law are macroscopic in nature. Microscopic reduction parameters such as Γ_E are potentially useful because they can be related to molecular-level processes, but macroscopic reduction parameters such as ρ or T can also be advantageous because they are easy to determine via experiment and have clear physical interpretations.

Notwithstanding the frequent use of the entropy scaling laws [10, 15, 28, 52, 64, 88, 94, 104, 119] and the various attempts to put them on a firmer theoretical ground using either mode coupling theory [95] or cell-theory models [51], the precise origin of this apparent connection between thermodynamics and dynamics of fluids is still uncertain. This view is perhaps best summarized by Rosenfeld [87]:

The excess-entropy scaling relation is a semi-quantitative model (like the van der Waals equation of state), rather than a theory. Like any corresponding-states relationship that links non-scaling force laws, it can only be approximate. However, in view of the ab-

sence of a unifying quantitative description of atomic transport in condensed matter, the excess-entropy scaling is important for estimating unknown transport coefficients and for providing guidelines for theoretical analysis.

1.4 Thesis Organization

In this thesis, we have used the ideas described above to propose a new approach for relating the self-diffusivity, the excess entropy (and the associated structural quantities) for the case of confined and supercooled fluids. We show that this relationship can be used for predicting the fluid dynamics in simple confinement such as 2- and 1-dimensional channels (Chapter 2, 3, 4) and more complex systems such as model porous media (Chapter 5). Moreover, we find that it highlights the underlying changes in the structure of supercooled liquids to clarify its dynamical nature (Chapter 6). Below is an outline of the latter chapters in this thesis:

Chapter 2: Thermodynamics predicts the dynamics of the confined equilibrium hard-sphere fluid

We study how confining the equilibrium hard-sphere fluid to restrictive one- and two-dimensional channels with smooth interacting walls modifies its structure, dynamics, and entropy using molecular dynamics and transition-matrix Monte Carlo simulations. Although confinement strongly affects local structuring, we find that the relationships between self-diffusivity, excess entropy, and average fluid density are, to an excellent approximation, indepen-

dent of channel width or particle-wall interactions. Thus, thermodynamics can be used to predict how confinement impacts dynamics.

Chapter 3: Average properties of the highly confined hard-sphere fluid

We use grand canonical transition-matrix Monte Carlo and discontinuous molecular dynamics simulations to generate precise thermodynamic and kinetic data for the equilibrium hard-sphere fluid confined between smooth hard walls. These simulations show that the pronounced inhomogeneous structuring of the fluid normal to the confining walls, often the primary focus of density functional theory studies, has a negligible effect on many of its average properties over a surprisingly broad range of conditions. We present one consequence of this insensitivity to confinement: a simple analytical equation relating the average density of the confined fluid to that of the bulk fluid with equal activity. Nontrivial implications of confinement for average fluid properties do emerge in this system, but only when the fluid is *both* (i) dense *and* (ii) confined to a gap smaller than approximately three particle diameters. For this limited set of conditions, we find that “in-phase” oscillatory deviations in excess entropy and self-diffusivity (relative to the behavior of the bulk fluid at the same average density) occur as a function of gap size. These paired thermodynamic/kinetic deviations from bulk behavior appear to reflect the geometric packing frustration that arises when the confined space cannot naturally accommodate an integer number of particle layers.

Chapter 4: Self-diffusivity, packing fraction, and excess entropy of

simple bulk and confined fluids

We explore the connections between self-diffusivity, density, and excess entropy in two of the most widely used models for “simple” liquids, the equilibrium Lennard-Jones and square-well fluids, in both bulk and confined environments. We find that the self-diffusivity data of the Lennard-Jones fluid can be approximately collapsed onto a single curve (i) versus effective packing fraction and (ii) in appropriately reduced form versus excess entropy, as suggested by two well-known scaling laws. Similar data collapse does not occur for the square-well fluid, a fact that can be understood based on the non-trivial effects that temperature has on its static structure. Nonetheless, we show that the implications of confinement for the self-diffusivity of both of these model fluids, over a broad range of equilibrium conditions, can be predicted based on knowledge of the bulk fluid behavior and either the effective packing fraction (approximately) or the excess entropy (accurately) of the confined fluid.

Chapter 5: Fluid diffusivity in random porous media

We propose a simple equation for predicting self-diffusivity of fluids embedded in random matrices of identical, but dynamically frozen, particles (i.e., quenched-annealed systems). The only nontrivial input is the volume available to mobile particles, which also can be predicted for two common matrix types that reflect equilibrium and non-equilibrium fluid structures. The proposed equation can account for the large differences in mobility exhibited by quenched-annealed systems with indistinguishable static pair correlations, illustrating the key role that available volume plays in transport.

Chapter 6: Thermodynamics, static structure and dynamics of supercooled liquids

Here we provide, to our knowledge, the first evidence that excess entropy also captures how supercooling a fluid modifies its diffusivity, suggesting that dynamics, from ideal gas to glass, is related to a single, standard thermodynamic quantity. Using standard thermodynamic expansion of excess entropy in terms of particle distribution functions, we also show that this information can be translated into a functional relationship between self-diffusivity and the pair correlation function.

Chapter 2

Thermodynamics predicts the dynamics of the confined equilibrium hard-sphere fluid

2.1 Introduction

The molecular dynamics of fluids confined to small spaces can differ significantly from the bulk. These differences have generated wide interest because confined fluids feature prominently in both nature and technology. Examples include dynamics of water near proteins or in concentrated cellular environments, transport processes across biological membranes, and fluid flows encountered in micro- or nanofluidic devices, to mention a few. Given that a significant fraction of the molecules in these systems populate highly inhomogeneous interfacial environments, it is easy to appreciate why confinement has nontrivial consequences for their transport coefficients (e.g., diffusivity and viscosity). Nonetheless, a theoretical framework that can reliably predict these consequences has been slow to develop.

One logical starting point is to ask whether confinement induced modifications to equilibrium fluid properties, such as the density, can explain some of the observed differences in dynamics [70, 76, 84]. For instance, if the presence of a strongly attractive substrate increases the local fluid density near the fluid-

substrate interface, one might naturally expect a corresponding decrease in particle mobility near that interface, and vice versa. This type of argument is physically intuitive, and it has been recently used to rationalize why nanoscale materials exhibit glass transition temperatures that are shifted relative to their bulk values [70]. However, it seems doubtful that average structural quantities alone can account for the wide variety of dynamical behaviors observed in both simulations and experiments of confined fluids [37, 56, 99]. As a result, it is natural to ask whether other equilibrium measures, such as the entropy, can provide additional insights. Unfortunately, it is currently difficult to obtain the necessary experimental data for testing these possible connections between thermodynamics and dynamics for confined fluids. Thus, simulation results on simple and well-defined model systems are of great complementary value.

One reason to speculate that entropy could be a reliable predictor for how confinement affects the diffusivity is its empirical success for capturing the dynamical behavior of bulk materials. In particular, computer simulation studies have demonstrated that the single-component HS and Lennard-Jones fluids, along with a variety of models for liquid metals, exhibit, to a very good approximation, a one-to-one relationship between diffusivity and excess entropy over a broad range of thermodynamic conditions [10, 15, 29, 89, 90]. Excess entropy has also been shown to accurately capture the behavior of diffusion phenomena in fluid mixtures [53, 94, 95] as well as those in solid-state ionic conductor and quasicrystalline materials [29].

To explain the origin of the correspondence between excess entropy and

diffusivity in bulk materials, several researchers have presented independent derivations of apparent scaling laws relating the two quantities. The earliest that we are aware of is due to Rosenfeld and is motivated by a variational thermodynamic perturbation theory [89, 90]. Dzugutov later used arguments based on kinetic theory to justify a similar scaling [29], and recently mode-coupling theory has been employed to establish an approximate basis for the observed connection [94, 95]. Despite the large amount of effort that has been devoted to justifying these scaling laws theoretically and testing their validity for bulk materials, to our knowledge the relationship between excess entropy and diffusivity has never been tested in inhomogeneous fluids, nor has it been used as a tool to understand how confinement affects dynamics.

In this Chapter, we advance the current understanding of the relation between thermodynamics and dynamics in inhomogeneous systems by addressing the following two questions. (i) Can either the entropy or the average density be used to determine the extent to which confinement alters the diffusivity of a hard-sphere (HS) fluid? (ii) If so, do the specific interactions between particles and the channel boundaries significantly impact the result? While the confined HS system represents arguably the most elementary and well-studied model for inhomogeneous colloidal and molecular fluids, there is still surprisingly little known about the possible connections between its basic thermodynamic and kinetic properties. If such connections do exist and prove to be robust, it suggests that equilibrium theories for inhomogeneous fluids might generally provide important information regarding how confinement

modifies the transport properties of fluids.

2.2 Simulation details

We studied how the structure, thermodynamics, and dynamics of the single component HS fluid confined to restrictive two-dimensional ($2d$) or one-dimensional ($1d$) channels bounded by smooth interacting walls differ from those of the bulk system. We considered five different $2d$ channel sizes that were effectively macroscopic in the x and y directions and had particle-center accessible dimensions in the confining z direction of $h_z = 15, 10, 7.5, 5,$ and $2.5,$ respectively. We also considered three $1d$ channel sizes that were effectively macroscopic in the x direction and had particle-center accessible dimensions in the confining y and z directions of $h_y \times h_z = 7.5 \times 7.5, 7.5 \times 5,$ and $5 \times 5,$ respectively. To simplify the notation, we have implicitly non-dimensionalized all lengths in this study by the HS particle diameter σ and all times by the combination $\sigma\sqrt{m\beta}$, where m is particle mass, $\beta = 1/k_B T$, k_B is Boltzmann's constant, and T is temperature. Consequently, all energies are given per unit $k_B T$. Position-dependent interactions between the particles and the confining channel walls $u(\zeta)$ were calculated using a square-well potential:

$$\begin{aligned}
 u(\zeta) &= \infty & \zeta < 1/2 \\
 &= \epsilon_w & 1/2 \leq \zeta < 1 \\
 &= 0 & \zeta \geq 1,
 \end{aligned} \tag{2.1}$$

where ζ represents the shortest distance between a given particle center and the wall of interest, and ϵ_w is the strength of the effective particle-wall interaction. We considered five specific particle-wall interactions for the $2d$ channels: $\epsilon_w = 1$ and $\epsilon_w = 0.5$ representing repulsive walls, $\epsilon_w = 0$ representing “hard” but neutral walls, and $\epsilon_w = -0.5$ and $\epsilon_w = -1$ representing attractive walls. Only the hard walls were considered for the three highly restrictive $1d$ channels. For the conditions investigated here, none of the model systems exhibit anomalous diffusion reported for some systems [75].

To monitor kinetic processes in these various systems, we performed a series of event-driven molecular dynamics simulations [82] in the microcanonical ensemble using $N = 4500$ hard spheres. Periodic boundary conditions were employed in the d “free” directions (i.e., directions not confined by walls). The dimensions of the simulation cell in the periodic directions were set to various values to simulate fluids with different average number densities that span the stable equilibrium range, from the dilute gas to the fluid at its freezing transition. We extracted the self-diffusivity of the fluid D by fitting the long-time ($t \gg 1$) behavior of the average mean-squared displacement of the particles to the Einstein relation $\langle \Delta \mathbf{r}_d^2 \rangle = 2dDt$, where $\Delta \mathbf{r}_d^2$ corresponds to the mean-square displacement in the d periodic directions. We also calculated D for several state points with both smaller ($N = 3000$) and larger ($N = 6000$) particle numbers to verify that system size effects in the periodic directions were negligible.

We determined the behavior of the excess entropy per particle s^{ex} using

grand canonical transition-matrix Monte Carlo (GC-TMMC) simulations [33]. Here, s^{ex} is defined to be the difference between the entropy per particle of the fluid and that of an ideal gas with the same spatial distribution of the particle number density. GC-TMMC simulations require fixed values for the activity ξ , the particle-center accessible dimensions $\{h_x, h_y, h_z\}$ that define the volume of the simulation cell $V = h_x h_y h_z$, and the reciprocal temperature β . The activity is defined as $\xi = \exp(\beta\mu)/\Lambda^3$, where μ is the chemical potential and Λ is the de Broglie wavelength. For all simulations conducted here, we set $\xi = 1$, $\beta = 1$, and we used the particle-wall interactions given by Eq. (2.1). The values of $h_y \times h_z$ or h_z are determined by the confining dimensions of the $1d$ or $2d$ channels, respectively, and the remaining periodic dimension(s) were chosen to satisfy $V = 1000$. Indistinguishable results were obtained for systems of size $V = 500$.

The key quantities extracted from the GC-TMMC simulations were the total particle number probability distribution $\Pi(N)$, the excess configurational energy $U^{\text{ex}}(N)$, and the N -specific spatial density distribution $\rho(N, \mathbf{r})$, each evaluated over a range of particle numbers spanning from $N = 0$ to $N = 984$. Using basic arguments from statistical mechanics [21, 79], one can relate these quantities to s^{ex} for the inhomogeneous HS fluid:

$$s^{\text{ex}}(N)/k_{\text{B}} = N^{-1} \{ \ln[\Pi(N)/\Pi(0)] - N \ln \xi + \ln N! - N \ln N + \beta U^{\text{ex}}(N) + \int \rho(N, \mathbf{r}) \ln \rho(N, \mathbf{r}) d\mathbf{r} \} \quad (2.2)$$

Given that $V = 1000$ is fixed, Eq. (2.2) provides $s^{\text{ex}}(\rho_h)$ within the range

$0 \leq \rho_h \leq 0.984$, where $\rho_h = N/V$ is the number density based on the particle-center accessible volume.

2.3 Results and discussion

In this section, we first discuss our observations for the utility of excess entropy s^{ex} in predicting how confinement affects dynamics. Next, we present results which suggests that even a much simpler measure, i.e. density can also be used to predict dynamics.

2.3.1 Self-diffusivity versus excess entropy

Fig. 2.1 shows a parametric plot of D versus $-s^{\text{ex}}$ for the HS fluid both in the bulk and confined to the 17 different $2d$ channels ($h_z = 2.5, 5, 10$ with $\epsilon_w = 1, 0.5, 0, -0.5, -1$ and $h_z = 7.5, 15$ with $\epsilon_w = 0$). The data, which encompasses the dynamic behavior of the equilibrium fluid from the dilute gas to the freezing transition, spans three decades in D . The collapse of the data onto a single master curve indicates that, to an excellent approximation, the simple one-to-one correspondence between D and s^{ex} for the bulk HS fluid also holds when the fluid is severely confined. Moreover, the quality of the data collapse is largely independent of either channel width (including “particle scale” channels with $h_z = 2.5$) and the sign or magnitude of the particle-wall interaction. Data for the HS fluid confined to the 3 rectangular $1d$ channels described above are superimposed in the Fig. 2.2. As can be seen, they also approximately collapse onto the bulk HS relationship between D and s^{ex} . In

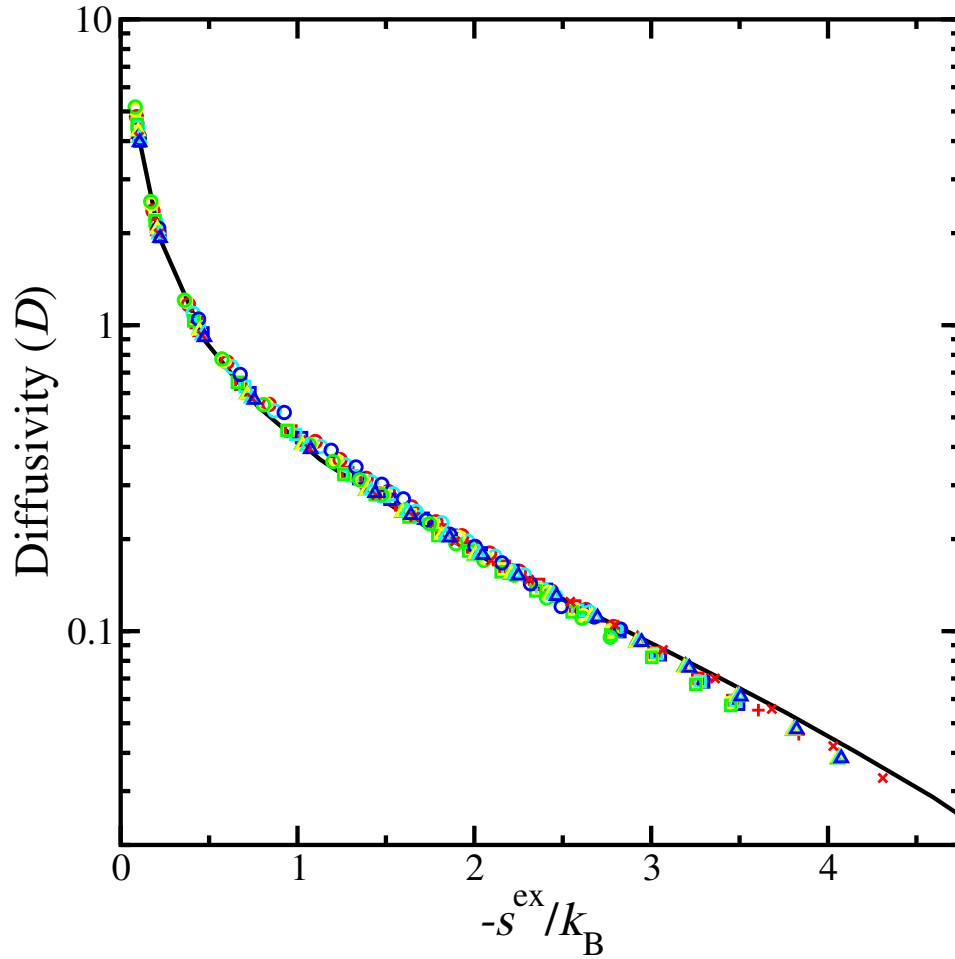


Figure 2.1: Self-diffusivity D versus the negative of excess entropy per particle $-s^{\text{ex}}/k_{\text{B}}$ for the bulk HS fluid (solid curve) and for the HS fluid in $2d$ channels (symbols). The symbols correspond to $h_z = 2.5$ (circle), 5 (square), 7.5 (plus), 10 (triangle up) and 15 (cross). The color codes are $\epsilon_w = 1$ (blue), 0.5 (cyan), 0 (red), -0.5 (yellow), and -1 (green).

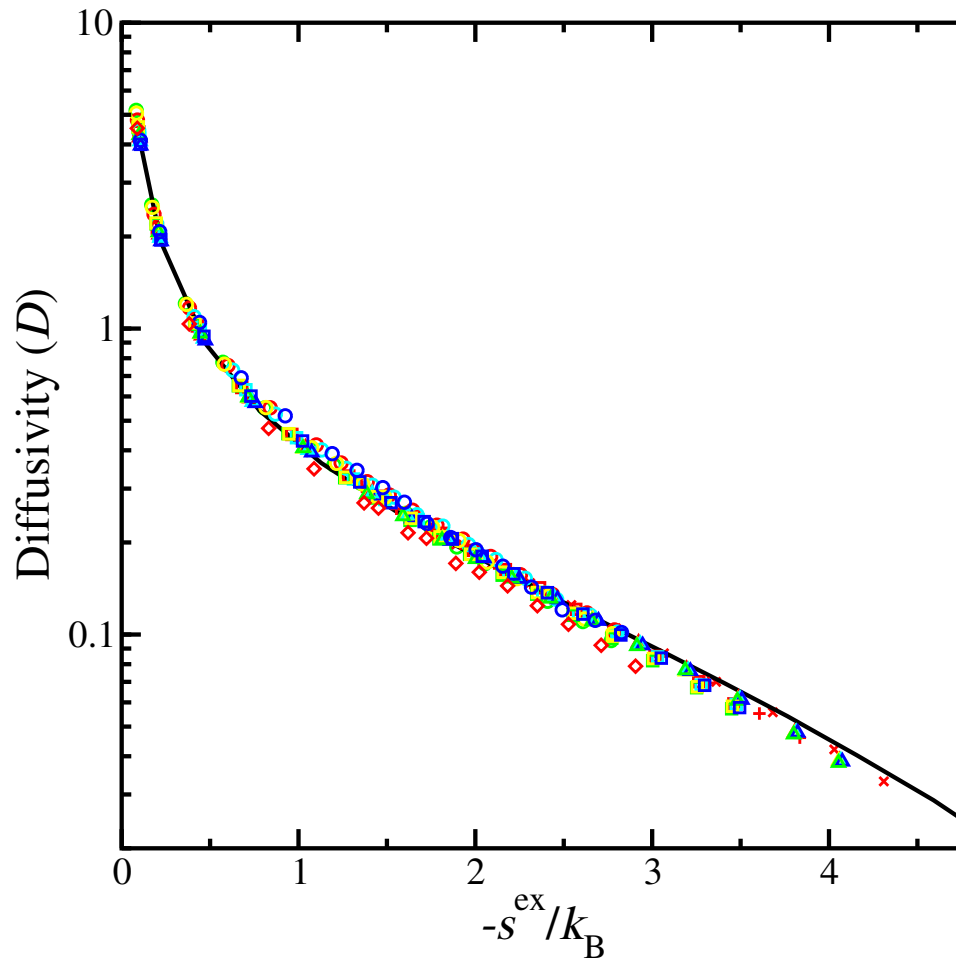


Figure 2.2: Self-diffusivity D versus the negative of excess entropy per particle $-s^{\text{ex}}/k_{\text{B}}$ for the same data as shown in Fig. 2.1 with added points for the $1d$ channels: 5×5 , 7.5×7.5 , and 5×7.5 shown by red diamonds.

fact the diffusivities for approximately 50, 70, and 90% of the confined state points shown in Fig. 2.2 are within 3, 5, and 10 % respectively of the bulk value at the same excess entropy.

2.3.2 Self-diffusivity versus average density

Having established that s^{ex} , an equilibrium thermodynamic property, can be used to predict how various confining environments impact the self-diffusivity of the HS system, it is natural to press forward and ask whether the same predictive information is contained in an even simpler structural measure: the average density.

Here, one needs to be specific because there are two different definitions of average density that are commonly used to characterize inhomogeneous HS fluids ($\rho_h = N/V_h$ and $\rho = N/V$). The former is based on the particle-center-accessible volume $V_h = h_x h_y h_z$, while the latter is based on the total system volume; i.e., $V = h_x h_y (h_z + 1)$ for $2d$ channels, and $V = h_x (h_y + 1)(h_z + 1)$ for $1d$ channels. Schmidt and Löwen [102] and, later, Zangi and Rice [120] demonstrated that ρ is in fact the relevant density for the lateral (i.e., periodic) component(s) of the pressure, and thus ρ is also a natural independent variable for the free energy of the system. Below, we investigate whether ρ is also an accurate predictor for how confinement effects HS diffusivity.

Fig. 2.3 shows D as a function of ρ for the bulk HS fluid as well as for the HS fluid confined to the $2d$ and $1d$ channels. The collapse of the data, while not perfect, demonstrates a very strong correlation between D and ρ

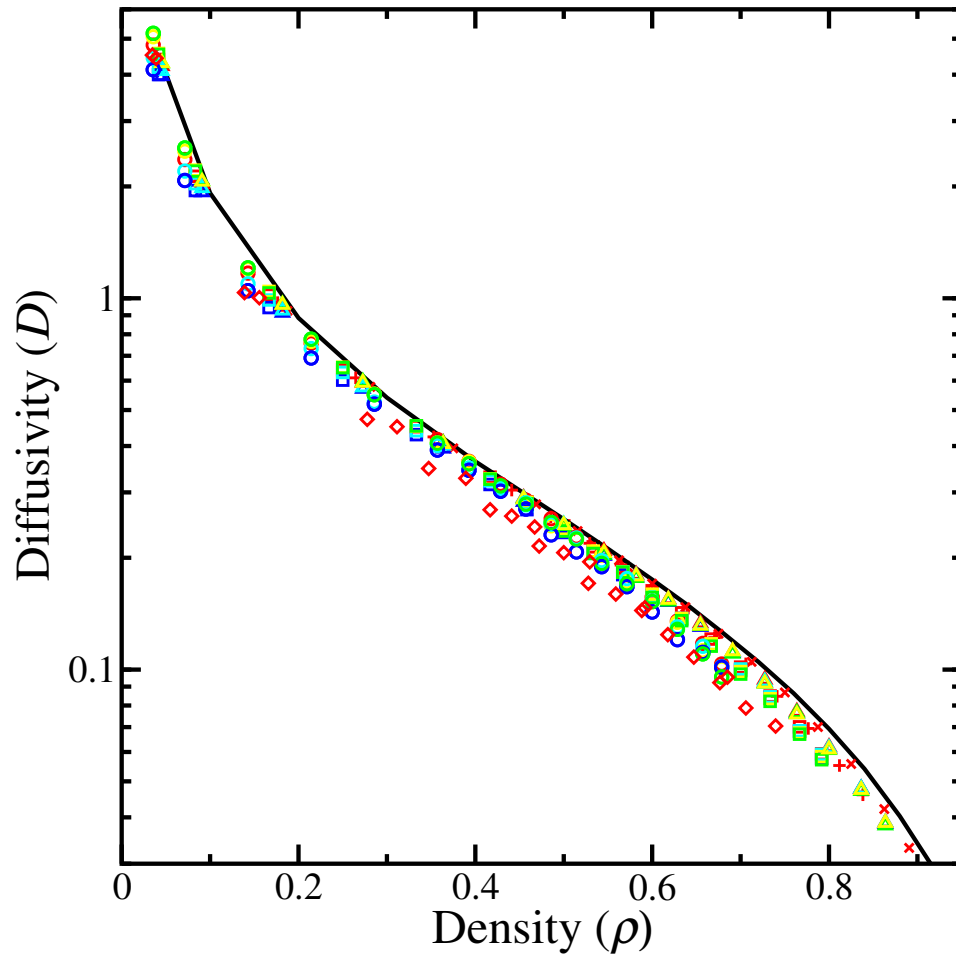


Figure 2.3: Self-diffusivity D vs average density $\rho = N/V$ based on the the total system volume V . Symbols are identical to those given in Fig. 2.2.

that is nearly independent of the confining dimensions and the particle-wall interactions. Approximately 70 and 90% of the diffusivities for the confined state points shown in Fig. 2.3 are within 10 and 20%, respectively, of the bulk value at the same average density. This is another significant result because, unlike s^{ex} , ρ is intuitively simple to understand and trivial to determine in simulations (e.g., it is specified in microcanonical and canonical simulations). As is expected, the systems that exhibit the most noticeable deviation from bulk behavior in Fig. 2.3 are the ones for which the fluid is under the most severe confinement, i.e., channels with dimensions comparable to the particle diameter. In these cases, it appears that specific fluid structuring (e.g., density enhancements in the channel corners) acts to only slightly reduce the diffusivity relative to what would be predicted by the average density ρ .

Now, we examine what conclusions regarding density follow if one instead chooses to plot D versus the alternative definition for average density, $\rho_h = N/V_h$, based on the total particle-center-accessible volume V_h . In particular, Fig. 2.4 compares the self-diffusivity for the HS fluid confined to 5 different $2d$ channels with hard walls ($\epsilon_w = 0$) as a function of ρ_h . Unlike when plotting versus ρ , there is no data collapse of D when plotting versus ρ_h . Thus, one might consider ρ a more natural independent variable than ρ_h , not only for thermodynamics of inhomogeneous fluids [102, 120], but also for dynamics.

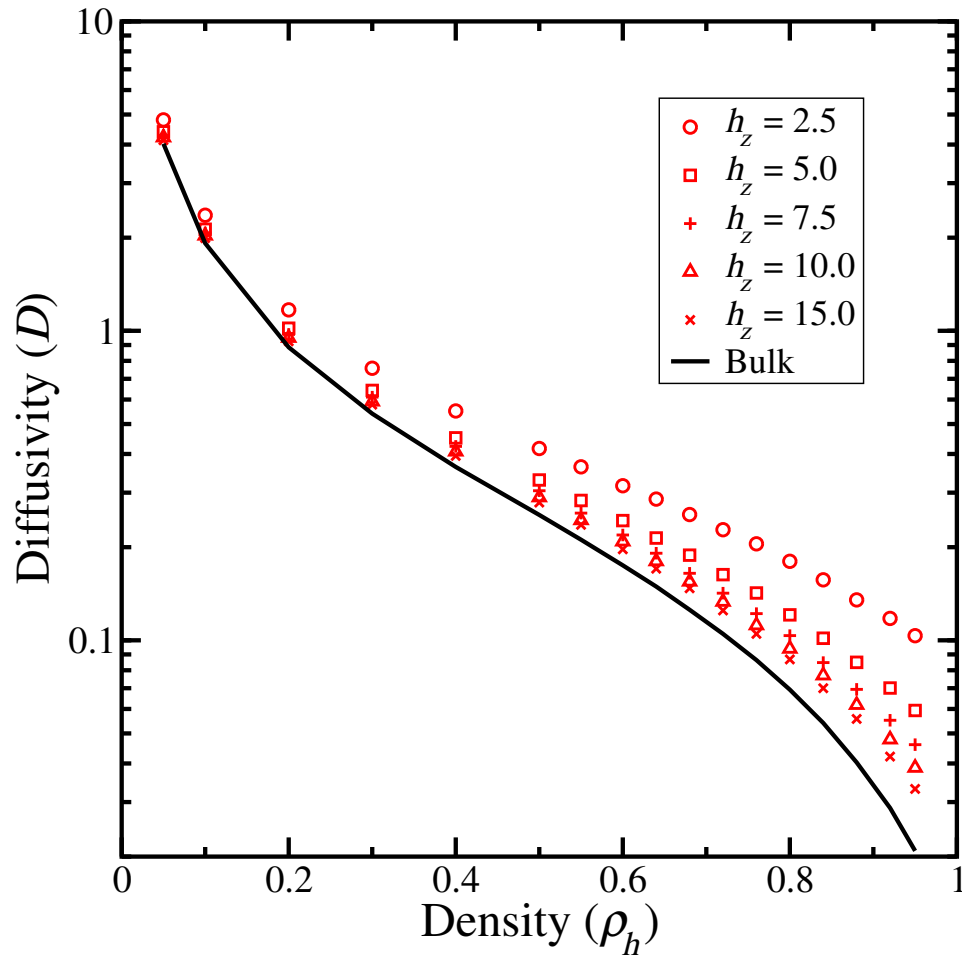


Figure 2.4: Self-diffusivity D versus average density $\rho_h = N/V_h$ based on the total particle-center accessible volume V_h . Systems shown include the bulk HS fluid (solid curve) and the HS fluid confined to the $2d$ channels between hard walls.

2.3.3 Local fluid structure versus diffusivity

Given the approximate collapse of the data in Fig. 2.3, it is natural to wonder whether it is simply the particle structuring that is determining the HS dynamics. To test this idea further, we examine in Fig. 2.5 the local density profiles $\rho(z)$ for a HS fluid confined to $2d$ channels of width $h_z = 2.5$ but with three different particle-wall interactions: $\epsilon_w = 1$ (repulsive walls), $\epsilon_w = 0$ (neutral walls), and $\epsilon_w = -1$ (attractive walls). All three systems exhibit the same average density ρ , and thus according to Fig. 2.3, display approximately the same self-diffusivity D as the bulk fluid. Clearly there are real and pronounced differences in the local structuring of the three confined fluids, especially when compared to the uniform bulk material. These types of structural differences are usually the main focus of studies of inhomogeneous fluids by classical density functional theories. Interestingly, these pronounced structural differences only slightly alter both s^{ex} and D when considering fluids with the same average ρ .

2.4 Conclusions

To conclude, we have probed the structure, entropy, and diffusivity of the HS fluid confined to $2d$ and $1d$ channels with a wide range of dimensions and particle-boundary interactions. Our main finding is that the relationships between diffusivity, excess entropy, and average density for the bulk HS fluid also remain valid, to within an excellent approximation, for the HS fluid confined to particle-scale geometries. Since statistical mechanical theories can

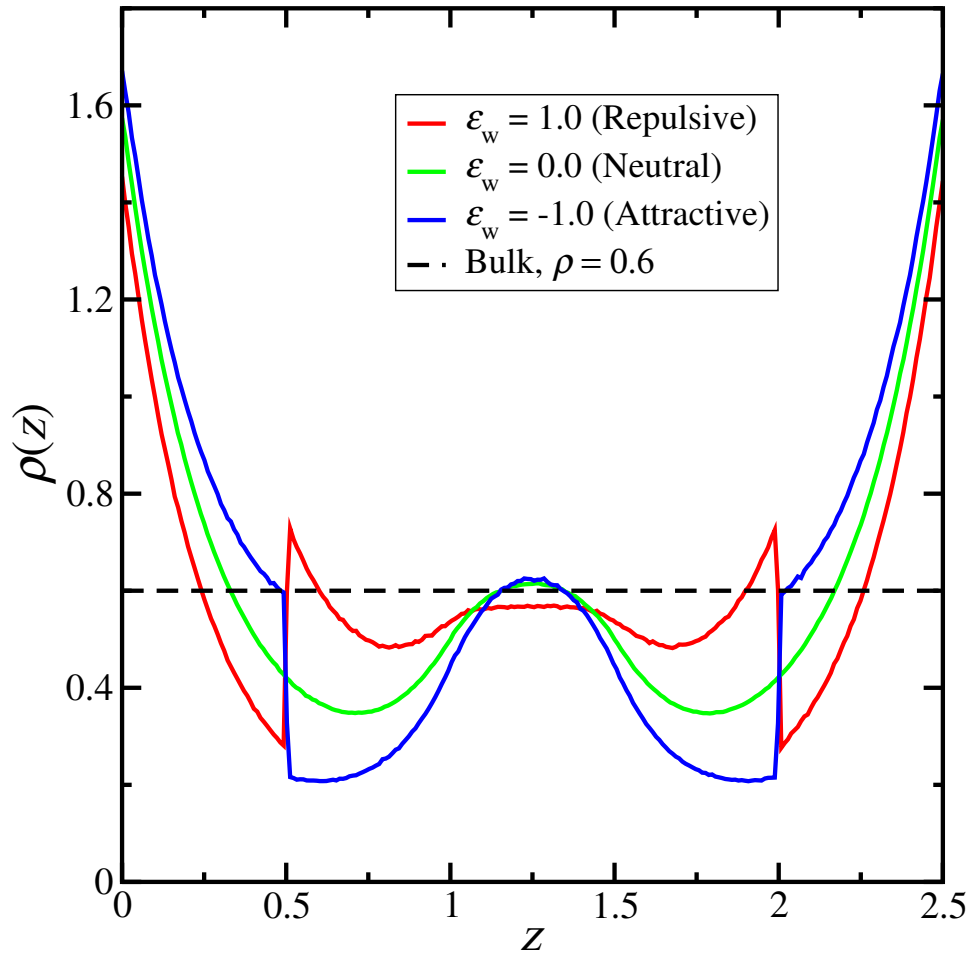


Figure 2.5: Density profiles $\rho(z)$ for HS fluids confined to a $2d$ channel of width $h_z = 2.5$. Although each system has different particle-wall interaction strengths ϵ_w , they share a common average density ρ (dashed) and self-diffusivity D .

provide accurate estimates for how confinement modifies the excess entropy and density, the robust connection between thermodynamics and dynamics reported here should have far-reaching implications for the prediction of dynamics in confined systems. In next chapters, we will test whether similar connections hold (i) for fluids with strong interparticle attractions that significantly affect local structuring, (ii) for the HS fluid in more general random environments (e.g., in quenched media, etc.), (iii) for non-equilibrium supercooled fluid states.

Chapter 3

Average properties of the highly confined hard-sphere fluid

3.1 Introduction

In the previous chapter, we demonstrated via molecular simulation that the self-diffusivity of the confined HS fluid parallel to the confining walls, over a broad range of equilibrium conditions, is very similar to the bulk HS fluid if the two systems are compared at the same value of density $\rho = N\sigma^3/V$. Here, N refers to the number of particles, σ is the particle diameter, $V = AH$ is the total volume of the confined fluid (i.e., A is the area of a wall in contact with the fluid, and H is the distance from “wall surface to wall surface”). In other words, the specific details of the inhomogeneous packing structures have only minor influence on the average single-particle dynamics of the confined fluid, as long as one controls for the average overall density ρ . Alternatively, if one instead compares the behaviors of the bulk and confined systems at equal values of $\rho_h = N\sigma^3/V_h$, one arrives at the conclusion that confining a HS fluid between hard walls has the effect of significantly speeding up its dynamics. Here, $V_h = Ah$ is the smaller volume accessible to the particle centers (i.e., $h = H - \sigma$). This latter artificial conclusion is related to the fact that N/A must vanish if ρ_h is to remain constant in the limit $H \rightarrow \sigma$. As a result, even

if the numerical value of ρ_h is chosen to be indicative of a dense bulk fluid, the actual average interparticle separation and particle mobility in the lateral direction will generally be very large (e.g., comparable to a dilute gas) when the fluid is confined to small enough H .

We are not aware of any systematic comparisons for how the thermodynamic properties of this system depend on ρ and ρ_h , respectively. However, even in the absence of such comparative studies, it is easy to imagine that one might indeed arrive at qualitatively different conclusions about the implications of confinement depending on whether ρ or ρ_h is chosen as the basis for comparison. To appreciate this point, consider that ρ_h diverges in the limit where the gap size H is reduced, at fixed N/A , to the size of one particle diameter σ (i.e., the two-dimensional fluid limit), whereas ρ and many other fluid properties of interest remain finite. This type of consideration alone hints that ρ might be the more suitable density variable of the two for making comparisons to the bulk fluid, and indeed ρ naturally emerges in the thermodynamic analysis of confined HS fluids [101, 120].

There is another important, but still poorly understood, conceptual point concerning this model. Specifically, it has not been entirely clear how one should compare the confined fluid to the bulk fluid in order to elucidate the main effects of confinement. One obvious possibility is to compare the two systems under conditions where they exhibit equal “average” density. The argument for choosing this basis of comparison is straightforward. Packing effects dominate the behavior of athermal systems, and average density is an

important factor in determining how the particles pack. Moreover, if one controls for average density in making the comparison, then one can hope to isolate more subtle effects due to, e.g., the finite size of the confined system (in one direction) and the shape of the density profile (i.e., the “layering”). Another possibility is to compare the two systems at equal activity, where the bulk and pore fluids exhibit different average densities. The advantage in doing so is also obvious. Equality of activity is a relevant experimental constraint on the chemical equilibrium that is established between the bulk and pore fluids.

The confinement model we use here is the equilibrium, monatomic hard-sphere (HS) fluid confined between smooth and parallel hard walls. Unfortunately, despite progress in elucidating some of the other properties of this system (see, e.g., [7, 21, 25, 40, 49, 58, 73, 100, 101, 110, 120]), a comprehensive picture for precisely how confinement modifies the average thermodynamic and kinetic behavior of this model fluid has yet to emerge.

One of the most basic hurdles to constructing this picture has been the lack of accurate molecular simulation data for the average properties of the confined HS fluid, a fact that may seem surprising given the apparent simplicity of the model. Ironically, the model’s simplicity has indirectly contributed to the lack of simulation data because it has allowed the system to be readily studied by approximate theories instead [67, 117], which are appealing because they require only modest computational resources. While such theories are also insightful, their predictions cannot be viewed as a replacement for molecular simulation data because they are not quantitatively accurate for conditions

of high fluid density and narrow confining geometries. Fortunately, the development of efficient algorithms for investigating systems with discontinuous potentials and the availability of fast computers have now made it feasible to use molecular simulation to fully characterize the behavior of this model with both accuracy and precision. One aim of the present study is to leverage these resources to take an important step toward completing this characterization.

Here, we follow up on some of the initial observations of Chapter 2 by presenting a more comprehensive study for how fluid density and confinement (between hard walls) affect the thermodynamic and kinetic properties of the HS fluid. We broadly focus our investigation on four main questions. The first pertains to the equation of state of the confined fluid (i.e., how the average transverse and normal components of its pressure tensor vary with average density). Specifically, we are interested in how the behaviors of these pressure components depend on the volume definition invoked, i.e., V versus V_h . Does use of either definition produce relationships similar to the equation of state the bulk HS fluid? Second, what are the effects of confinement and average density on the transverse self-diffusivity of fluids confined to pores narrower than those previously examined in Chapter 2 (i.e., $H < 3.5\sigma$)? Third, how do the behaviors of the confined and bulk HS fluid systems compare under conditions of equal activity as opposed to equal density? Finally, does the robust relationship between excess entropy s^{ex} (relative to ideal gas) and self-diffusivity D , previously discovered for fluids confined to gap sizes larger than $H = 3.5\sigma$ in this system [73], continue to hold for very narrow pores ($H <$

3.5 σ)? By addressing these four questions, we can make significant headway not only in indentifying the regions in the $H - \rho$ and $H - \xi$ planes of parameter space where the confined HS system significantly deviates from the bulk HS fluid, but also in probing the microscopic mechanisms for such deviations.

3.2 Simulation Methods

To explore these issues, we have calculated the thermodynamic properties of confined and bulk HS fluids using grand canonical transition-matrix Monte Carlo (GC-TMMC) simulations [30, 34], and we have tracked their single-particle dynamics via discontinuous molecular dynamics (DMD) simulations [82]. To simplify the notation, we have implicitly non-dimensionalized all quantities by appropriate combinations of a characteristic length scale (which we take to be the HS particle diameter σ) and time scale (which we choose to be $\sigma\sqrt{m\beta}$, where m is particle mass, $\beta = [k_B T]^{-1}$, k_B is the Boltzmann constant, and T is temperature). As a result, all quantities with dimensions of energy are understood to be “per $k_B T$ ”, the only energy scale in the problem.

The DMD simulations each involved $N = 1500$ identical HS particles. For the bulk fluid, the particle centers were contained within a cubic simulation cell of $V_h = N/\rho_h$, and periodic boundary conditions were applied in all three directions. For the confined fluid, particle centers were contained within a rectangular parallelepiped simulation cell of $V_h = h_x h_y h_z$, where $h_z = H - 1$ and $h_x = h_y = [N/(h_z \rho_h)]^{1/2}$. Periodic boundary conditions were applied in the x and y directions and perfectly reflecting, smooth hard walls were

placed so that particle centers were trapped in the region $0 < z < h_z$. The self-diffusivity D of the fluid was obtained by fitting the long-time ($t \gg 1$) behavior of the average mean-squared displacement of the particles to the Einstein relation $\langle \Delta \mathbf{r}_d^2 \rangle = 2dDt$, where $\Delta \mathbf{r}_d^2$ corresponds to the mean-square displacement per particle in the d periodic directions ($d = 2, 3$ for the confined and bulk fluid, respectively). To verify that system-size effects in the periodic directions on D were insignificant, we checked that our calculated values for D for several state points compared favorably with those we obtained using either $N = 3000$ or $N = 4500$ particles.

The GC-TMMC simulations each utilized a simulation cell of size $V_h = 1000$. For the bulk fluid, the cell was cubic with $h_x = h_y = h_z = 10$. For the confined fluid, the cell was a rectangular parallelepiped with $h_z = H - 1$ and $h_y = h_x = \sqrt{1000/h_z}$. GC-TMMC simulations require a specified value for the activity ξ (i.e., N is allowed to fluctuate), which is defined as $\xi = \exp(\beta\mu)/\Lambda^3$, where μ is the chemical potential and Λ is the de Broglie wavelength. For all simulations conducted here, we set $\xi = 1$. The key quantities that we extracted from the simulations were the normalized total particle number probability distribution $\Pi(N)$ and the N -specific spatial density distribution $\rho(N, \mathbf{r})$, both evaluated over a range of particle numbers spanning from $N = 0$ to $N = 984$. Thermodynamic properties at other values of activity ξ were readily obtained via the histogram reweighting technique [38] to shift the original $\Pi(N)$ distribution to one representative of the particle numbers visited at the selected ξ . We found that we obtained statistically indistinguishable results

for systems with $V_h = 500$, indicating again that noticeable artifacts associated with system size were not present.

By employing basic arguments from statistical mechanics [21, 79], one can use the equilibrium information from GC-TMMC simulations to compute thermodynamic properties of interest. Specifically, the grand potential Ω can be calculated directly from the normalized particle number distribution [31, 79],

$$\Omega = \ln \Pi(0). \quad (3.1)$$

For the bulk HS fluid, we also have $V = V_h$, and thus $\rho = \sum_N N \Pi(N)/V = \rho_h$. Moreover, the pressure of the bulk fluid P is equal to the negative of the grand potential density, $P = -\Omega/V$. On the other hand, for the HS fluid confined between hard walls, we have $V = V_h/(1-H^{-1})$, and thus $\rho = \sum_N N \Pi(N)/V = (1 - H^{-1})\rho_h$. In this case, negative grand potential density $-\Omega/V$ represents an average transverse pressure acting parallel to the confining walls [48]. In the reduced units adopted here, the component of the pressure tensor acting normal to the walls is equal to the local fluid density in contact with a hard wall, $P_z(N) = \rho(N, z = 0.5) = \rho(N, z = H - 0.5)$, a consequence of an exact statistical mechanical sum rule for this system [39]. Finally, the molar excess entropy $s^{\text{ex}} = S^{\text{ex}}/N$ is determined using the following expression [32, 73],

$$\begin{aligned} S^{\text{ex}}(N) &= \ln[\Pi(N)/\Pi(0)] - N \ln \xi + \ln N! \\ &\quad - N \ln N + \int \rho(N, \mathbf{r}) \ln \rho(N, \mathbf{r}) d\mathbf{r}. \end{aligned} \quad (3.2)$$

Below, we describe how the above methods were employed in this study to characterize the behaviors of the confined and bulk HS fluids.

3.3 Results and Discussion

3.3.1 Volume definition and the equation of state

One of the most practically important and well-understood properties of the bulk, equilibrium HS fluid is its equation of state $P(\rho)$, which quantifies how its pressure varies with density. For densities below the freezing transition, this relationship is accurately described by the semi-empirical Carnahan-Starling equation $P(\rho) \approx P_{\text{CS}}(\rho) = \rho(1 + \phi + \phi^2 - \phi^3)/(1 - \phi)^3$ [18], where $\phi = \pi\rho/6$ is the packing fraction of the spheres.

Much less is known about the global behavior of the pressure tensor for the HS fluid confined between smooth hard walls. One obvious question is, do the relationships between the transverse and normal components of the pressure tensor and “average” density (defined as either ρ or ρ_h) show quantitative similarities to the equation of state of the bulk fluid? Although the inhomogeneous structuring of the fluid might be expected to give rise to some nontrivial deviations from bulk fluid behavior, the main qualitative trends should be the same: compressing the fluid increases the interparticle collision rate and, consequently, the individual components of the pressure tensor.

In Fig. 3.1, we compare the bulk fluid equation of state to our GC-TMMC simulation data for the average transverse and normal components of

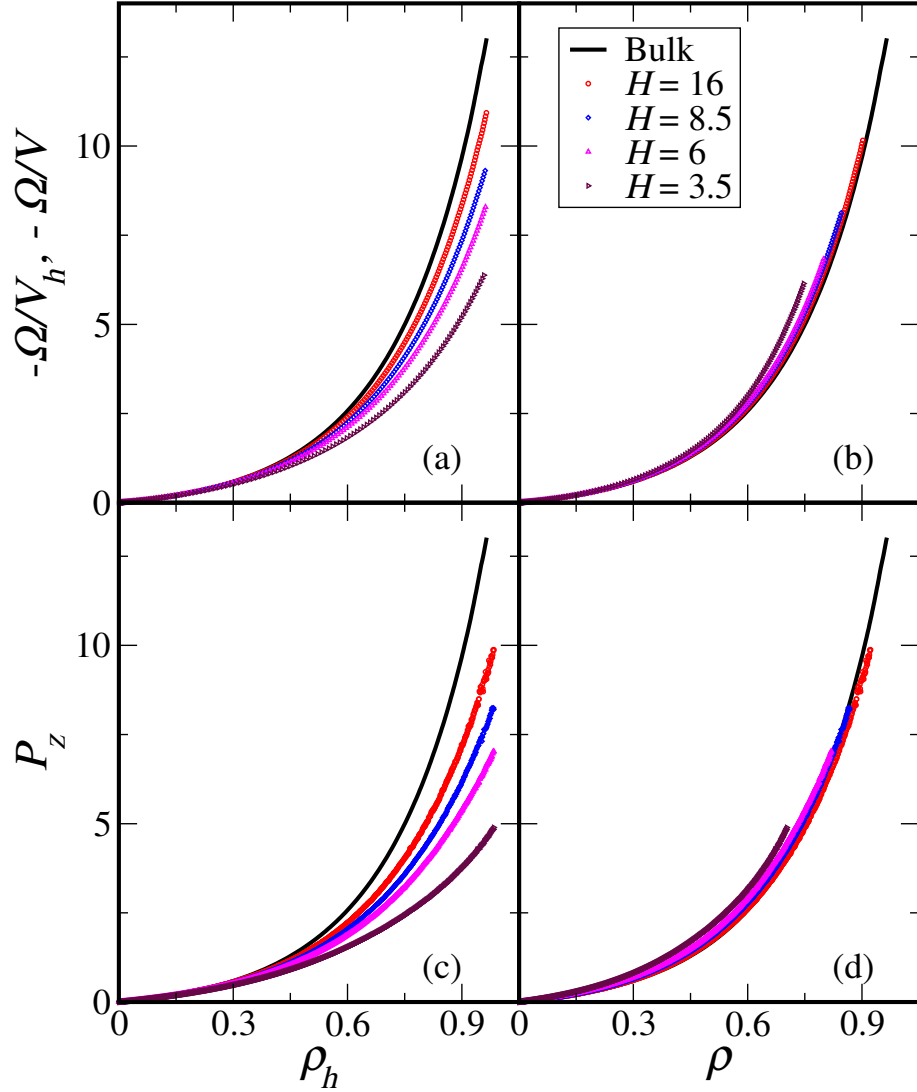


Figure 3.1: Equation of state of a confined HS fluid between hard walls separated by center-accessible distance $H - 1$. Top panels show the negative of the grand potential density (average transverse pressure) versus average fluid density calculated using (a) the center-accessible volume V_h and (b) the total volume V . Bottom panels illustrate the normal pressure versus average density calculated using (c) the center-accessible volume V_h and (d) the total volume V .

the pressure tensor. We focus here on confined fluids with $H = 3.5, 6, 8.5,$ and 16 . In top panels (a) and (b), negative grand potential density is plotted versus average density, adopting the V_h (center accessible) and V (total) volume conventions, respectively. The density dependencies of P_z are similarly displayed in panels (c) and (d). Focusing on plots (a) and (c), one finds a family of curves for $-\Omega/V_h$ and P_z that are qualitatively similar to the bulk fluid behavior, with the main difference being that systems with smaller H have weaker ρ_h dependencies (higher apparent compressibilities). This difference appears logically consistent with the earlier observation [73] that confined HS fluids also have faster single-particle dynamics as compared to the corresponding bulk fluid with the same ρ_h .

Interestingly, the corresponding quantities plotted in (b) and (d) using the total volume V convention approximately collapse onto a single curve. This means that the ρ dependencies of both $-\Omega/V$ and P_z , for each value of H investigated, can approximately be described by the equation of state of the bulk fluid $P(\rho)$. This trend also appears consistent with the approximate collapse of self-diffusivities for confined HS fluids onto the bulk behavior when plotted together on a single graph versus ρ [73]. Although there are clearly some quantitative deviations from bulk behavior for the smallest pores in panels (b) and (d) of Fig. 3.1, we found that the following simple relationship can describe the ρ dependence of the grand potential density to within at least 25% for $H \geq 3.5$:

$$\Omega(\rho, H)/V \approx -P_{\text{CS}}(\rho). \quad (3.3)$$

We will use this approximate relationship below to help construct an analytical model for predicting the excess adsorption of fluid in a model slit pore.

3.3.2 Interfacial free energy and excess adsorption

Given the approximate collapse of the thermodynamic data for the confined HS fluid when plotted against average density ρ , it is natural to ask whether there is a connection to the behavior of the interfacial free energy and the surface excess adsorption of the fluid at a single hard wall.

The interfacial free energy of the HS fluid near a hard wall is defined as the excess grand potential of the fluid (relative to bulk) per unit fluid-wall contact area. Similar to average density, its numerical value depends on the choice of dividing surface [16, 47]. If one chooses the plane of closest approach of the particle centers to the wall as the dividing surface, then the following expression yields the interfacial free energy:

$$\gamma_h^\infty = \lim_{H \rightarrow \infty} \left[\frac{\Omega(\rho, H)}{V_h} + P_b \right] \frac{(H-1)}{2}, \quad (3.4)$$

where P_b is the pressure of the bulk fluid in equilibrium with the pore fluid. Stated differently, ρ of the pore fluid is determined by H and the requirement that it adopt the same activity ξ as the bulk HS fluid of pressure P_b . There is an accurate approximate equation due to Henderson and Plischke [46] for predicting how γ_h^∞ depends on the packing fraction of the bulk fluid $\phi_b = \pi\rho_b/6$,

$$\gamma_h^\infty \approx -\frac{9}{2\pi}\phi_b^2 \frac{[1 + (44/35)\phi_b - (4/5)\phi_b^2]}{(1 - \phi_b)^3}. \quad (3.5)$$

If one instead chooses the physical surface of the wall to be the dividing surface, then a slightly different equation emerges:

$$\gamma^\infty = \lim_{H \rightarrow \infty} \left[\frac{\Omega(\rho, H)}{V} + P_b \right] \frac{H}{2} \quad (3.6)$$

$$= \gamma_h^\infty + P_b/2 \quad (3.7)$$

Substituting the Carnahan-Starling equation of state for P_b and Eq. 3.5 for γ_h^∞ into Eq. 3.7 results in the following analytical estimate for γ^∞ ,

$$\gamma^\infty \approx \frac{3}{\pi} \phi_b \frac{[1 - (1/2)\phi_b - (31/35)\phi_b^2 + (1/5)\phi_b^3]}{(1 - \phi_b)^3} \quad (3.8)$$

Given that we have already observed that other properties of the confined HS fluid approximately collapse when plotted versus ρ (based on total volume V), we choose to focus from this point forward on γ^∞ , the interfacial free energy that is also based on V .

As we demonstrated in the previous section, one can readily determine the quantities on the right-hand side of Eq. 3.6 for finite values of H using GC-TMMC simulations. As a result, these simulations might also provide a reasonably accurate means for estimating γ^∞ , assuming that H can be chosen large enough so that the perturbations to the fluid caused by the two confining walls do not significantly interfere with one another (i.e., so that so-called “finite-size” or frustration effects of confinement do not occur). Although, it is not clear *a priori* how large H must be to achieve this, one might reasonably expect that the pore would need to be at least several particle diameters in width.

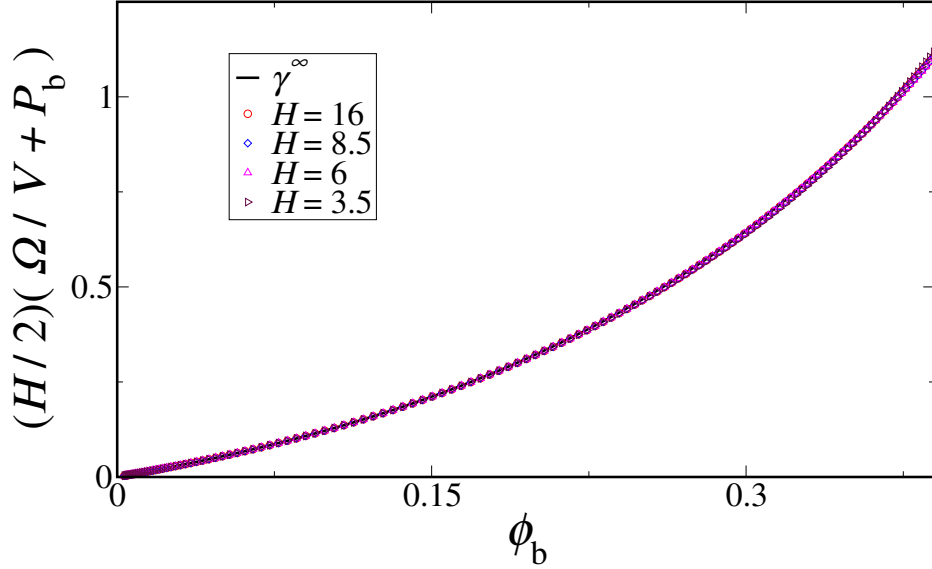


Figure 3.2: The quantity $(H/2) [\Omega/V + P_b]$ calculated from our GC-TMMC simulations for various H along with the $H \rightarrow \infty$ limit, γ^∞ , computed using Eq. 3.8. Data are plotted as a function of ϕ_b , the packing fraction of the bulk HS fluid that is in equilibrium with the pore fluid.

As a test of this idea, we present in Fig. 3.2 values of the quantity $[\Omega(\rho, H)/V + P_b] (H/2)$ calculated from our GC-TMMC simulations for various H along with the single-wall quantity γ^∞ of Eq. 3.8, which is the $H \rightarrow \infty$ limit. All data are plotted as a function of bulk packing fraction ϕ_b . Interestingly, the plot reveals that the simulated curves for $H \geq 3.5$ all collapse, to within an excellent approximation, onto that for γ^∞ . In other words,

$$\gamma^\infty \approx \left[\frac{\Omega(\rho, H)}{V} + P_b \right] \frac{H}{2} \quad (3.9)$$

independent of H for $H \geq 3.5$. This implies that single-wall behavior such as γ^∞ can be estimated with great accuracy in this system from a simulated slit-

pore of width $H = 3.5$, which can only accomodate a fluid film three particle layers thick. This result, while very robust, is somewhat surprising because the single-wall density profiles decay slowly enough to expect appreciable interference or frustration effects at pore sizes as small as $H = 3.5$. However, similar to the picture that emerged from the behavior of the equation of state in the previous section, any interference that does occur apparently cancels in determining the average properties of the confined HS fluid, which remain remarkably “bulk-like” even for these very thin films.

So, when do interference effects due to packing frustration of the wall-induced particle layers begin to occur? We can probe this issue by taking the analysis one step further. Specifically, if one uses Eq. 3.3 to substitute for $\Omega(\rho, H)/V$ in Eq. 3.9, differentiates both sides of Eq. 3.9 with respect to chemical potential, and invokes the Gibbs adsorption equation $\partial\gamma^\infty/\partial\mu = -\Gamma^\infty$, then upon rearranging one arrives at the following simple equation for predicting the pore density ρ :

$$\rho \approx \rho_b + \frac{2\Gamma^\infty}{H} \quad (3.10)$$

The quantity Γ^∞ is the standard surface excess density for a HS fluid next a to *single* hard wall, and, within the above approximations, it is given by

$$\Gamma^\infty = -\frac{3\phi_b [1 + a_1\phi_b + a_2\phi_b^2 + a_3\phi_b^3 + a_4\phi_b^4]}{\pi(1 + 4\phi_b + 4\phi_b^2 - 4\phi_b^3 + \phi_b^4)}, \quad (3.11)$$

where $a_1 = 1$, $a_2 = -221/70$, $a_3 = 4/5$, and $a_4 = -1/5$.

Fig. 3.3 shows the predictions of the simple analytical model of Eq. 3.10 and 3.11 compared to the simulated pore density ρ as a function of H . From

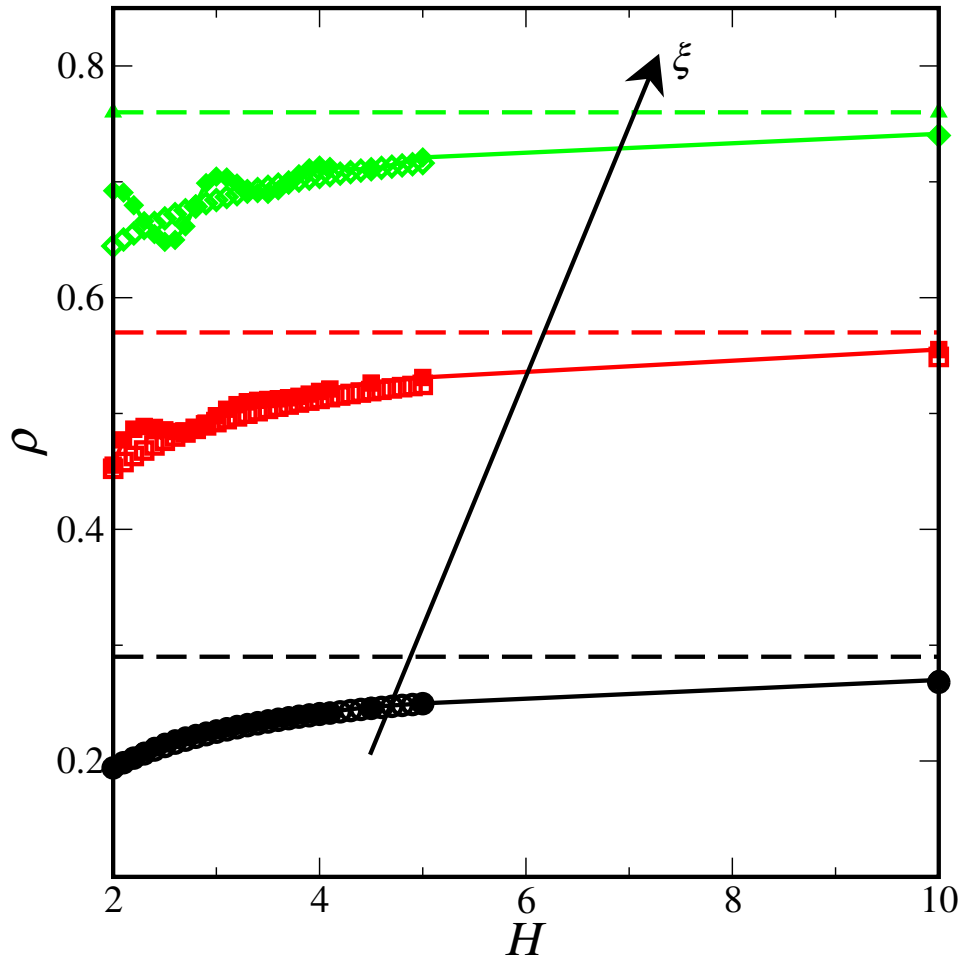


Figure 3.3: Pore fluid density ρ as a function of pore width H at different values of activity [$\ln \xi = 0.4, 4.4, \text{ and } 8.8$]. Filled and open symbols correspond to the GC-TMMC data and the predictions of Eq. 3.10, respectively. The dashed lines correspond to the bulk density ρ_b for a given activity ξ .

the plot, it is evident that the average pore density can be predicted based on knowledge of only the single-wall surface excess Γ^∞ unless the fluid is *both* dense *and* confined to pores narrower than approximately three particle diameters. Under those restrictive conditions, the single-wall model misses the emergence of oscillations in the pore density. These oscillations cannot be solely attributed to single-wall “layering” in the density profile because pronounced layering also occurs for dense fluids with $H \gg 3$, where the analytical model is still very accurate. Rather, the oscillations must be due to packing frustration associated with the interference of the layers emerging from the two confining walls, which apparently becomes significant in this system only for very narrow pores and high fluid density.

3.3.3 Comparing bulk and pore fluid self-diffusivities

The last two sections demonstrated that some of the average thermodynamic properties of the confined HS fluid are very similar to those of the bulk fluid if the two systems are compared at equal values of the average density ρ (based on the total system volume). Deviations occur only when the fluid is both dense and confined to pores narrower than approximately three particle diameters. In the previous chapter, we have also shown that the self-diffusivity D of the confined HS fluid is approximately equal to that of the bulk fluid with the same ρ for $H > 3.5$ over a fairly broad range of ρ . Here, we carefully investigate the H -dependency of pore self-diffusivity at constant ρ for narrow pores, with a focus on understanding when packing frustration

causes the correlation between D and ρ to break down. We also investigate the H -dependency of D for the confined fluid under the constraint of constant imposed activity ξ . We find that this latter behavior can be essentially predicted in advance, given the known connection between D and ρ [73] and the ability to predict ρ from ξ and H discussed in the previous section.

We begin here by examining how H affects D at constant ρ using the DMD simulations described earlier. Specifically, we plot in Fig. 3.4 the self-diffusivity D of the bulk and confined HS fluid for $H = 2$ to 5 and various pore packing fractions ($\phi \equiv \pi\rho/6 = 0.15, 0.30, 0.40,$ and 0.45). What is plainly evident is that up to fairly dense packing fractions ($\phi < 0.40$), D of the confined fluid shows no significant deviations from bulk behavior (dashed line) even when in very restrictive pores (e.g. $H = 2$). In fact, quantitative deviations are prominent ($> 25\%$) only in the high density ($\phi \geq 0.4$) and small pore ($H < 3$) limit. Note that an equilibrium fluid at $\phi = 0.45$ cannot be accessed over the full H range because the system penetrates into the fluid-solid coexistence region or the solid phase region on its phase diagram [40].

To gain a more physical understanding of the variations in D at constant ϕ that occur under conditions of high ϕ and low H , we plot in Fig. 3.5 the 2D projections of instantaneous particle configurations of the confined HS fluid for $H = 2.0, 2.4,$ and 3.0 at $\phi = 0.40$, state points that show very different dynamical behaviors. We also present the corresponding density profiles $\rho(z)$ normal to the walls. This figure shows well-developed layering structures for both $H = 2.0$ (two particle layers) and $H = 3.0$ (three particle layers).

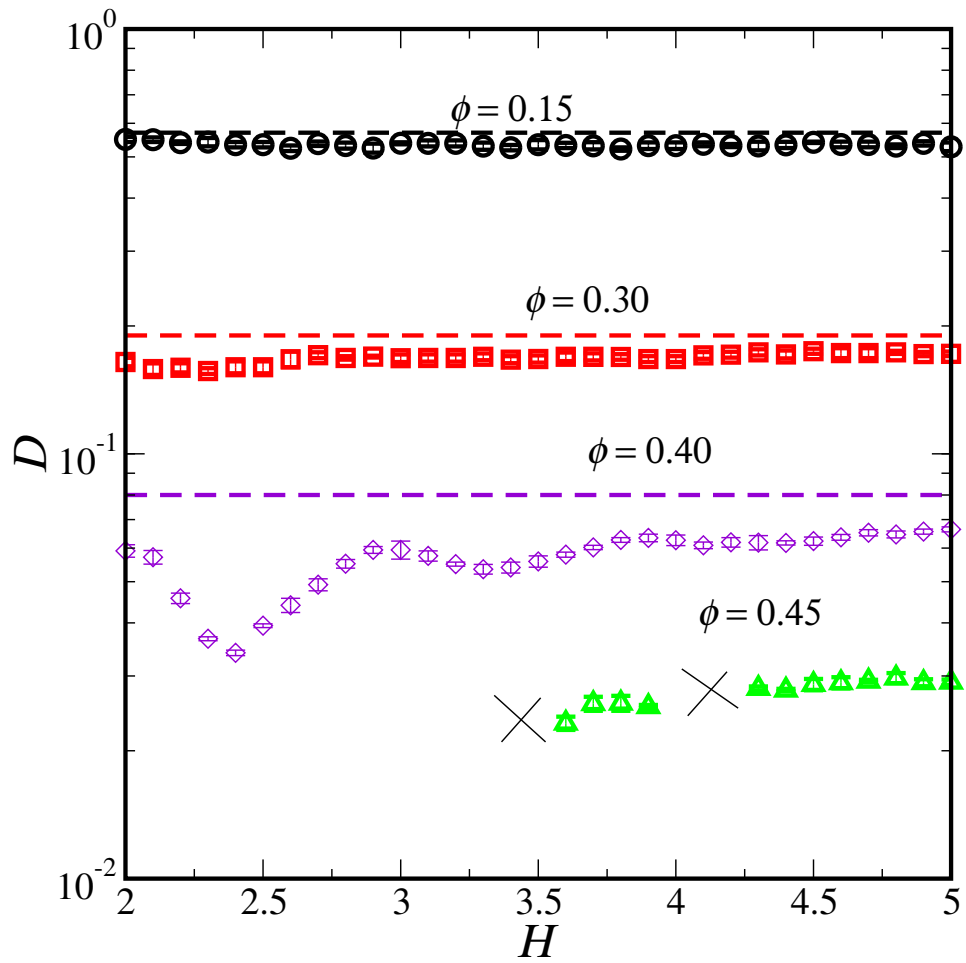


Figure 3.4: Self-diffusivity D as a function of pore width H at different pore fluid packing fractions ϕ . For $\phi = 0.45$, crosses mark regions for which the confined system penetrates into the fluid-solid coexistence region or the solid phase region on its equilibrium phase diagram [40].

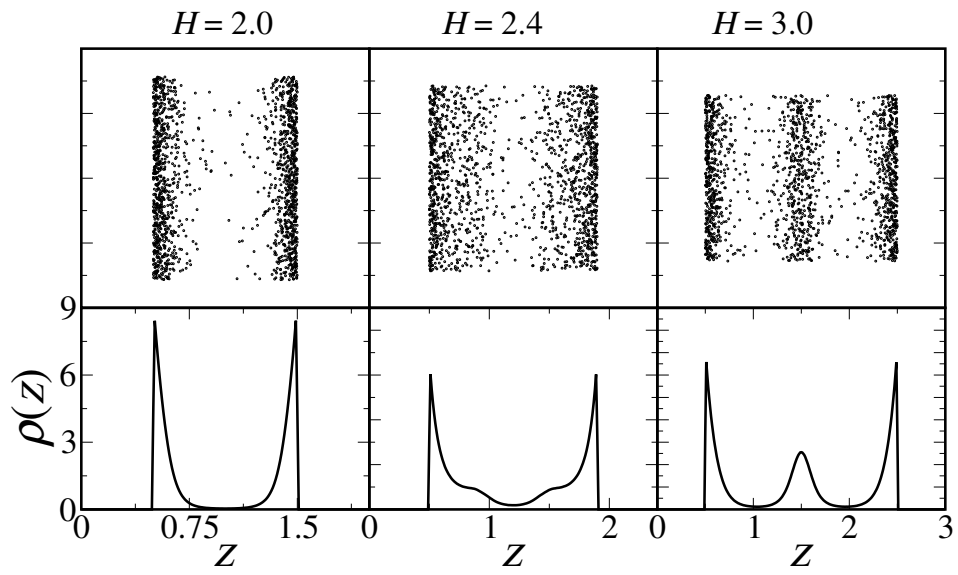


Figure 3.5: 2D projections of typical instantaneous particle configurations of the confined HS fluid are shown (top) along with equilibrium density profiles $\rho(z)$ (bottom), where z represents the positional coordinate normal to the walls.

However, the system at $H = 2.4$ shows considerably more packing frustration. In particular, the individual density peaks are reduced in this case because the spacing is such that it is “in between” distances that naturally accommodate either two or three layers. The pore diffusivity is also lowest for $\phi = 0.4$ at $H = 2.4$ as shown in Fig. 3.4. Similar oscillations in D , which are much smaller in magnitude and decay with increasing H , occur at larger separations with the minima again coinciding with spacings that do not naturally accommodate an integer number of particle layers. In short, for small enough pores and high enough densities, the frustrated layering of particles normal to the confining walls significantly slows down the single-particle dynamics in the direction parallel to the walls.

The trend that increased layering leads to faster dynamics may initially appear counter-intuitive, especially if one tries to understand it by drawing an analogy with the bulk HS system. In the bulk HS system, compressing the fluid increases the structural ordering [112, 113] but *reduces* the self-diffusivity. In contrast, as can be clearly seen in Fig. 3.4 and 3.5, increased layering in the normal direction (i.e., less uniform density profiles) correlates with faster dynamics. However, these two represent fundamentally different systems undergoing different changes. In the bulk HS system, increasing the density not only increases the structural order, but it also reduces the entropy (or average free volume) of the particles in the fluid. This compression-induced reduction in free volume is not surprisingly correlated with slower dynamics. However, the confined HS system actually maximizes its entropy (or average free vol-

ume) at fixed average density and H by adopting an inhomogeneous density profile with pronounced layering [59]. Our results show that, for constant ρ , the values of (small) H that frustrate the ability of the system to form an integral number of particle layers also tend to reduce the single-particle mobility in the direction parallel to the walls. We return to investigate the potential connection between dynamics and entropy of the confined HS fluid in the next section.

Another important point concerning the frustration-induced oscillations in D of Fig. 3.4 is that they are distinct from the oscillations in D that occur as a function of H at constant activity ξ [67, 117]. The latter are inevitably impacted by oscillations in average pore density, whereas the average density is being controlled for (held constant) in Fig. 3.4. Deviations from bulk behavior at fixed average density are purely frustration-induced *finite-size effects*, and the relative importance of these types of deviations has been a long-standing question in the study of confined fluids [2].

Interestingly, if one compares the locations of the oscillations in D versus H at $\phi = 0.40$ in Fig. 3.4 with the fluid-solid phase boundary of this system presented in Fig. 2 of Ref. [40], one also finds a strong correlation between slow dynamics and proximity of the fluid to the phase boundary. In other words, the same packing frustration that is giving rise to slow dynamics also appears to ultimately promote the formation of an ordered solid phase. This argues that the effect of confinement on the phase diagram of the system can provide important insights into how confinement impacts single-particle

dynamics. The consequences of this could be significant for the strategies that are typically employed to study supercooled and confined liquids. For example, weak polydispersity is commonly incorporated into model fluid systems in order to study them under conditions where the corresponding monatomic fluid would rapidly crystallize. A cautionary note that follows from the above discussion is that one should not readily assume that the behaviors of the polydisperse and monatomic systems are trivially related, and that the former only differs from the latter in that its liquid state is kinetically accessible over a broader range of conditions. The phase diagrams of polydisperse materials are considerably more complex than monatomic systems (even in the bulk [105]). Thus, one should expect confinement to impact the dynamics of polydisperse systems in ways that are not easily relatable to the behavior of the corresponding monatomic fluids.

We now turn our attention to the H -dependent diffusivity behavior of the confined HS fluid at fixed activity ξ (i.e., in chemical equilibrium with the bulk). As can be ascertained from the strong correspondence between D and ρ in Fig. 3.4, the dynamical behavior at constant ξ can be largely predicted in advance if one simply has knowledge of how H influences ρ at constant ξ (e.g., from simulation or the analytical model of Eq. 3.10 and 3.11). In Fig. 3.6, we provide the H -dependent data along constant ξ paths for the quantities ρ and D determined from GC-TMMC and DMD simulations, respectively. One initial observation is that ρ is always less than ρ_b for finite H , and, as should be expected based on this, D is larger in the pores than in the equilibrium bulk

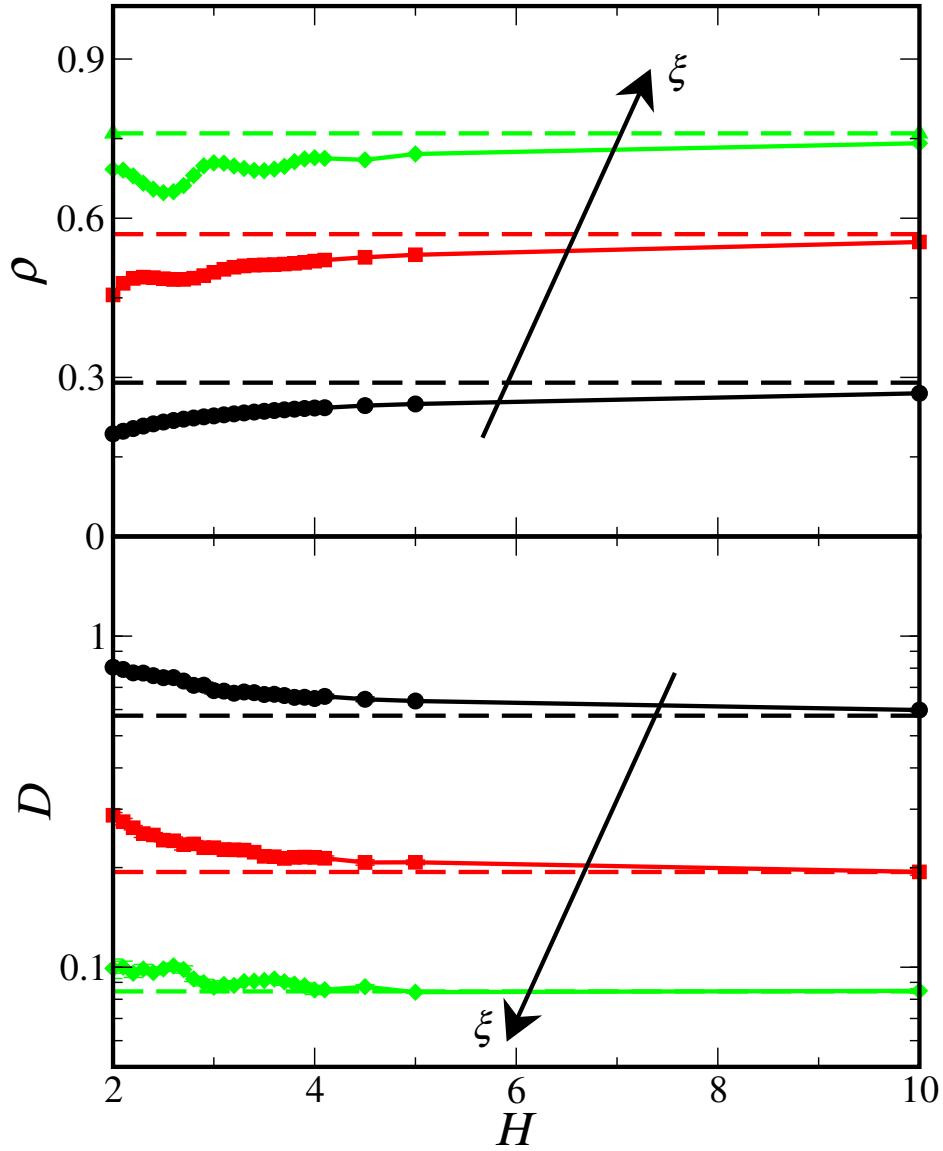


Figure 3.6: Average density ρ and self-diffusivity D as a function of pore size H for the confined HS fluid in equilibrium with the bulk HS fluid at a given activity ξ [$\ln \xi = 0.4, 4.4, \text{ and } 8.8$]. Dashed lines correspond to the density ρ_b and self-diffusivity D of the bulk HS fluid at the given activity ξ .

fluid. Note that this type of physically-intuitive connection between average density and dynamics would be completely lost, however, if one instead chooses ρ_h as the definition for average density, which is significantly greater than ρ_b for finite H . More generally, the reliability of approximate theories for transport properties in inhomogeneous fluids could be particularly sensitive to how averaging is handled, which might help to explain why an earlier kinetic theory [117] predicts that confining a fluid at constant ξ significantly decreases D , the opposite of what is seen in the MD simulation data of Fig. 3.6.

A second observation about the data in Fig. 3.6 is that there are negative oscillatory deviations in ρ (relative to bulk) with H at high ξ in small pores, which one might expect to produce similar positive oscillations in D . However, the frustration-induced negative deviations from bulk behavior in the D versus H relationship at constant ρ shown in Fig. 3.4 appear to largely cancel this effect. The net result is that D is strikingly similar to bulk behavior, even for small H , along paths of constant (and sufficiently high) ξ .

3.3.4 Diffusivity and excess entropy

The oscillatory data in Fig. 3.4 clearly show that average density alone cannot predict the self-diffusivity of the HS fluid if the fluid is both dense and confined to a pore smaller than approximately three diameters. Is there another thermodynamic quantity that can predict diffusivity behavior in these narrow pores? One promising candidate is the excess entropy s^{ex} (relative to ideal gas), which Chapter 2 results demonstrate, to an excellent approximation,

determines the self-diffusivity of the HS fluid confined between hard walls for $H > 3.5$. Here, we explore its relationship to self-diffusivity in smaller pores.

Fig 3.7 shows the data for D and s^{ex} of the confined fluid collected from our DMD and GC-TMMC simulations [data at fixed pore packing fraction ϕ provided in panels (a) and (c), and data at fixed activity ξ provided in (b) and (d)]. Irrespective of the thermodynamic path, strong qualitative correspondence is observed between D and s^{ex} , including the “in-phase” oscillations that emerge at small H . In other words, self-diffusivity and excess entropy appear to be affected in a very similar way by confinement, even for the very narrow pores.

To scrutinize the quantitative accuracy of the relation between the two variables, we also plot all data corresponding to constant pore packing fraction ϕ (filled symbols) and constant ξ (empty symbols) paths in Fig 3.8 in the D - s^{ex} plane. As can be seen, most of the data falls very close the curve for the bulk HS fluid, indicating that excess entropy (a static quantity) can indeed approximately predict the implications of confinement for self-diffusivity. The largest deviations are for the fluid that has the highest pore packing fraction of $\phi = 0.4$.

This data is yet one more manifestation of a larger trend seen throughout this chapter. Namely, that the confined HS fluid, by measure of many of its average properties, has behavior very similar to that of the bulk fluid. It changes character only under a fairly restrictive set of conditions, when the pore fluid is dense ($\phi \geq 0.4$) and when it is confined to pores smaller than

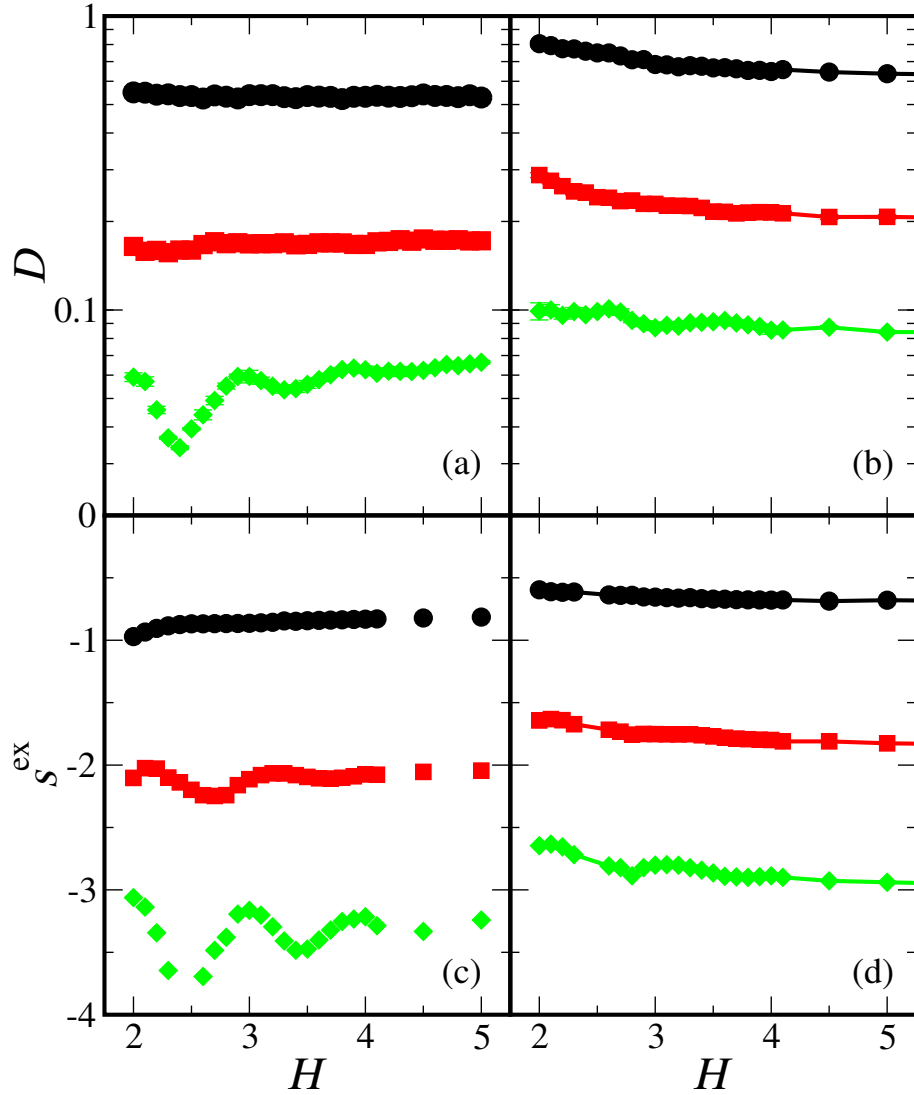


Figure 3.7: (a) Self-diffusivity D and (b) excess entropy s^{ex} as a function of pore size H for the confined HS fluid at a given pore packing fraction $\phi = \pi\rho/6$. Data from top to bottom correspond to $\phi = 0.15, 0.3, \text{ and } 0.4$. (c) Self-diffusivity D and (d) excess entropy s^{ex} as a function of pore size H for the confined HS fluid at a given activity ξ . Data from top to bottom correspond to $\ln \xi = 0.4, 4.4, \text{ and } 8.8$.

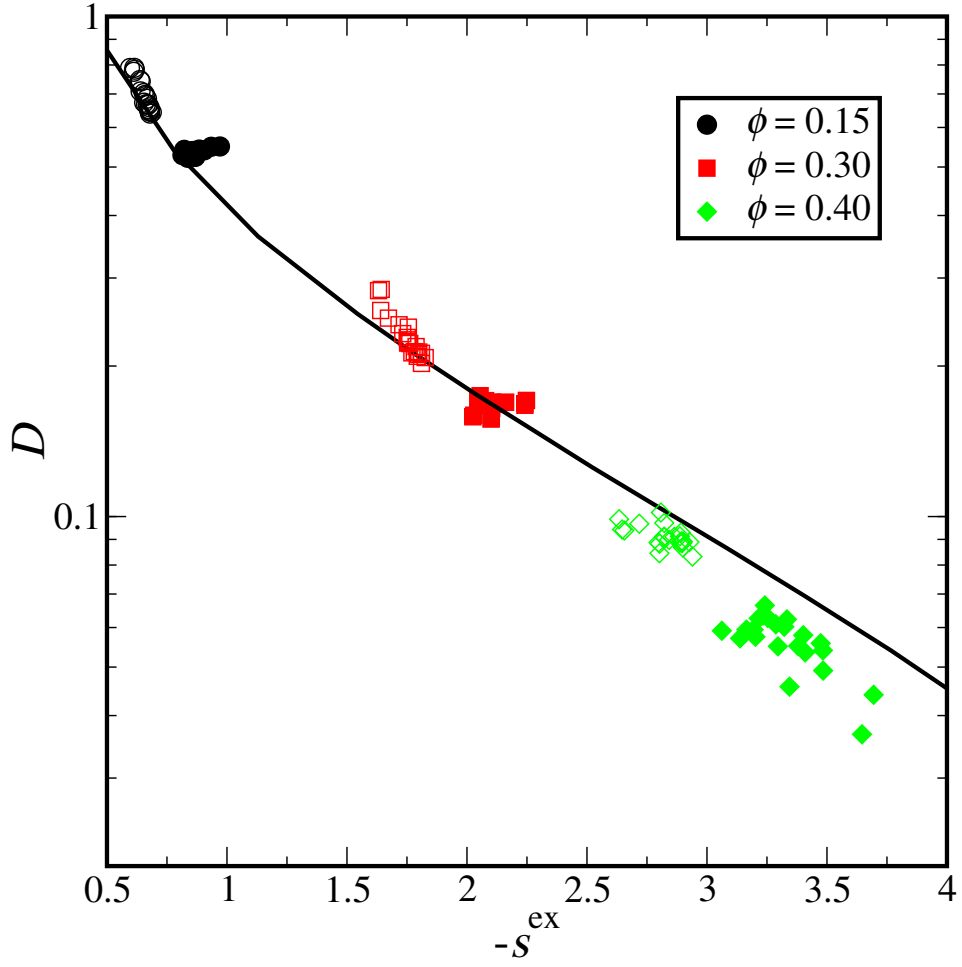


Figure 3.8: Self-diffusivity D vs negative excess entropy per particle $-s^{\text{ex}}$ for the bulk HS fluid (solid curve) and for the HS fluid confined between smooth hard walls (symbols). The filled symbols correspond to the confined system at a fixed pore packing fraction ϕ as shown on the legend and empty symbols are for system at a given activity ξ for which bulk packing fraction is given on the legend.

approximately three particle diameters in width.

3.4 Conclusions

In conclusion, we have presented new comprehensive simulation results for the HS fluid confined between smooth hard walls. The results elucidate thermodynamic and dynamic behavior of this system over a wide range of system conditions, further clarifying the precise role of confinement on average fluid properties and the most useful way to define average density for this system. One perhaps unexpected result is that, for most conditions, the average behavior of the confined HS fluid is very similar to that the bulk fluid. Frustration-induced finite effects do emerge in this system, but they are only prominent for very small pores (dimensions smaller than approximately three particle diameters) and high fluid densities where the system approaches the confinement-shifted fluid-solid phase boundary.

Chapter 4

Self-diffusivity, packing fraction and excess entropy of simple bulk and confined fluids

4.1 Introduction

Perturbation theories [9, 45, 57, 68, 91, 118, 121] are successful in predicting thermodynamic properties of dense, simple liquids because the pair-wise structuring in those systems is primarily determined by the short-range (approximately hard-core) repulsive interactions between the particles [19]. However, does the ability to approximate the structure of a simple liquid by an effective hard-sphere (HS) reference fluid also have implications for understanding its single-particle dynamics? More specifically, should one expect the self-diffusivity, D , of an atomic liquid to be approximately equal to that of a HS fluid if compared at the same effective packing fraction? This intuitive line of thinking appears promising, especially when one considers that diffusion is intimately connected to interatomic “collisions”, which are in turn linked to pair-wise structural correlations. In fact, ideas such as these have already led to the development of a theoretical approach for predicting the dynamics of a repulsive soft-sphere fluid [92]. Unfortunately, a number of attempts to further extend this type of conceptual framework to compute D of the Lennard-Jones (LJ) fluid have only been able to achieve qualitative agreement with simulation

data [50, 62, 106, 109]. In addition, adjustments made to improve upon these approaches have ultimately relied on semi-empirical corrections to account for the presence of the attractive interactions [65, 106]. All of this would appear to imply that attractions may have an effect on the single-particle dynamics that is more subtle than one might surmise based on their approximately “mean-field” contribution to the free energy.

On the other hand, it has been independently demonstrated that the self-diffusivity of several simple liquids, when cast in an appropriately reduced form, show an approximate scaling with s^{ex} , the excess entropy per particle of the fluid (relative to an ideal gas with the same number density) [26, 86, 87]. Interestingly, excess entropy can also be used as a tool for predicting how confinement modifies the single-particle dynamics of equilibrium fluids. In particular, we showed in Chapter 2 and 3 via molecular simulation that while confining the equilibrium HS fluid generally changes both its excess entropy and self-diffusivity, the relationship between the two remains, to an excellent approximation, unaltered. Since classical density functional theories for inhomogeneous fluids can be used to accurately estimate how confinement impacts the excess entropy, the existence of this “master curve” for excess entropy and self-diffusivity has potentially broad implications for using thermodynamics to predict the dynamics of confined fluids. One of the main open questions raised in previous chapters is whether these observations apply more generally to other simple liquid systems with attractive interactions.

Here, we report results from extensive grand canonical transition matrix

Monte Carlo and molecular dynamics simulations, which are used to explore some basic questions regarding the thermodynamic and dynamic behaviors of such simple fluids with attractive interactions. Our main focus is elucidating the various connections between the excess entropy, the effective packing fraction, and the self-diffusivity of LJ and SW fluid systems in both bulk and confined environments.

4.2 Model Systems and Simulation Methods

In order to simplify the notation, we implicitly non-dimensionalize all quantities by appropriate combinations of the characteristic energy scale ϵ and length scale σ corresponding to the strength of the interparticle attraction and the particle diameter, respectively, in the pair potentials of the aforementioned fluids. For example, all temperatures are implicitly per unit ϵ/k_B , energies per unit ϵ , entropies per unit k_B , densities per unit σ^{-3} , self-diffusivities per unit $\sqrt{\epsilon\sigma^2/m}$, and so forth.

In the case of the LJ system, we describe the interactions between fluid particles with a truncated and quadratically-shifted version of the pair potential for which the energy and force go continuously to zero at an interparticle separation r equal to the cut-off distance, $r = r_c$. The form of the potential is given by [108],

$$\mathcal{V}(r) = 4 \left\{ r^{-12} - r^{-6} + [6r_c^{-12} - 3r_c^{-6}] \left(\frac{r}{r_c} \right)^2 - 7r_c^{-12} + 4r_c^{-6} \right\}. \quad (4.1)$$

In this work, we set $r_c = 2.5$. For the confined LJ fluid, we consider parallel

boundary walls that interact with fluid particles via the following external field,

$$\mathcal{V}_{\text{fw}}(z) = \mathcal{V}_{9-3}(z) + \mathcal{V}_{9-3}(H_z - z) \quad (4.2)$$

where H_z is the particle center-accessible separation between the confining walls ($0 < z < H_z$) and the single-wall “9-3” potential is given by

$$\mathcal{V}_{9-3}(z) = \epsilon_{\text{fw}} \left[\frac{2}{15} \left(\frac{\sigma_{\text{fw}}}{z} \right)^9 - \left(\frac{\sigma_{\text{fw}}}{z} \right)^3 \right]. \quad (4.3)$$

Here, we set $\sigma_{\text{fw}} = 1$ for all cases, and we investigate the system for different values of ϵ_{fw} ($\epsilon_{\text{fw}} > 0$ for attractive walls). Because the fluid-wall repulsions are steep in this potential, there will be finite regions near the walls that will not be populated by the particle centers with any statistical significance at finite temperature. We will return to this issue later in our discussion of the role that the effective packing fraction of the confined fluid plays in determining its average dynamic behavior.

The particles in the SW fluid that we explore interact with one another via the following pair potential,

$$\begin{aligned} \mathcal{V}(r) &= \infty & r < 1 \\ &= -1 & 1 \leq r < \lambda \\ &= 0 & r \geq \lambda, \end{aligned} \quad (4.4)$$

and we take $\lambda = 1.5$. For the confined SW fluid, we also consider parallel boundary walls that interact with fluid particles via the following SW potential,

$$\mathcal{V}_{\text{fw}}(z) = \mathcal{V}_{\text{SW}}(z) + \mathcal{V}_{\text{SW}}(H_z - z), \quad (4.5)$$

where $\mathcal{V}_{\text{SW}}(z)$ is given by

$$\begin{aligned}
\mathcal{V}_{\text{SW}}(z) &= \infty & z < 0 \\
&= -\epsilon_{\text{fw}} & 0 \leq z < (\lambda_{\text{fw}} - 1)\sigma_{\text{fw}} \\
&= 0 & z \geq (\lambda_{\text{fw}} - 1)\sigma_{\text{fw}}.
\end{aligned} \tag{4.6}$$

As with the “9-3” wall potential, we set $\sigma_{\text{fw}} = 1$ for all cases, and we simulate the system for different values of ϵ_{fw} ($\epsilon_{\text{fw}} > 0$ for attractive walls and $\epsilon_{\text{fw}} < 0$ for repulsive walls). Most of the confined systems that we investigate have $\lambda_{\text{fw}} = 1.5$, but we also study a few systems with a shorter range fluid-wall interaction ($\lambda_{\text{fw}} = 1.1$).

To monitor kinetic processes in the LJ fluid, we performed molecular dynamics simulations of $N = 1500$ particles in the microcanonical ensemble using the velocity Verlet algorithm [3]. We analyzed the dynamics of the the HS and SW fluids using $N = 4500$ and $N = 1000$ particles, respectively, in the microcanonical ensemble via discontinuous (event-driven) molecular dynamics simulations [82]. Periodic boundary conditions were employed in all three directions (x , y , and z) for the bulk fluid simulations and in the two “macroscopic” directions (x and y) for the simulations of the confined fluid films. Self diffusion coefficients, D , were extracted by fitting the long-time ($t \gg 1$) behavior of the average mean-squared displacement $\Delta \mathbf{r}_d^2$ of the particles in the d periodic directions to the Einstein relation $\langle \Delta \mathbf{r}_d^2 \rangle = 2dDt$.

The excess entropy per particle s^{ex} for each of these models was obtained using grand-canonical transition-matrix Monte Carlo (GC-TMMC) sim-

ulations [33]. In general, s^{ex} is defined to be the difference between the entropy per particle of the fluid and that of an ideal gas with the same spatial distribution of the particle number density. GC-TMMC simulations require fixed values of the activity ξ , particle center-accessible volume of the simulation cell V_h , and temperature T as inputs. The activity is defined as $\xi = \exp(\mu T^{-1})\Lambda^{-3}$, where μ is the chemical potential and Λ is the thermal de Broglie wavelength. For all GC-TMMC simulations employed here, we set $V_h = 1000$ and $\xi = 1$, and we investigated the system as a function of temperature T . Thermodynamic properties at other values of activity ξ were readily obtained via the histogram reweighting technique [38].

The key quantities extracted from the GC-TMMC simulations were the total particle number probability distribution $\Pi(N)$, and the particle-number-specific spatial density distribution $\rho(N, \mathbf{r})$, and the excess configurational energy $U^{\text{ex}}(N)$, each evaluated over a range of particle numbers to span the required density values. Using basic arguments from the statistical mechanics [21, 79], one can relate these quantities to the excess entropy per particle $s^{\text{ex}} = S^{\text{ex}}/N$, which can be determined from the following relation [32, 72],

$$S^{\text{ex}}(N) = U^{\text{ex}}(N)/T + \ln[\Pi(N)/\Pi(0)] - N \ln \xi + \ln N! - N \ln N + \int \rho(N, \mathbf{r}) \ln \rho(N, \mathbf{r}) d\mathbf{r}. \quad (4.7)$$

Given that V_h is fixed, Eq. 4.7 readily provides information for how excess entropy is related to average density or packing fraction, a subject that we will return to in the next section.

4.3 Results and discussion

4.3.1 Effective packing fraction and self-diffusivity: Bulk fluids

The determination of the effective packing fraction $\phi_{\text{eff}}(T, \rho)$ of a bulk fluid usually involves two steps. The first step is the separation of the intermolecular potential of the fluid into a repulsive, $\mathcal{V}_0(r)$, and a perturbation, $\mathcal{V}_1(r)$, contribution [i.e., $\mathcal{V}(r) = \mathcal{V}_0(r) + \mathcal{V}_1(r)$]. Here, we invoke the well-known WCA method [19] for achieving this decomposition. The second step is the determination of an effective HS diameter $\sigma_{\text{HS}}(T, \rho)$ for the particles of the bulk fluid [9, 11, 19], which is ultimately used to determine $\phi_{\text{eff}}(T, \rho) = \pi\rho\sigma_{\text{HS}}^3(T, \rho)/6$. Perturbation theories have traditionally approached the calculation of $\sigma_{\text{HS}}(T, \rho)$ from the view that it should ensure some level of thermodynamic consistency between the free energy of the repulsive fluid with potential $\mathcal{V}_0(r)$ and that of a HS fluid of particles with effective diameter $\sigma_{\text{HS}}(T, \rho)$, which generally involves numerical minimization of an integral equation [19, 63]. However, a simpler approach for determining the effective HS diameter called the “Boltzmann factor criterion” (BFC) has also been employed in the study of liquids [11, 106]. In the BFC approach, $\sigma_{\text{HS}}(T)$ depends on temperature only, and it is determined from the following basic equation,

$$\mathcal{V}_0(r = \sigma_{\text{HS}}) = aT. \quad (4.8)$$

The physical interpretation of this criterion is that it finds a diameter such that only a very small (a -dependent) fraction of interparticle “collisions” in the model fluid will have sufficient kinetic energy to cause overlap of the effective

hard cores (i.e., $r < \sigma_{\text{HS}}(T)$). A detailed discussion of the BFC can be found in a recent article by Ben-Amotz and Stell [11]. Formal justifications for choosing parameter values of $a = 1, 1.5,$ and 2 in the BFC have been previously advanced by Hsu, Chandler, and Loweden [54], Andrews [5], and Speedy *et al.* [106], respectively. In this work, we calculate $\sigma_{\text{HS}}(T)$ of the bulk LJ fluid using Eq. 4.8 and each of three aforementioned values of a .

Our main goal in carrying out this analysis is to provide, to our knowledge, the first comprehensive test of whether the single-particle dynamics of the equilibrium LJ fluid (as measured by self-diffusivity plotted versus effective packing fraction) are in fact significantly different than what would be expected based on the behavior of the HS fluid. Fig. 4.1(a-c) shows data for the product $DT^{-1/2}$ versus $\phi_{\text{eff}}(T)$ of Eq. 4.8 employing BFC parameter values $a =$ (a) 1, (b) 1.5, and (c) 2 discussed above. Temperatures and effective packing fractions over wide intervals $1 \leq T \leq 10$ and $0 < \phi_{\text{eff}} < 0.48$, respectively, are considered. By plotting the product of $DT^{-1/2}$ instead of simply D , we have removed the trivial differences in single-particle dynamics that arise due to thermal velocity effects. The behavior of the bulk HS fluid is also presented as a single solid curve in each of the three panels in Fig. 4.1 for comparison.

Perhaps the most striking aspect of Fig. 4.1 is that the data for $DT^{-1/2}$ of the bulk LJ fluid, irrespective of the precise BFC “ a ” parameter employed, approximately collapse onto a single curve when plotted in this fashion. Moreover, the collapsed data has a dependency on $\phi_{\text{eff}}(T)$ that is consistent with what would be expected based on the behavior of the HS fluid. In fact, by

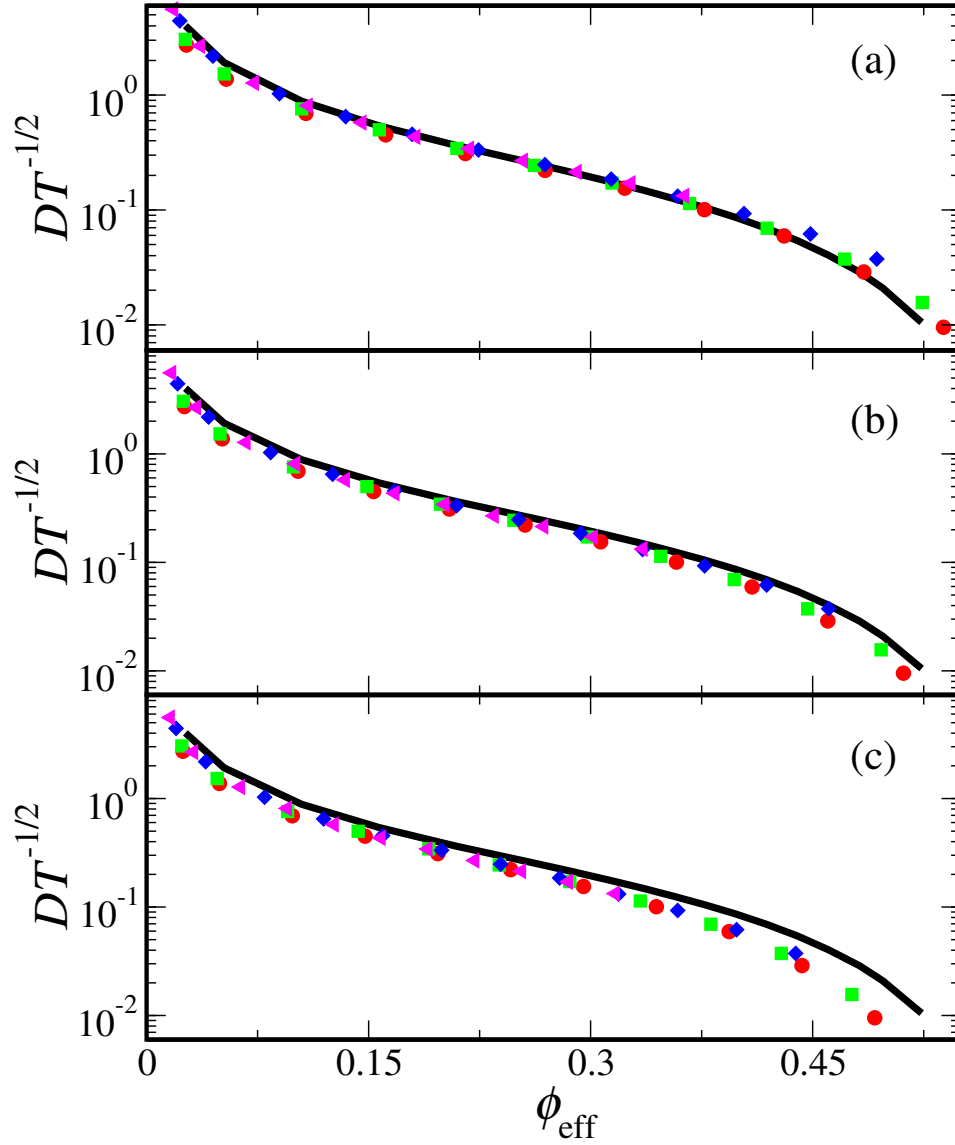


Figure 4.1: Scaled self diffusivity $DT^{-1/2}$ of the bulk LJ fluid versus effective packing fraction ϕ_{eff} defined using the Boltzmann factor criterion of Eq. 4.8 with parameter values, $a =$ (a) 1, (b) 1.5, and (c) 2. Symbols correspond to $T = 1$ (filled circle), 1.2 (filled square), 3 (filled diamond), and 10 (filled triangle left). The curve corresponds to data for the bulk HS fluid.

choosing the parameter value $a = 1$ in the BFC to determine $\phi_{\text{eff}}(T)$, one would be able to use the bulk HS data alone to produce fairly accurate estimates for the self-diffusivity of the bulk LJ fluid over an impressive range of temperatures and densities. Interestingly, we were also recently able to employ a similar analysis to successfully estimate the self-diffusivity of the LJ fluid in a random matrix of quenched LJ particles from knowledge of the behavior of an equivalent HS reference system [74]. When taken together with the data provided in Fig. 4.1, this indicates that the single-particle dynamics of the LJ model are essentially reflecting those of a HS system with the same effective packing fraction.

Unfortunately, as we will see, the “collision” perspective provided by the BFC outlined above does not provide a particularly accurate mapping of the T -dependent SW fluid behavior onto a HS fluid with the same effective packing fraction. The reason why is easy to understand. In the LJ fluid, the repulsive part of the potential can be treated as an effective HS contribution with a temperature-dependent diameter, and the slowly-varying (r^{-6}) intermolecular attractions have only minor implications for local particle structuring and collisions. In contrast, the attractions in the SW potential “turn off” via an infinitely steep step function at the outer edge of the attractive well ($r = \lambda$), a feature that can cause both the local structuring and the collisions in this model to be qualitatively different from what is observed in the HS and LJ fluids. We will return to this point in the next section when discussing the differences between SW and HS fluid structures.

The repulsive contribution to the SW potential simply comes from the impenetrable diameter of the SW particle itself. In that sense, the actual particle diameter of the SW potential represents the most obvious basis for calculating the effective HS packing fraction, i.e., $\phi_{\text{eff}} = \pi\rho/6$. Using this definition, we show our simulated SW fluid data for $DT^{-1/2}$ plotted versus ϕ_{eff} in Fig. 4.2. Again, wide ranges of temperature ($0.8 \leq T \leq 10$) and packing fraction ($0 < \phi_{\text{eff}} < 0.45$) are presented. As might be expected based on the above discussion, the T -dependent data for the SW fluid do not collapse onto a single curve as they do for the bulk LJ fluid, although the ϕ_{eff} dependencies at each T appear qualitatively similar.

It is worth noting that Speedy *et al.* [106] have previously used molecular simulation data to propose a simple empirical equation for relating the T -dependent self-diffusivity of the SW fluid (D_{SW}) to that of the HS fluid with the same density (D_{HS}). In particular, they proposed that one can estimate the former by multiplying the latter by $(1 - \alpha T^{-1})$, where α is a constant, i.e.,

$$D_{\text{SW}} = D_{\text{HS}} \times (1 - \alpha T^{-1}). \quad (4.9)$$

The inset of Fig. 4.2 shows a comprehensive test of this equation (using $\alpha = 0.68$, obtained by a least-squares fit) for the SW self-diffusivity data generated in this study. Although the proposed scale factor cannot quantitatively account for all of the deviations apparent in the main panel, the empirical expression does a remarkably good job given its simplicity. To appreciate the physics that might underlie this type of empirical expression, first recall that

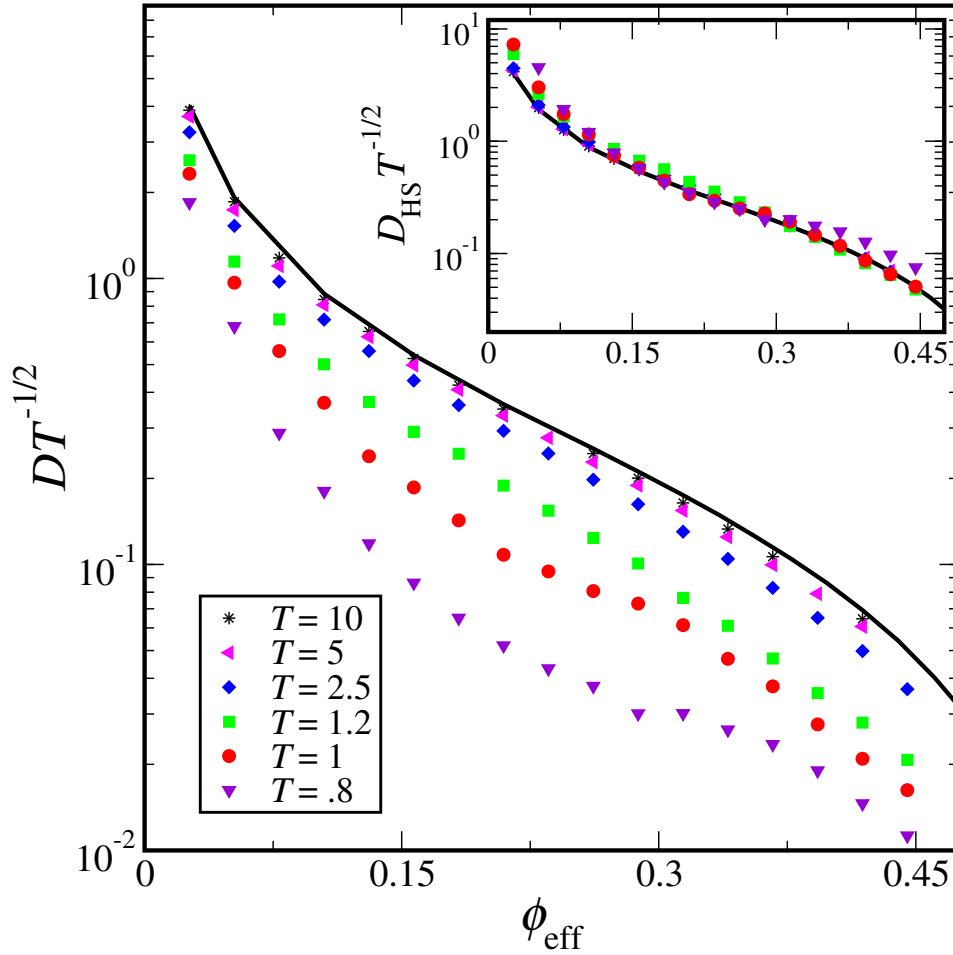


Figure 4.2: Scaled self diffusivity $DT^{-1/2}$ versus effective packing fraction ϕ_{eff} for the SW fluid (symbols) at the various temperatures T described in the legend. The black curve corresponds to the bulk HS data (or, equivalently, the data for the SW fluid in the $T \rightarrow \infty$ limit). Speedy *et al.* [106] proposed that the T -dependent SW self-diffusivity data might collapse onto the HS curve if divided by an empirical factor of the form $(1 - \alpha T^{-1})$, where α is a constant. The inset shows the scaled HS diffusivity $D_{\text{HS}} T^{-1/2}$ that is predicted by applying this type of normalization to the scaled SW diffusivity data, $D_{\text{SW}} T^{-1/2}$, in the main panel [i.e., $D_{\text{HS}} = D_{\text{SW}} / (1 - 0.68 T^{-1})$].

the behavior of the SW fluid, at any given ϕ_{eff} , must approach that of the HS fluid as $T \rightarrow \infty$. However, as T is lowered, the diffusion coefficient of the SW fluid becomes systematically reduced. One possible way to view this trend is that the attractions of the SW potential cause the particles to take on larger effective diameters (i.e., higher ϕ_{eff}), which naturally results in more sluggish dynamics. Of course, attractive interactions could further impede particle mobility in ways that are qualitatively different than the “crowding” effect associated with larger HS particle diameters. At this stage, however, it would be difficult to pin down any specific microscopic mechanisms, especially in the absence of a more rigorous justification of the functional form presented in Eq. 4.9.

To briefly summarize, the results presented in this section for the bulk LJ and SW fluids provide some evidence that it is possible to relate the dynamics of these systems to those of a bulk HS fluid with an equivalent effective packing fraction. This suggests that perturbation ideas for the thermodynamics of simple attractive fluids might also have some value in understanding, and eventually predicting, their single-particle dynamics. Unfortunately, the relationships in both cases between the behaviors of the fluids and the corresponding HS system involve parameters that are, at least at present, not known *a priori*. In the case of the LJ fluid, one needs to know the value of the parameter a in the BFC used to obtain the effective packing fraction. Interestingly though, as our data shows, collapse of the T -dependent self-diffusivity of the bulk LJ fluid onto a single curve appears to be fairly insensitive to the

precise value of a chosen. The situation for the SW fluid is not nearly as clean. Both the functional form of the scale factor provided in Eq. 4.9 and the value of the parameter α required to collapse the data, to our knowledge, lack rigorous justification. In the next section, we explore the extent to which the self-diffusivities of these bulk fluid systems might be alternatively predicted using knowledge of their excess entropy.

4.3.2 Excess entropy and self-diffusivity: Bulk fluids

Below, we use our molecular dynamics and GC-TMMC simulation data to put the excess entropy scalings of Rosenfeld [86] and Dzugasov [26] (see section 1.3 for more detail) to stringent tests for the bulk LJ and SW fluids examined in the previous section. Earlier studies provided preliminary evidence that the scaling laws could indeed adequately describe the behavior of the dense, equilibrium LJ fluid [26, 86], and we are not aware of any tests of the scaling laws for the SW model. However, an important point to keep in mind is that the GC-TMMC method used here, described in section 4.2, provides an accurate means for directly computing s^{ex} in our simulations, and thus we were able to readily explore its behavior over a wide range of thermodynamic conditions for these systems. In contrast, earlier studies (e.g., [10, 15, 26, 28, 52, 64, 86, 88, 94, 119]) have relied on estimating s^{ex} via its two-body approximation or by thermodynamic integration using approximate equations of state or simulation data over a fairly limited set of conditions. In short, the new data that we present here provide the first comprehensive

picture for how self-diffusivity and excess entropy (calculated without approximation) are related for these two basic model fluids.

The Rosenfeld scaling predicts the following approximate functional relationship, $D_R \approx 0.58 \exp(As^{\text{ex}})$, between the reduced diffusion coefficient $D_R = DT^{-1/2}\rho^{1/3}$ and the excess entropy per particle s^{ex} of dense, equilibrium fluids. The parameter A has been found to be an $\mathcal{O}(1)$ number that varies only slightly between different model fluids. Rosenfeld also pointed out that this functional form must give way to a different behavior in the dilute gas limit. In particular, he used Enskog theory for D and a virial expansion for s^{ex} to argue that $D_R \approx 0.37(-s^{\text{ex}})^{-2/3}$ [87] for low-density fluids of soft-sphere particles with potentials of the form r^{-n} , where $n > 3$.

The “universal” entropy scaling law of Dzugutov is given by $D_D \approx 0.078 \exp(s^{\text{ex}})$ [28], and it relates a slightly different reduced self-diffusivity $D_D = D\rho^{2/3}\Gamma_E^{-1}$ to the excess entropy per particle s^{ex} . The parameter $\Gamma_E = 4\pi\rho g(\sigma)\sqrt{T/\pi}$ is an effective Enskog interparticle collision frequency, σ is the interparticle separation corresponding to the first peak in the radial distribution function, and $g(\sigma)$ is the magnitude of that first peak. As with the Rosenfeld scaling, the available data suggests that it applies for dense, simple liquids above their freezing temperature (or below their freezing density).

We begin here by examining the entropy scaling behavior for the self-diffusivity of the bulk LJ fluid. Specifically, Fig. 4.3 shows the reduced self-diffusivity as calculated based on the aforementioned Rosenfeld (top) and Dzugutov (bottom) forms, respectively. The data span the same wide range

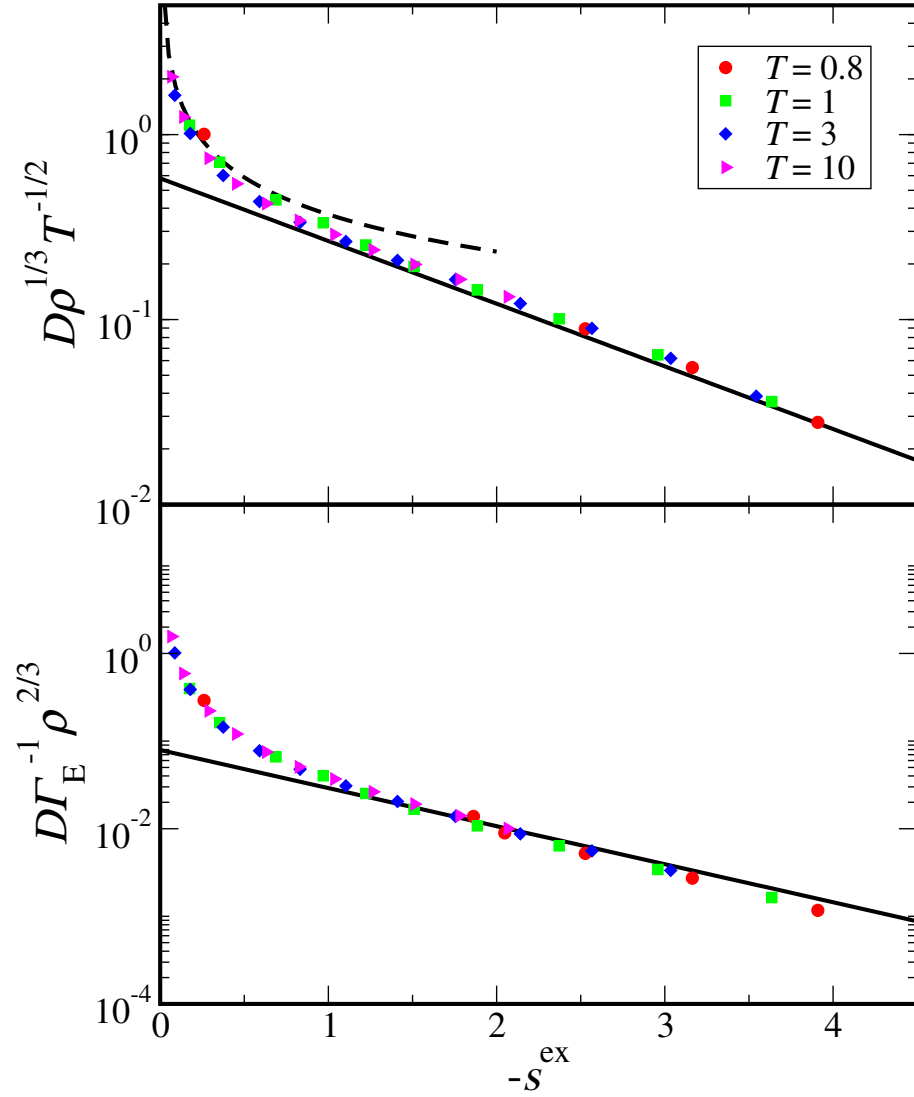


Figure 4.3: Scaled self diffusivity data (symbols) versus negative excess entropy per particle for the bulk LJ fluid using the (top) Rosenfeld and (bottom) Dzugutov reduction parameters discussed in the text. In the top panel, the solid line represents the Rosenfeld scaling law, $0.58\exp(0.78s^{\text{ex}})$, for the dense fluid, and the dashed curve shows the low-density behavior expected for fluids with soft-sphere potentials, $0.37(-s^{\text{ex}})^{-2/3}$ [87]. In the bottom panel, the solid line represents the Dzugutov scaling law, $0.078\exp(s^{\text{ex}})$.

of parameter space discussed in the previous section, i.e., $1 \leq T \leq 10$ and $0 < \phi_{\text{eff}} < 0.48$. Three points are worth noting here. First, both reduced forms appear to collapse the data, to a good approximation, onto single curves when plotted versus $-s^{\text{ex}}$. Next, the scaling laws provided by Rosenfeld and Dzugutov (shown in Fig. 4.3 by the black lines) capture the LJ model behavior reasonably well in the interval $1.5 < -s^{\text{ex}} < 4$, which spans the dense fluid range [26, 86]. Finally, the low-density power-law scaling behavior derived by Rosenfeld for repulsive soft-sphere fluids (dashed line) [87] appears to capture the behavior of the attractive LJ fluid very well. This good agreement was not necessarily expected in advance because attractions can have a pronounced influence on fluid structure at low-to-intermediate densities. Nonetheless, the key generic point of Fig. 4.3 is that a standard thermodynamic quantity, the excess entropy, seems to determine the (reduced) self-diffusivity of the LJ fluid over an extraordinarily broad range of conditions.

Now, we turn our attention to exploring the behavior of the bulk SW fluid with respect to the Rosenfeld and Dzugutov entropy scaling laws. To the best of our knowledge, Fig. 4.4 represents the first examination of the dependencies of reduced self-diffusivity on $-s^{\text{ex}}$ for this model. Interestingly, there are significant deviations in the SW fluid behavior from the scaling laws of both Rosenfeld (top) and Dzugutov (bottom), the latter of which was thought to provide a “universal” description for the behavior of simple atomic fluids such as this. In both cases, the deviations reflect the fact that, similar to what was found in the packing fraction analysis of Section 4.3.1, temperature effects

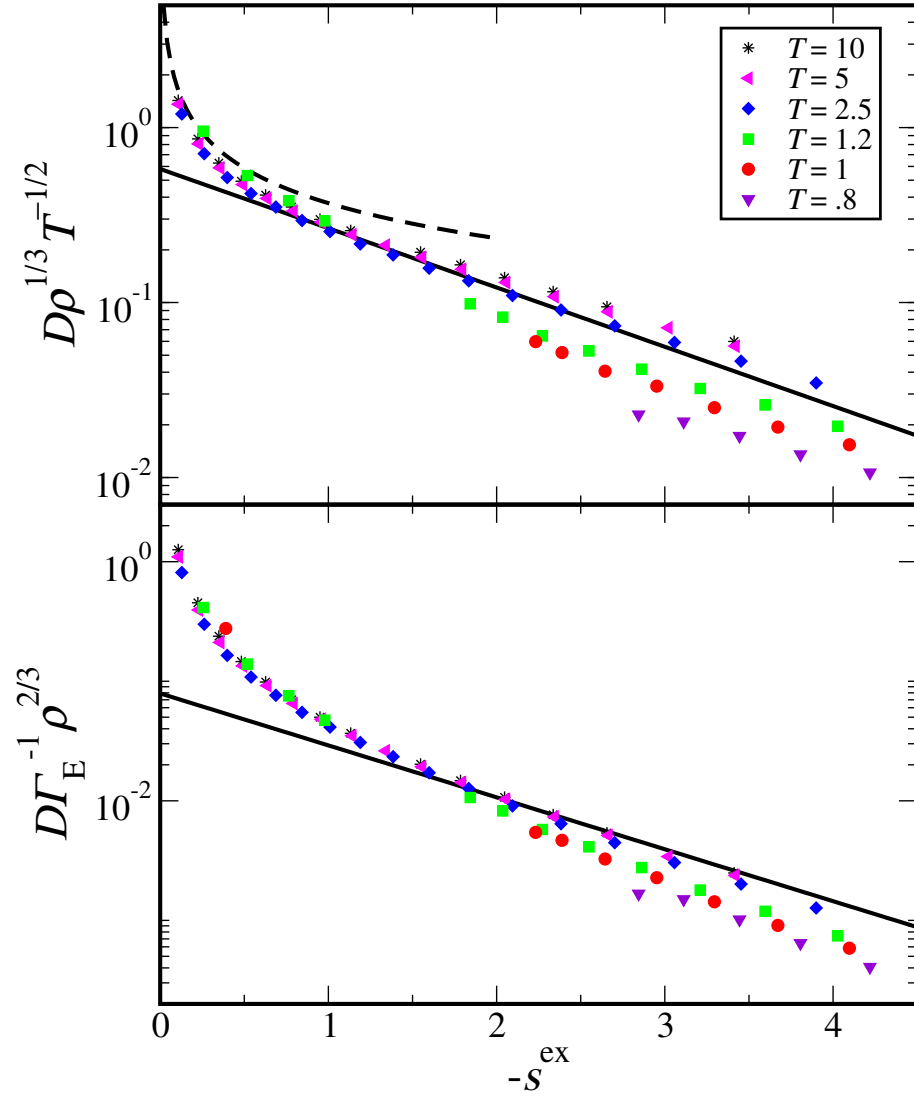


Figure 4.4: Scaled self diffusivity data (symbols) versus negative excess entropy per particle for the bulk SW fluid using the (top) Rosenfeld and (bottom) Dzugutov reduction parameters discussed in the text. In the top panel, the solid line represents the Rosenfeld scaling law, $0.58\exp(0.78s^{\text{ex}})$, for the dense fluid, and the dashed curve shows the low-density behavior expected for fluids with soft-sphere potentials, $0.37(-s^{\text{ex}})^{-2/3}$ [87]. In the bottom panel, the solid line represents the Dzugutov scaling law, $.078\exp(s^{\text{ex}})$.

on self-diffusivity of the bulk SW fluid cannot be collapsed in the same way that they can for the bulk LJ fluid.

To try to understand the deviations of the SW fluid from the entropy scaling laws, it may help to recall the basic arguments originally made in justifying these approximate relationships. The scaling law of Rosenfeld was motivated by the success of a variational perturbation theory that used the excess entropy to parametrize the structure of simple equilibrium fluids [87]. Thus, one might expect it to lose validity for fluids that do not satisfy the basic assumptions of perturbation theory, the most important being that the structure of the fluid can be adequately approximated by that of a HS reference system. Indeed, as was discussed in the previous section, unlike the LJ fluid, the SW fluid will fail in this basic assumption under certain thermodynamic conditions. Specifically, its attractive interactions are not slowly-varying, and, as a result, they can greatly impact fluid structure, especially at low temperature and intermediate fluid densities. In fact, Fig. 4.5 illustrates the stark contrast between the low-temperature SW fluid structure and that of the HS fluid at the same density. Given these basic differences, it is perhaps not too surprising that the Rosenfeld scaling fails to quantitatively describe the temperature dependencies of the SW fluid behavior.

Similarly, the Dzugutov scaling assumes that the Enskog parameter Γ_E provides the relevant microscopic information about the collisional processes that mediate self-diffusion in the fluid. However, since the Enskog approach is intrinsically a hard-sphere collision theory that focuses on the first peak in

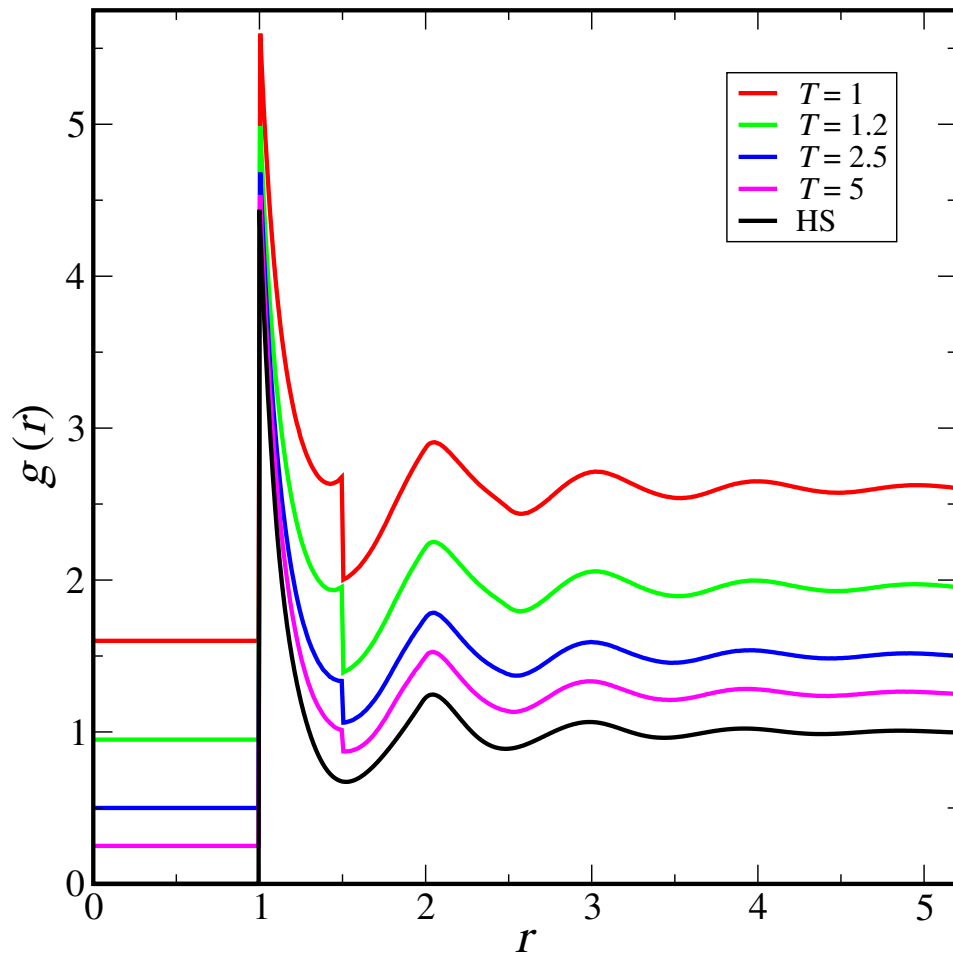


Figure 4.5: Pair correlation function $g(r)$ for the SW fluid at density $\rho = 0.84$ and various T values presented in the legend (T increases from top to bottom for SW fluid). The bottom curve corresponds to $g(r)$ for the HS fluid with the same density. Curves for the SW fluid have been vertically shifted for clarity.

$g(r)$, then it also stands to reason that it might break down when the liquid structure differs qualitatively from that of the HS fluid, as is it does for the SW fluid at lower temperatures (Fig. 4.5). In fact, similar deviations from the Dzugutov scaling have also been noticed for the Stillinger-Weber model of Si and have been ascribed to the very different liquid structure of that fluid due to its angular bonding [52].

The results presented above reinforce the notion, suggested in the last section, that the single-particle dynamics of the bulk LJ fluid are effectively mediated by HS-like collisions, which are connected to the effective HS-like structuring of that system. As a result, like the HS fluid, the self-diffusivity of the LJ fluid can be approximately determined a single static quantity that is intimately tied to structure, the excess entropy. In this sense, the LJ fluid is an extraordinarily “simple” liquid. However, as we have seen, a similar description does not apply to the T -dependent behavior of the SW fluid. This appears intimately connected to the fact that the SW fluid structure becomes markedly different from the HS fluid at low T , which is itself tied to the fact that its attractive interactions are not slowly-varying in r .

In the next section, we put the connections between self-diffusivity, effective packing fraction, and excess entropy to a much more stringent test for these systems. Namely, we explore how confinement of these attractive fluids affects the various relationships between these basic quantities.

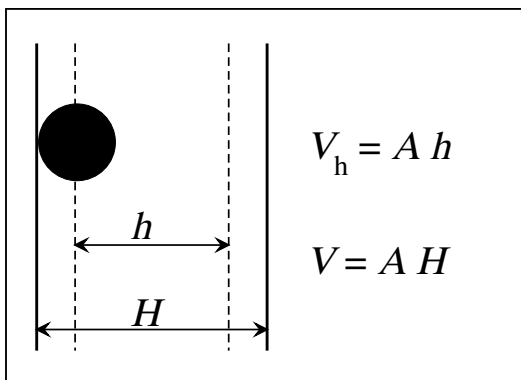


Figure 4.6: Schematic showing a particle confined in a slit-pore geometry. The effective packing fraction of this system can be defined based either on the volume that the particle centers access ($V_h = Ah$) or the “total” volume that the particle surfaces access ($V = AH$), where A is the fluid contact area at a single wall.

4.3.3 Effective packing fraction and self-diffusivity: Confined fluids

Here, we explore how the effective packing fraction approach for studying the single-particle dynamics of bulk fluids introduced in Section 4.3.1 can be extended to understand and predict the kinetic behavior of confined fluids. Before moving forward, however, we first need to clarify what we mean by the effective packing fraction of particles in a slit-pore geometry. Specifically, there are two different types of definitions that are commonly invoked: $\phi_{\text{eff}} = N\pi\sigma_{\text{HS}}^3/6V_h$ and $\phi_{\text{eff}} = N\pi\sigma_{\text{HS}}^3/6V$, where σ_{HS} is the Boltzmann diameter of Eq. 4.8 associated with the repulsive interaction between two fluid particles. The difference, shown in Fig. 4.6, is that $V_h = Ah$ is the volume that the particle centers effectively access (A is the contact area between a single wall and the fluid), and $V = AH$ is the larger “total” volume that the fluid

particle surfaces access (i.e., $H = h + \sigma_{\text{HS}}^{\text{fw}}$, where $\sigma_{\text{HS}}^{\text{fw}}$ is the Boltzmann diameter of the fluid wall-interaction). While these two definitions must converge in the limit $H \rightarrow \infty$, they generally have very different numerical values for severely confined fluids.

In Chapter 2, we presented some compelling arguments based on our simulations of HS fluids confined to both thin film and square-channel geometries that the most natural definition of the two is the one based on the total volume [72]. Specifically, our results showed that D of the confined HS fluid, over a wide range of equilibrium conditions, approximately collapsed onto that of the bulk HS fluid if the two systems are compared at the same value of $\phi_{\text{eff}} = \pi N/6V$ (recall that $\sigma_{\text{HS}}^{\text{fw}} = \sigma_{\text{HS}} = 1$ for the HS fluid confined between hard walls). In other words, the microscopic details of the inhomogeneous packing structures have only minor influence on the average single-particle dynamics of the confined HS fluid, as long as one controls for the average packing fraction based on V . Alternatively, if one instead compared the behaviors of the bulk and confined systems at equal values of packing fraction based on V_h , one arrived at the conclusion that confining a HS fluid between hard walls generally has the effect of significantly increasing its self-diffusivity.

Given this background, we now move on to explore whether the effective packing fraction of the LJ fluid confined between “9-3” walls separated by a distance H_z (see model description in section 4.2) also provides a good predictive measure for its single-particle dynamics. In this system, the effective packing fraction based on the total (i.e., “particle surface” rather

than “particle center”-accessible) volume is $\phi_{\text{eff}}(T) = N\pi\sigma_{\text{HS}}^3(T)/[6AH]$, where $H = H_z - \sigma_{\text{HS}}^{\text{fw}}(T)$. Here, we have used Eq. 4.8 and the repulsive WCA contributions to the fluid-fluid and fluid-wall potentials of Eq. 4.1 and 4.3, respectively, to determine $\sigma_{\text{HS}}(T)$ and $\sigma_{\text{HS}}^{\text{fw}}(T)$. We have employed a BFC parameter of $a = 1$ in determining these diameters because of the excellent data collapse that this choice produced for the bulk LJ fluid (recall Fig. 4.1a).

The predictions for the scaled self-diffusivity $DT^{-1/2}$ versus ϕ_{eff} for the confined LJ fluid are presented in Fig. 4.7. As for the bulk LJ fluid, data have been generated for wide ranges of temperature and packing fraction, $0.8 \leq T \leq 10$ and $0 < \phi_{\text{eff}} < 0.48$, respectively. Slit-pores with $H_z = 5$ and $H_z = 10$ and fluid-wall interaction parameters $\epsilon_{\text{fw}} = .01$ and $\epsilon = 1$ were considered. In short, one can see that, although there is some visible deviation, most of the data for the inhomogeneous systems fall very close to the collapsed curves of the bulk LJ and HS fluids. Stated differently, the average packing fraction ϕ_{eff} seems to approximately determine the single-particle dynamics of the LJ and HS fluids, even when they are confined to thin films.

Can packing fraction provide similar insights into how confining the SW fluid between interacting walls modifies its dynamics? One might initially be skeptical given that the data for $DT^{-1/2}$ versus ϕ_{eff} did not even collapse for different T in the bulk SW fluid (recall Fig. 4.2). However, T dependencies and confinement may be different issues altogether. As we discussed earlier, the lack of a data collapse for the bulk fluid at various T is likely due to the fact that lowering T causes pronounced structural changes in the SW fluid,

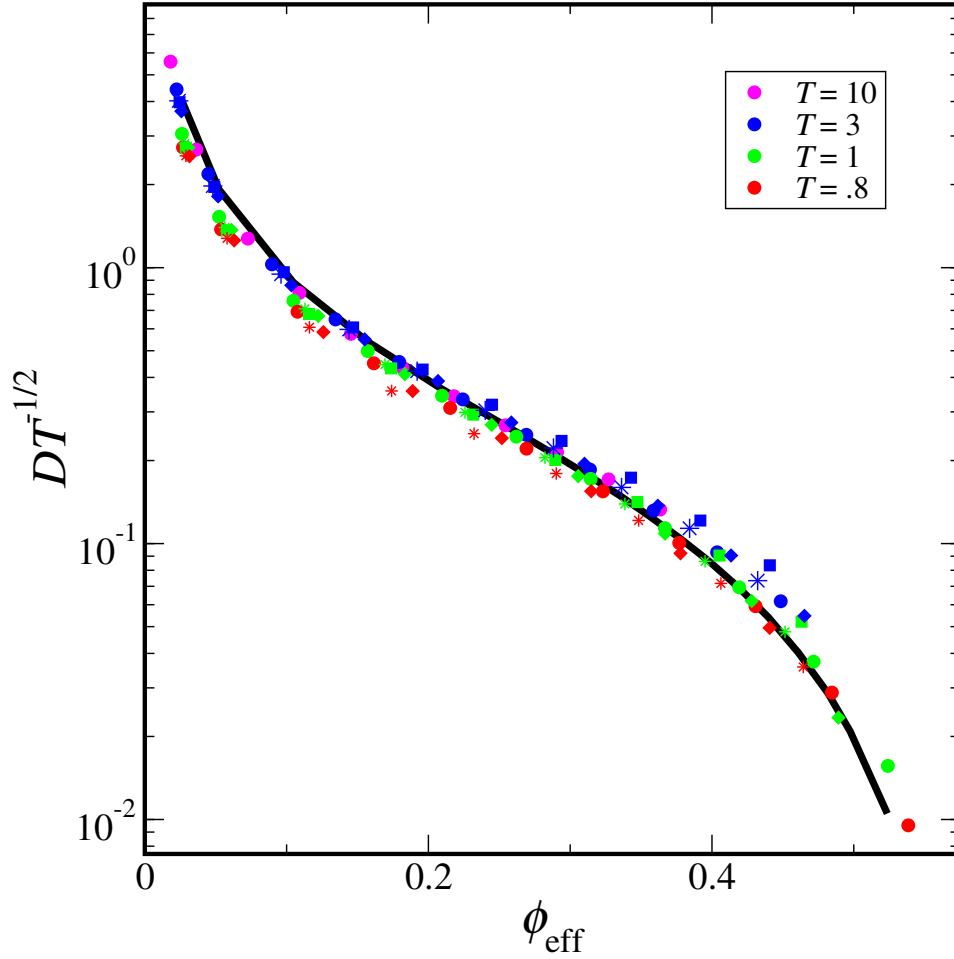


Figure 4.7: Scaled self diffusivity $DT^{-1/2}$ for bulk and confined LJ fluids versus effective packing fraction $\phi_{\text{eff}}(T)$ based on the total (i.e., “particle surface” rather than “particle center”-accessible) volume, as discussed in the text. Temperatures for data points follow the color code shown in the legend. Various fluid-wall interactions used are effective “hard wall” (HW, $\epsilon_{\text{fw}} = .01$), and neutral wall (NW, $\epsilon_{\text{fw}} = 1$) both modeled by a 9-3 LJ interaction potential described in the text. The symbols correspond to bulk (filled circle), HW: $H_z = 5$ (filled square), NW: $H_z = 5$ (filled diamond), and NW: $H_z = 10$ (asterisk). The solid curve corresponds to the bulk HS fluid data.

i.e., the fluid evolves from HS-like ordering at high T to qualitatively different structuring at low T (recall Fig. 4.5). However, if we restrict ourselves to making comparisons between SW fluid systems *at the same temperature*, it is still possible that ϕ_{eff} might explain the implications of confinement for single-particle dynamics.

To test this idea, we simulated the SW fluid confined between SW walls separated by distances $H_z = 2.5$ and $H_z = 7.5$ with different values of the fluid-wall energy parameter ϵ_{fw} : hard walls ($\epsilon_{\text{fw}} = 0$), repulsive walls ($\epsilon_{\text{fw}} = -1$), and attractive walls ($\epsilon_{\text{fw}} = 1$). We also considered two different values of the fluid-wall potential range parameter ($\lambda_{\text{fw}} = 1.5$ and $\lambda_{\text{fw}} = 1.1$). Here, $\phi_{\text{eff}} = N\pi/[6AH]$ again describes the packing fraction based on total (i.e., “particle surface” rather than “particle center”-accessible) volume, where $H = H_z + 1$. Recall that the full description of the fluid-wall interaction in this model system is provided in methods section.

Fig. 4.8 shows the relationship between self-diffusivity D and ϕ_{eff} for the bulk and confined SW fluids over a wide range of thermodynamic conditions. The interesting point here is that, without any rescaling of the diffusion coefficient, the effective packing fraction of the SW fluid appears to account for the main effects that confinement has on the single-particle dynamics at any given temperature. Although the data along each isotherm in Fig. 4.8 does show more scatter than is apparent for the LJ fluid presented in Fig. 4.7, the ability of a single static quantity to approximately capture the diffusivity behavior is still remarkable, especially considering the complexity of the local structuring

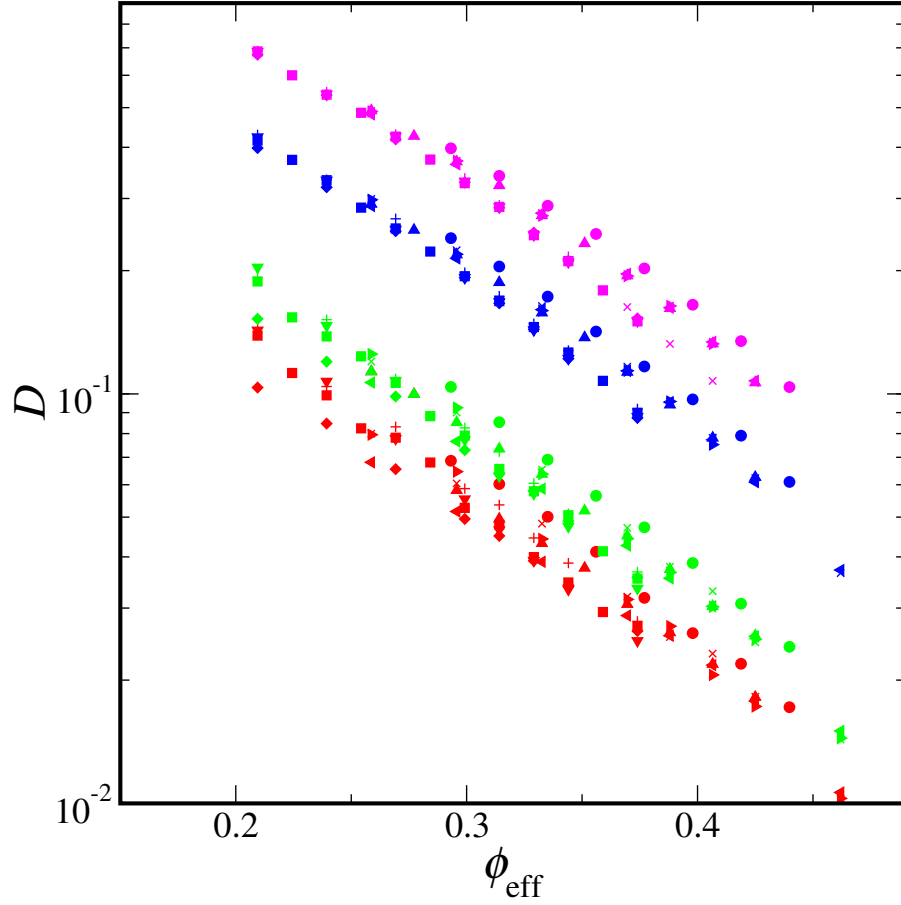


Figure 4.8: Self diffusivity D of the confined SW fluid versus ϕ_{eff} based on the total (i.e., “particle surface” rather than “particle center”-accessible) volume, as discussed in the text. Temperatures for data points follow the color code shown in the legend. Various fluid-wall interactions used are hard wall (HW, $\epsilon_{\text{fw}} = 0$), repulsive wall (RW, $\epsilon_{\text{fw}} = -1$), attractive wall, (AW, $\epsilon_{\text{fw}} = 1$). The range of the fluid-wall potential is $\lambda_{\text{fw}} = 1.5$ except for a few data sets (SR) where it is $\lambda_{\text{fw}} = 1.1$. Symbols correspond to bulk (filled circle), HW: $H_z = 3.5$ (filled square), HW: $H_z = 8.5$ (filled triangle up), RW: $H_z = 3.5$ (filled diamond), RW: $H_z = 8.5$ (filled triangle left), AW: $H_z = 3.5$ (filled triangle down), AW: $H_z = 8.5$ (filled triangle right), AW-SR: $H_z = 3.5$ (plus), and AW-SR: $H_z = 8.5$ (times).

of the SW fluid and the number of different types of confining environments investigated. In this sense, confinement effects on dynamics of the SW fluid are easier than temperature effects to understand and predict.

Given the results of this section and those presented earlier for bulk fluids, it is natural wonder whether excess entropy can in fact capture the confinement effect for attractive liquids even more reliably than effective packing fraction. In this next section, we explore that issue.

4.3.4 Excess entropy and self-diffusivity: Confined fluids

We examined in detail two different excess entropy scaling laws in Section 4.3.2, both of which can be utilized to predict the (reduced) self-diffusivity of the bulk LJ fluid from knowledge of its excess entropy. In this section, we first first investigate whether the same scaling laws can also be used to collapse the single-particle dynamics data of the bulk and confined LJ fluids.

Fig. 4.9 shows the reduced self-diffusivity data for both the bulk and confined LJ fluids utilizing the Rosenfeld (top) and Dzugutov (bottom) reduction parameters discussed earlier. The conclusion from this plot is a simple one: both scaling laws are able to collapse, to a very good approximation, the data from all simulations onto a single curve. In other words, although confinement can change the the reduced self-diffusivity (in either form) and the excess entropy of a fluid, the relationship between these two variables is apparently preserved. This seems like a very powerful conclusion because the excess entropy of confined LJ fluids can be predicted by classical density functional

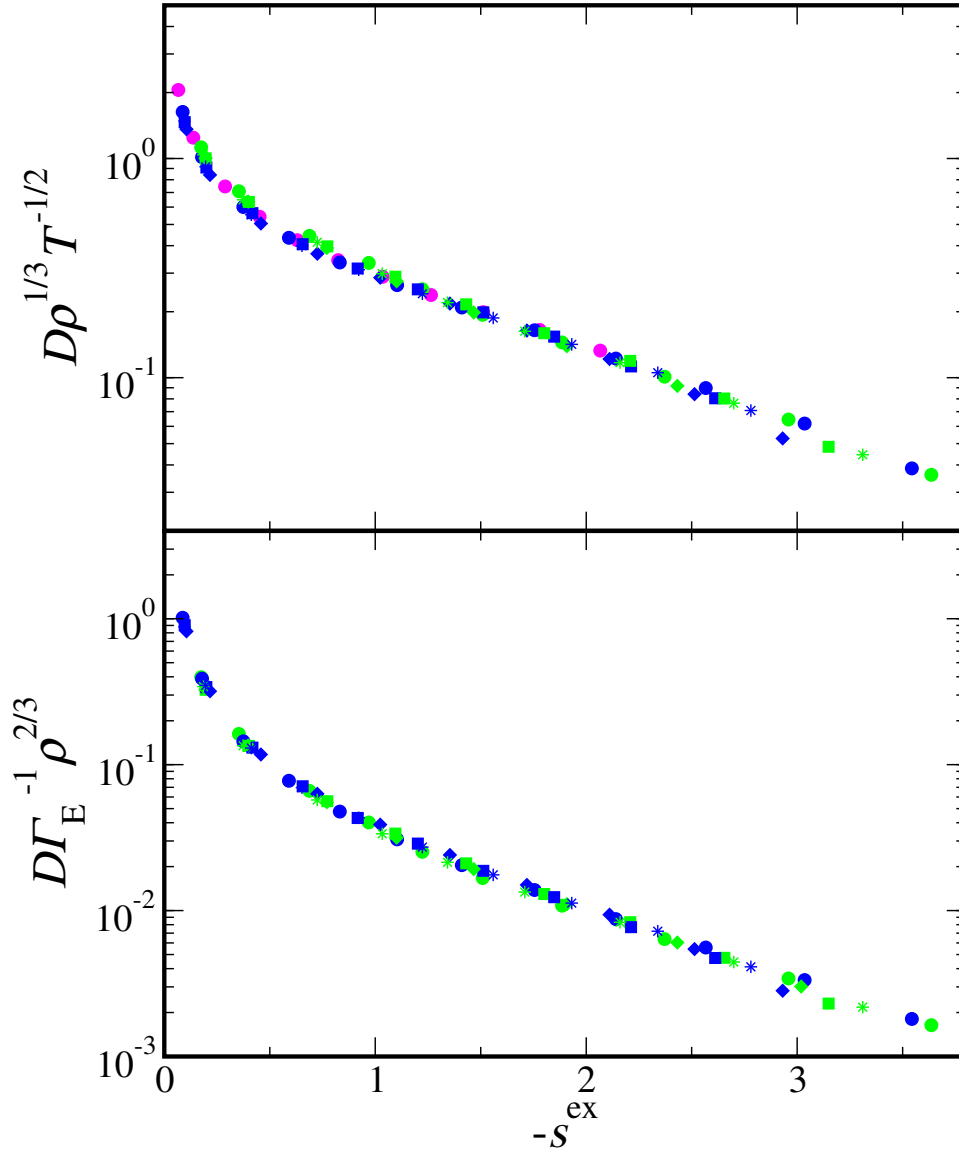


Figure 4.9: Scaled self diffusivity data (symbols) versus negative excess entropy per particle for the bulk and confined LJ fluids using the (top) Rosenfeld and (bottom) Dzugutov reduction parameters discussed in the text. Symbols are the same as those presented in Fig. 4.7.

theories, and thus one could use the “master curves” presented in Fig. 4.9 to ascertain how confinement impacts the reduced self-diffusivity.

However, there are two potential issues with using the scaling laws for studying the implications of confinement that need to be addressed. First, one generally is interested in predicting the self-diffusivity itself and not the reduced self-diffusivity. Second, one would also like to be able to make predictions about the effects of confinement for the dynamics of the SW fluid, and we already know that the Rosenfeld and Dzugutov scalings break down for that system. The natural solution is ask a different, but related, question. Does confining a fluid *at constant temperature* affect the relationship between the self-diffusivity itself (i.e., no reduction parameters) and excess entropy. If not, than one can use accurate predictions about the latter (e.g., from density functional theory) to infer information about the former.

As can be seen in Fig. 4.10, the relationship between the self-diffusivity and excess entropy, for a given temperature, is indeed approximately unaltered by confinement for both the LJ and the SW fluids. Note that this is a much more powerful conclusion than the one presented in the last section where the effective packing fraction, instead of the excess entropy, was the independent variable. The reason why is two-fold. First, the data shows much less scatter when excess entropy is the independent variable in the plot. Second, effective packing fraction relies on a definition for the Boltzmann diameters of the system (e.g., the parameter a in the BFC given by Eq. 4.8), whereas the excess entropy is a standard thermodynamic quantity that is unambiguously

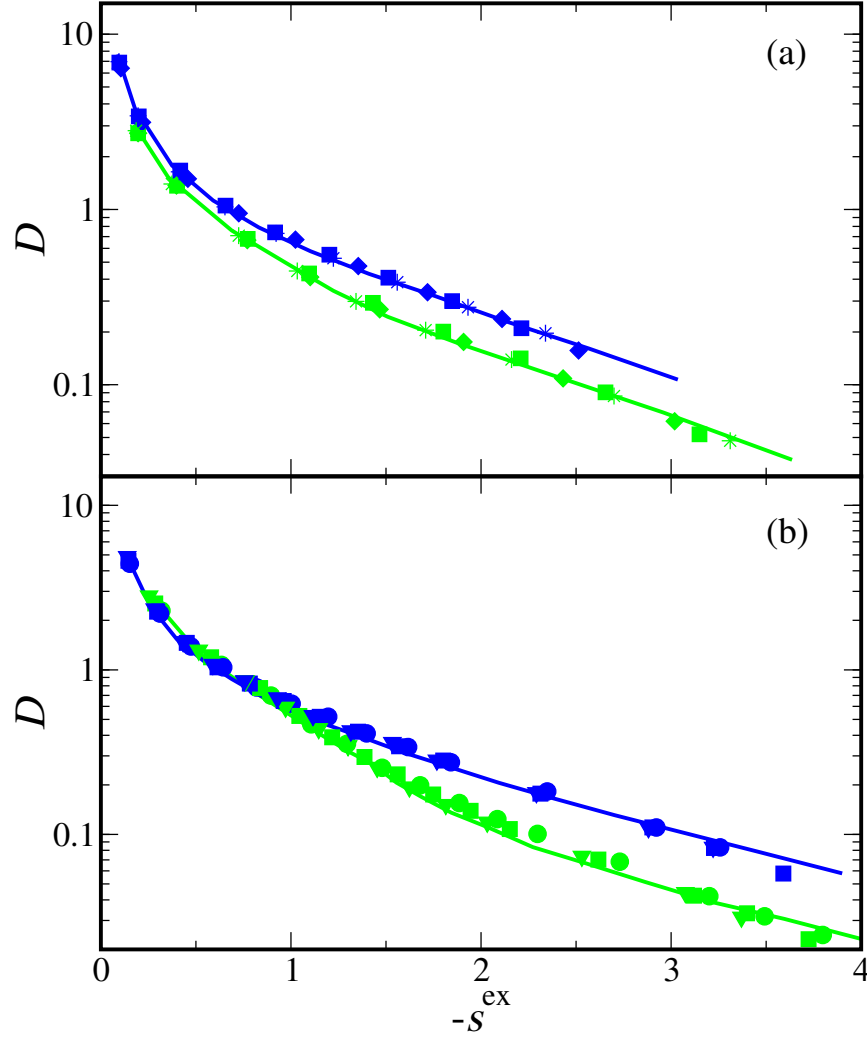


Figure 4.10: Self diffusivity versus negative excess entropy per particle. (a) Bulk and confined LJ fluids at temperatures $T = 1$ and 3. Symbols and color code are the same as in Fig. 4.7. (b) Bulk and confined SW fluids at temperatures $T = 1.2$ and 2.5 from bottom to top curve. Various fluid-wall interactions used are hard wall (RW, $\epsilon_{\text{fw}} = -1$), repulsive wall (HW, $\epsilon_{\text{fw}} = 0$), attractive wall, (AW, $\epsilon_{\text{fw}} = +1$). The range of the fluid-wall potential is $\lambda_{\text{fw}} = 1.5$. Symbols correspond to bulk (line), RW: $H_z = 4$ (filled circle), HW: $H_z = 4$ (filled square), AW: $H_z = 4$ (filled triangle down).

defined, even for confined fluids.

4.4 Conclusions

In this chapter, we presented a systematic investigation of the relationships between the self-diffusivity, effective packing fraction, and excess entropy of the LJ and SW fluids in both bulk and confined environments. We find that the entropy scaling laws of Rosenfeld and Dzugutov can collapse (appropriately reduced) self-diffusivities of the bulk and confined LJ fluids as a function of excess entropy over a wide range of thermodynamic conditions. Moreover, the self-diffusivities of the LJ fluids can be approximately collapsed onto a single, HS-like, curve versus effective packing fraction. Interestingly, the SW fluid data cannot be collapsed by either the entropy scaling laws or the effective packing fraction. We explain how this can be understood based on the non-trivial effects that temperature has on its static structure. Even still, we show that the consequences of confinement for the self-diffusivity of both of these liquids, over a broad range of equilibrium conditions, can be estimated based on knowledge of the bulk fluid behavior and either the packing fraction or the excess entropy of the confined fluid. Excess entropy is perhaps the most preferable route since it is a standard, unambiguous thermodynamic quantity that can be readily predicted via classical density functional theories of inhomogeneous fluids.

Chapter 5

Fluid diffusivity in random porous media

5.1 Introduction

Fluid transport in random porous media is central to a host of natural phenomena and technological applications, from the function of biological cells to the performance of materials for membrane separations and heterogeneous catalysis. Although it is now appreciated that kinetic processes in these systems are intimately connected to their microstructures (pore volume, surface area, connectivity, etc.) [111], determining the precise structure-property relationship for the transport property of interest remains a formidable challenge.

One promising line of inquiry has been the exploration of simple model systems for which both transport properties and structure are amenable to theoretical analysis. In the case of diffusivity, earlier work has focused primarily on single particle transport through random configurations of static obstacles [17]. At low obstacle densities, particles show anomalous, sub-diffusive motion over intermediate time and length scales but recover normal diffusive behavior in the long time limit. On the other hand, sub-diffusive motion is observed for all times at high obstacle densities. Similar behavior is predicted for transport of single ions in disordered matrices of quenched charges [24].

Self-diffusivities of highly coupled fluids in random media pose additional challenges and are also of great interest. Very recently, insightful molecular dynamics simulation [20] and mode-coupling theory [61] studies have been presented for the hard-sphere (HS) fluid embedded in disordered matrices of obstacle spheres. This type of model, introduced originally by Madden and Glandt [66], is referred to as a quenched-annealed (QA) system. To the best of our knowledge, no simple theoretical relationship between self-diffusivity of mobile particles, densities of mobile and matrix particles, and matrix microstructure has been proposed for QA media. As a result, a general consensus on which physical parameters are most important for understanding mobility in these model porous materials is lacking.

In this Chapter, we introduce one such approximate relationship that we motivate by using a physical argument for how the matrix reduces the volume available for diffusion of the mobile particles. We test its predictions against the numerical results of molecular dynamics simulations for HS QA systems with matrices that reflect equilibrium and non-equilibrium structures, which serve as idealizations for two different classes of physically realizable materials. We then demonstrate how the available volume in both types of matrices can be accurately predicted directly from equilibrium properties of the bulk HS fluid. Finally, we test our equation for diffusivity against simulation results of QA systems comprising Lennard-Jones (LJ) particles. For all models investigated, we find good agreement with simulations over a wide range of parameters, with significant overpredictions of diffusivity occurring only for

high matrix densities where limited connectivity of the available volume (not accounted for in our approximate equation) also hinders transport.

5.2 Model and simulation details

The protocols that we use to generate static matrices represent two of the most commonly employed in studies of QA systems [20, 66, 116]. In the first, N_M particles of diameter σ are initially equilibrated in a volume V at temperature T . They are subsequently quenched (i.e., frozen in place) in an equilibrium configuration, and a “fluid” (F) of N_F identical particles is added, equilibrated, and studied. This method of matrix generation is referred to as QA-M because the matrix (M) itself reflects an equilibrium configuration of density $\rho_M = N_M\sigma^3/V$ for the bulk system. QA-M matrices serve as elementary models of amorphous solid materials prepared, e.g, by very rapidly cooling gel-forming suspensions of proteins or colloids [116].

The second matrix generation protocol we study is referred to as QA-FM because it involves first equilibrating $N_F + N_M$ identical particles of diameter σ in a volume V at temperature T . Then, N_M of the particles are randomly selected and quenched to create the solid matrix. The other N_F particles constitute the mobile “fluid” of density $\rho_F = N_F\sigma^3/V$. QA-FM matrices are idealized models for templated porous solids synthesized by depleting a high density material of one of its components by, e.g., dissolution, reaction, or desorption [116].

We performed molecular dynamics simulations [82] for HS QA-M and

QA-FM systems in the microcanonical ensemble using $N_F = 1500$ mobile particles and a periodically-replicated simulation cell. Runs were performed at different values of N_M and V/σ^3 to obtain results for specific combinations of ρ_F and ρ_M . We extracted self-diffusivity of the mobile particles $D(\rho_F, \rho_M)$ by fitting the long-time ($t \gg 1$) behavior of the average mean-squared displacement to the Einstein relation $\langle \Delta \mathbf{r}^2 \rangle = 6Dt$.

5.3 Simple diffusion equation from scaling

Our approach for predicting the fluid self-diffusivities of these systems is motivated by three basic observations about their behaviors. (i) The mobile particle pair correlation functions of HS QA-M and QA-FM configurations, averaged over matrix particles at the same total density $\rho_F + \rho_M$, are indistinguishable [20]. (ii) Yet, their fluid self-diffusivities generally differ significantly, even when compared at the same ratio of matrix to mobile particles. This has previously been interpreted as evidence that the differences in the dynamics of QA media cannot be predicted based on static structural information alone [20]. (iii) However, there is a key static property that distinguishes individual QA systems: the fraction of volume available to the mobile particle centers in the matrix, V_0/V [116]. As we demonstrate below, differences in this quantity can largely account for the wide range of self-diffusivities exhibited by QA materials that are otherwise “structurally similar”.

For example, contrast the behavior of a bulk HS fluid with density $\rho = \rho_F + \rho_M$ to a HS QA system (produced by either -M or -FM protocols)

with matrix and mobile particle densities of ρ_M and ρ_F , respectively. The binary collisions that mediate diffusion in these two systems are expected to be comparable, since their pair correlation functions and mobile-particle thermal velocities are the same. Nonetheless, mobile particles in the QA system will diffuse over a shorter characteristic length scale per unit time compared to those of the bulk because the volume available for diffusion (per particle) in the QA matrix, V_0/N , is smaller than V/N . If we assume that the characteristic length scales for diffusion are proportional to the cube root of the respective available volumes and, in turn, that the associated self-diffusivities are proportional to the square of the length scales, we arrive at the following approximate relationship:

$$D(\rho_F, \rho_M) \approx D(\rho_F + \rho_M, 0) \times (V_0/V)^{2/3}, \quad (5.1)$$

where $D(\rho_F, \rho_M)$ and $D(\rho_F + \rho_M, 0)$ are the self-diffusivities of the mobile particles in QA and bulk fluid systems. As we show below, the appeal of this relation is its ability to predict the self-diffusivity of non-trivial QA systems from knowledge of well-characterized equilibrium properties of the *bulk* HS fluid.

In order to predict HS QA diffusivity using Eq. 5.1, we now require V_0/V of both QA-M and QA-FM matrices and an expression for the self-diffusivity of the bulk HS fluid, $D(\rho, 0)$. For $D(\rho, 0)$, we adopt Speedy's empirical fit to molecular dynamics simulation data [107],

$$D(\rho, 0) = \frac{A}{\rho} \left(1 - \frac{\rho}{1.09}\right) [1 + \rho^2(0.4 - 0.83\rho^2)], \quad (5.2)$$

where $A = 3/(8\sqrt{\pi})$. We implicitly non-dimensionalized $D(\rho, 0)$ of Eq. 5.2, and all other self-diffusivities in this study, by σ^2/τ , where $\tau = \sigma\sqrt{m/k_B T}$, k_B is the Boltzmann’s constant, and m is particle mass. In the next section, we explain in detail different routes to calculate V_0/V .

5.4 Calculating available space

In HS QA-M systems, matrices are drawn from equilibrium configurations of the bulk HS fluid with density ρ_M , and thus V_0/V is given by [83]

$$V_0/V = \exp[-\mu^{\text{ex}}(\rho_M)/k_B T]. \quad (5.3)$$

The excess chemical potential (relative to ideal gas) of the HS fluid, μ^{ex} , can be obtained analytically from, e.g., either scaled particle theory [83] or the Carnahan-Starling (CS) equation of state [18] (here, we adopt the latter, which is very accurate for $\rho_M < 0.9$).

In HS QA-FM media, however, the matrix structure is different than that of an equilibrium HS fluid because it is quenched in the presence of mobile particles. Nonetheless, as Van Tassel and co-workers [115, 116] have demonstrated, because of the specific protocol by which “non-equilibrium” QA-FM matrices are created, one can still apply equilibrium liquid-state approaches (e.g., integral equation theories) to estimate V_0/V . Here, we introduce an accurate information-theory (IT) based strategy for accomplishing this task. As we show, its main advantage is that it only requires knowledge of ρ_M , ρ_F , and the pair correlation function $g(r)$ of the bulk HS fluid.

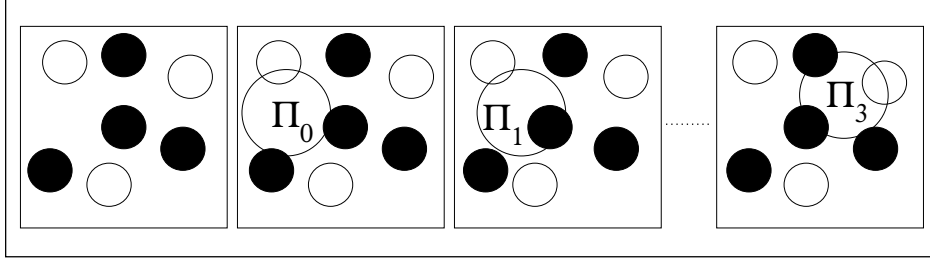


Figure 5.1: Schematic of a QA system. Equi-sized filled and empty circles are matrix and fluid particles, respectively. The bigger circle is a window with radius equal to the one particle diameter. Π_i is the probability that it will be occupied by exactly i matrix or fluid particle centers.

Our strategy implicitly uses the fact that the pair correlations of the HS QA-FM system are indistinguishable from those of an equilibrium HS fluid with density $\rho_F + \rho_M$. Since the QA-FM particle identities (matrix or mobile) are randomly distributed, one can write down an exact expression for V_0/V in the QA-FM matrix in terms of equilibrium properties of bulk HS fluid:

$$V_0/V = \sum_{i=0}^{\infty} \Pi_i(\rho_M + \rho_F) \times \left[1 + \frac{\rho_M}{\rho_F} \right]^{-i}. \quad (5.4)$$

Here $\Pi_i(\rho_M + \rho_F)$ represents the probability that a randomly placed spherical window (with radius equal to one particle diameter) in a bulk HS fluid of density $\rho_F + \rho_M$ will contain precisely i particle centers (see Fig. 5.1). The quantity $[1 + \rho_M/\rho_F]^{-i}$ is the probability that, in the structurally equivalent QA-FM system, all of the i centers in the window would be fluid particles.

IT provides expressions for the Π_i ,

$$\Pi_i = \exp[\lambda_0 + \lambda_1 i + \lambda_2 i^2]/i!, \quad (5.5)$$

which maximize a relative information entropy subject to some experimental constraints [55]. In particular, λ_0, λ_1 , and λ_2 are Lagrange multipliers determined (see, e.g., [55]) by imposing the normalization condition $\sum_i \Pi_i = 1$ and the first two moments of the window occupancy, \bar{i} and $\overline{i^2}$,

$$\begin{aligned}\bar{i} &= 4\pi\rho/3, \\ \overline{i^2} &= \bar{i} + \rho^2 \int_w d\mathbf{r} \int_w d\mathbf{r}' g(|\mathbf{r} - \mathbf{r}'|).\end{aligned}\tag{5.6}$$

Here, $\rho = N\sigma^3/V$, and the subscript w in the last expression indicates that the integrals are constrained to the spherical observation window. Fig. 5.2 shows a numerical comparison of V_0/V predicted by Eq. 5.4 and 5.5 to the “exact” results for V_0/V obtained from applying the available space algorithm of Sastry et al. [97] to HS QA-FM matrices. As is evident, the simple IT approach provides accurate predictions over a wide range of matrix parameters.

5.5 Comparison between diffusion equation and exact results

Fig. 5.3 (a,b) provides a fairly comprehensive comparison of $D(\rho_F, \rho_M)$ from Eq. 5.1 to the results of our molecular dynamics simulations. Interestingly, the predictions show semi-quantitative agreement with simulations of QA systems for matrix densities in the wide range $0 \leq \rho_M \leq 0.25$, which includes systems where matrix particles exclude mobile particle centers from over 70% of the total volume (see, e.g., Fig. 5.2). Given that matrix particles reduce $D(\rho_F, \rho_M)$ by more than an order of magnitude across this range of

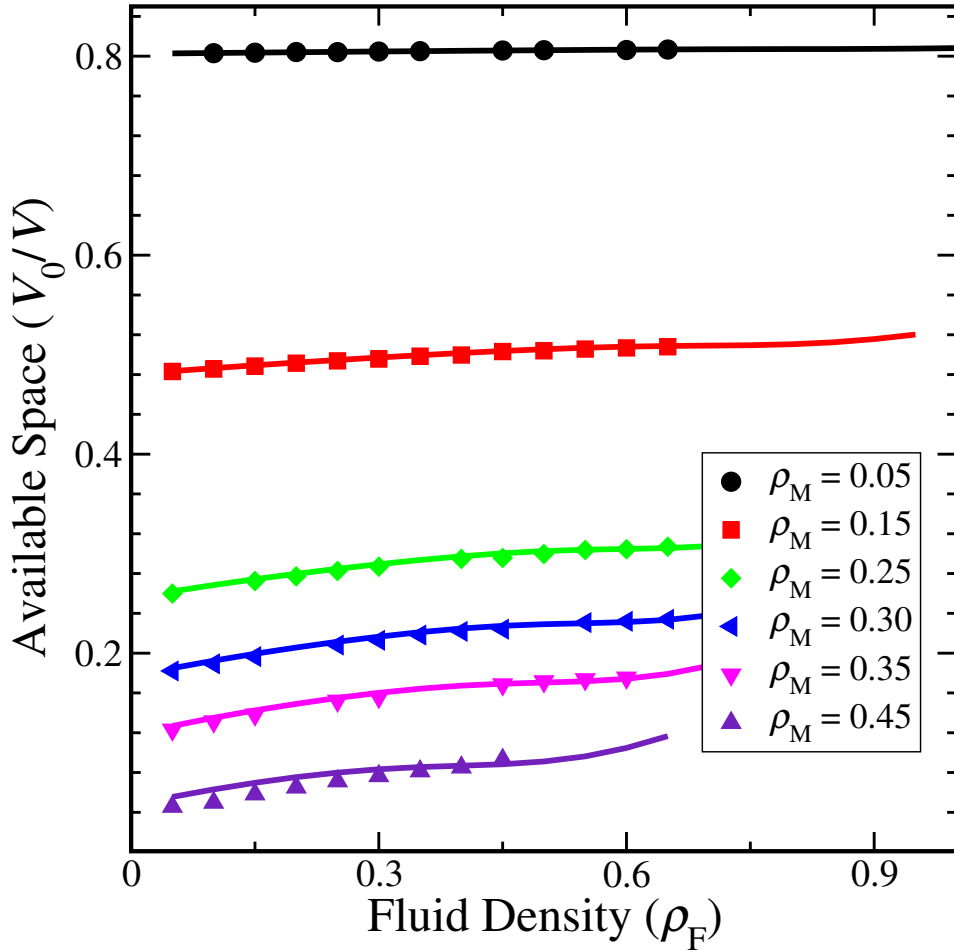


Figure 5.2: The fractional available volume V_0/V in HS QA-FM matrices computed using the IT approach of Eq. 5.4 and 5.5 (curves) and “exact” results (filled circles) using the available space algorithm of Ref [97].

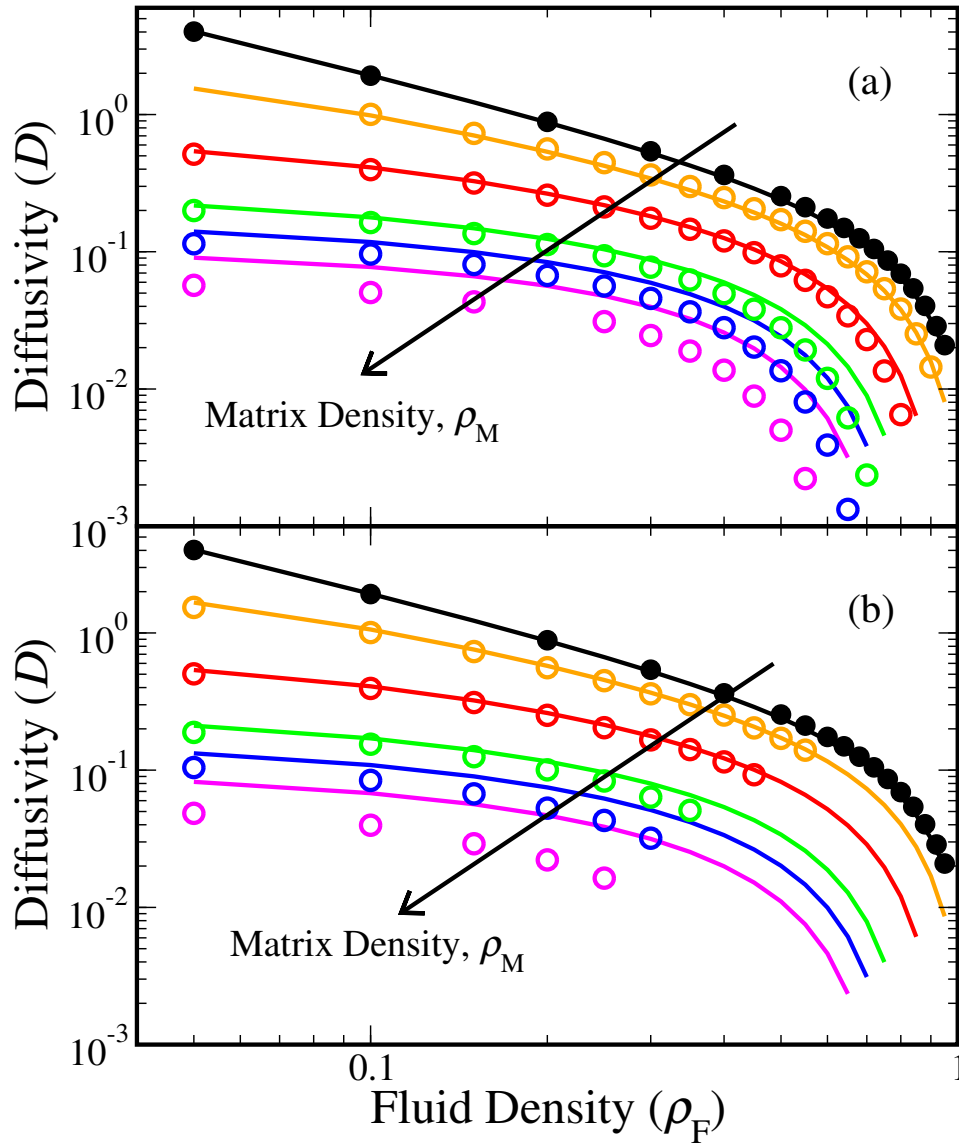


Figure 5.3: Fluid self-diffusivity D versus fluid density ρ_F for HS (a) QA-FM and (b) QA-M system with matrix densities $\rho_M = 0.0, 0.05, 0.15, 0.25, 0.30,$ and 0.35 . Curves are predictions of Eq. 5.1 and circles are molecular dynamics simulation results.

densities, the success of Eq. 5.1 argues that available volume plays a primary role in controlling the single-particle dynamics. For matrix densities greater than $\rho_M = 0.25$ (i.e., systems with less than 30% of volume available to mobile particle centers), Eq. 5.1 captures the qualitative trends, but it systematically overpredicts the simulated self-diffusivities. However, this overprediction is expected, given that Eq. 5.1 only accounts for the reduction of available volume and not the fact that available volume also becomes highly disconnected (i.e., some pockets of available volume are inaccessible or are accessible by only small number of paths) at high matrix densities [111], which acts to further hinder transport.

In order to test whether the connection between diffusivity and available volume holds more generally for fluids confined to random media, we also performed molecular dynamics simulations of QA-FM systems comprising LJ particles (truncated and shifted with a quadratic function in r [108] to insure that both the potential and its gradient vanish at $r_{\text{cut}} = 2.5$). The details of the simulations are identical to those of the HS QA systems described earlier, except that the equations of motion were integrated via the velocity Verlet algorithm [82], and $N_F = 1000$ mobile particles were considered. The goal was to test if one could employ techniques commonly used in thermodynamic perturbation theory to map the QA LJ system onto an equivalent QA HS system, and then use Eq. 5.1 to predict the self-diffusivity. The specific mapping that we used in this study is a Boltzmann factor criterion [11, 54], which determines the temperature-dependent “effective” HS diameter $\sigma(T)$ (and hence the cor-

responding reduced matrix and fluid densities, ρ_M and ρ_F) of the LJ system through the following relationship $u_0(r = \sigma) = k_B T$, where u_0 is the repulsive part of the Weeks-Chandler-Andersen decomposition of the pair potential [19]. The hypothesis is that LJ QA systems will exhibit similar reduced diffusivities $D(\rho_F, \rho_M)$ as HS QA systems when compared at the same values of ρ_F and ρ_M (see section 4.3.1 for more detail).

As a first test of this idea, we compare in Fig. 5.4 (a) the diffusivities $D(\rho_F, \rho_M)$ of the HS QA-FM and LJ QA-FM systems obtained by our molecular dynamics simulations. In this plot, the LJ QA-FM system is at a temperature $T = \epsilon/k_B$, where ϵ is the characteristic energy of the LJ pair potential [108]. Except for at very low fluid densities (conditions for which the LJ fluid structure is not accurately approximated by an equivalent HS reference fluid [35]), the mapping brings the dynamics of the LJ and HS QA systems into excellent agreement.

A final test is to check whether the simple aforementioned mapping allows direct prediction of LJ QA-FM dynamics at other temperatures using Eq. 5.1. Fig. 5.4 (b) shows the comparison of the predicted $D(\rho_F, \rho_M)$ versus the results of our molecular dynamics simulations at $T = 3\epsilon/k_B$. The agreement between the predictions and the simulations again confirm the pivotal role that available volume plays in controlling the single-particle dynamics of fluids in porous media.

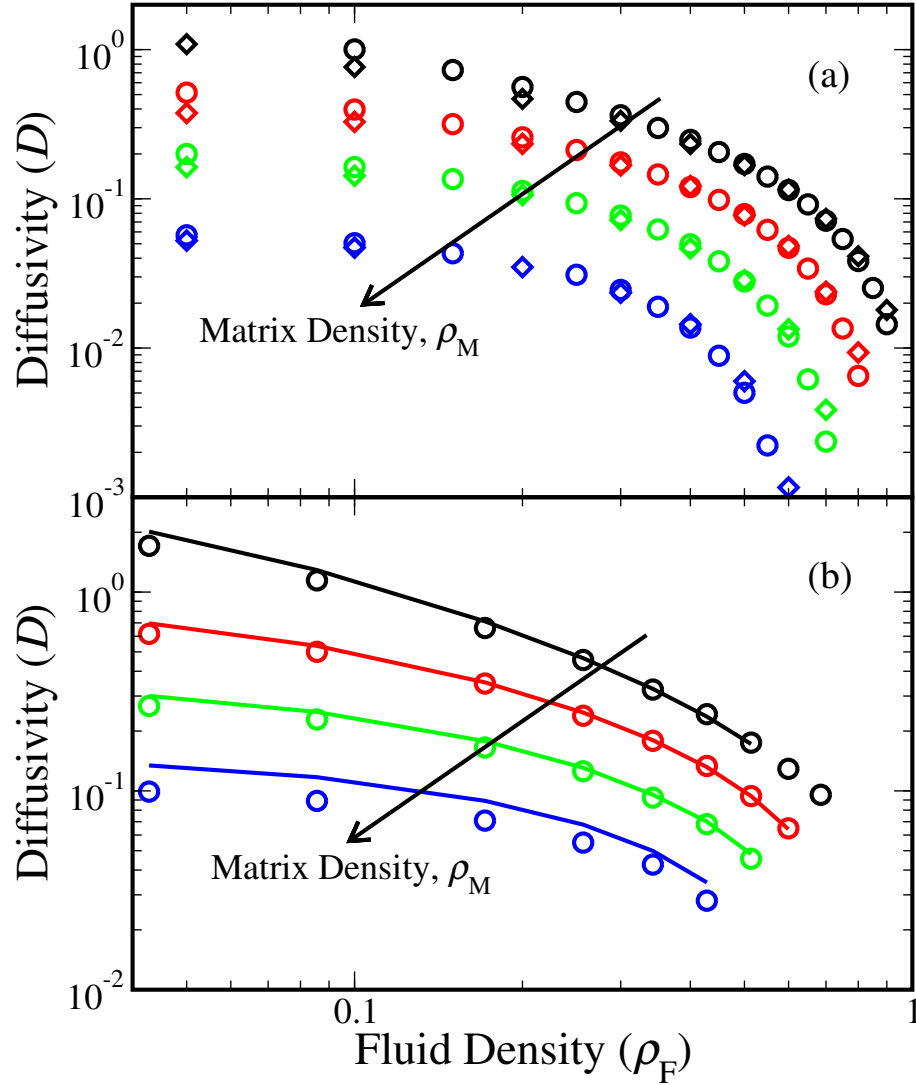


Figure 5.4: (a) Fluid self-diffusivity D versus fluid density ρ_F for HS QA-FM (circles) and LJ QA-FM (diamonds) systems obtained via molecular dynamics simulations. The LJ QA-FM system is at $T = \epsilon/k_B$. Matrix densities of $\rho_M = 0.05, 0.15, 0.25,$ and 0.35 are presented. (b) Results for the LJ QA-FM system at $T = 3\epsilon/k_B$: molecular dynamics simulations (circles) and Eq. 5.1 (curves). Matrix densities of $\rho_M = 0.043, 0.128, 0.214,$ and 0.3 are presented.

5.6 Conclusions

To conclude, we proposed a simple equation for predicting the self-diffusivity of mobile particles in quenched-annealed systems that only requires knowledge of the diffusivity of the bulk, homogeneous fluid and the statistical geometry of the matrix particles. Comparison between predictions of this equation and the “exact” results obtained via molecular dynamics simulations shows a very good agreement over a wide range of fluid densities. The general applicability of this approach is demonstrated by analyzing diffusivity of hard-sphere and Lennard-Jones mobile particles within different types of random matrices which qualitatively correspond to different physically realizable systems.

Chapter 6

Thermodynamics, static structure and dynamics of supercooled liquids

6.1 Introduction

We provided evidence in Chapter 2, 3, and 4 that the quasi-universal scaling that links single-particle dynamics to excess entropy for the transport coefficients of simple bulk [29, 89, 90] also holds for confined fluids above their freezing points. But this relationship hasn't been tested for supercooled liquids and if found to be true will indicate that the empirical connection between thermodynamics and dynamics for simple fluids is broader, perhaps spanning from “from ideal gas to glass”. Moreover, excess entropy can be approximated based on structural data from, e.g., scattering experiments, it also promises to provide the elusive link between structure and dynamics of the liquid state.

In this Chapter, we explore the possibility of such a relationship between excess entropy and diffusivity via molecular simulations of two very different models of supercooled fluids, the Kob-Andersen binary Lennard-Jones alloy [60] and a “core-softened” water-like model [22]. Further, we utilize the entropy expansion to examine the feasibility of a relationship between the pair-correlation function and diffusivity via molecular dynamics simulations of

three different model systems two of which are known to display anomalous structural, thermodynamic, and kinetic behaviors in their supercooled fluid states: SPC/E water [12] and a recently introduced model for attractive colloids [80, 81].

6.2 Relationship between thermodynamics and dynamics

The excess entropy s^{ex} is defined as the molar entropy of the liquid minus that of an ideal gas with the same number density. In systems interacting with spherically-symmetric interparticle potentials, s^{ex} quantifies the entropic penalty associated with the translational structural correlations that result from the Boltzmann-sampled interparticle interactions. The physical idea is that these static correlations reflect the local caging structures that surround each particle and act as a barrier to the dynamic particle rearrangements required for self-diffusion.

Because the relationship investigated here involves s^{ex} instead of configurational entropy s_C (see section 1.2 for detail), it has three important practical advantages over the AG relationship that make it a particularly intriguing subject of this investigation. First, unlike s_C , the quantity is a standard thermodynamic variable that does not require knowledge of the detailed topographical information about the potential energy landscape. Second, the determination of the two-body approximation for s^{ex} , only requires knowledge of the radial distribution function, which is an experimentally accessible quan-

tity. As a result, may lend new insights into the elusive connection between structure and dynamics of supercooled liquids as we discuss in the next section. Third, while s_C is not thought to be particularly relevant for the dynamics of fluids above their freezing point, s^{ex} is known to provide scaling relationships for the transport coefficients of simple equilibrium fluids.

6.2.1 Core-softened water-like model

We first examine the behavior of a core-softened fluid that belongs to a larger class of model potentials known to reproduce many of liquid waters distinctive properties. In particular, we perform simulations for a broad range of thermodynamic conditions where the model displays pronounced increases in self-diffusivity D upon isothermal compression, a well-known experimental signature of supercooled liquid waters dynamics.

To obtain self-diffusivity, we performed molecular dynamics simulations of 1000 particles interacting via a core-softened potential (i.e., a Lennard-Jones potential plus a Gaussian repulsion). We extracted self-diffusivity by fitting the long-time ($t \gg 1$) behavior of the average mean-squared displacement to the Einstein relation $\langle \Delta \mathbf{r}^2 \rangle = 6Dt$. We determined the behavior of the excess entropy per particle s^{ex} using grand canonical transition-matrix Monte Carlo (GC-TMMC) simulations [33]. Here, s^{ex} is defined to be the difference between the entropy per particle of the fluid and that of an ideal gas at the particle number density and temperature. A more detailed account on how this is done can be found in section 2.2, 3.2 and 4.2.

Figure 6.1(a, b) shows that the excess entropy s^{ex} and diffusivity D of this fluid have strikingly similar dependencies on density ρ for a wide range of temperatures T . In fact, when plotted along curves of constant ρ (Figure 6.2), we find $D \propto \exp[A(\rho)s^{\text{ex}}]$, where $A(\rho)$ is a T -independent parameter.

6.2.2 Binary Lennard-Jones mixture

The second type of supercooled fluid that we examine in this section is a well-studied model glass former and is a binary mixture of Lennard-Jones particles. The individual as well as cross particle diameters σ and energy parameters ϵ for this model has been parameterized to avoid freezing at the time scale of the simulations. One proof of this model's popularity is that all the relevant data required for its thermodynamics and dynamic behavior can be obtained easily from the literature over a very wide temperature and density range. We obtained excess entropy from the semi-empirical free energy and internal energy expressions reported in Ref. 18. The diffusivity has been extracted from the Figure 3 in Ref. 18.

Figure 6.3 shows that the robust scaling based on s^{ex} is also exhibited by this model binary alloy for conditions where it displays many of the experimental characteristics of fragile supercooled liquids. This is a stringent test since this alloy has become one of the most well-characterized model glass-formers.

Adam-Gibbs theory predicts a different form of exponential relationship between D and configurational entropy s_C , where is a T -independent

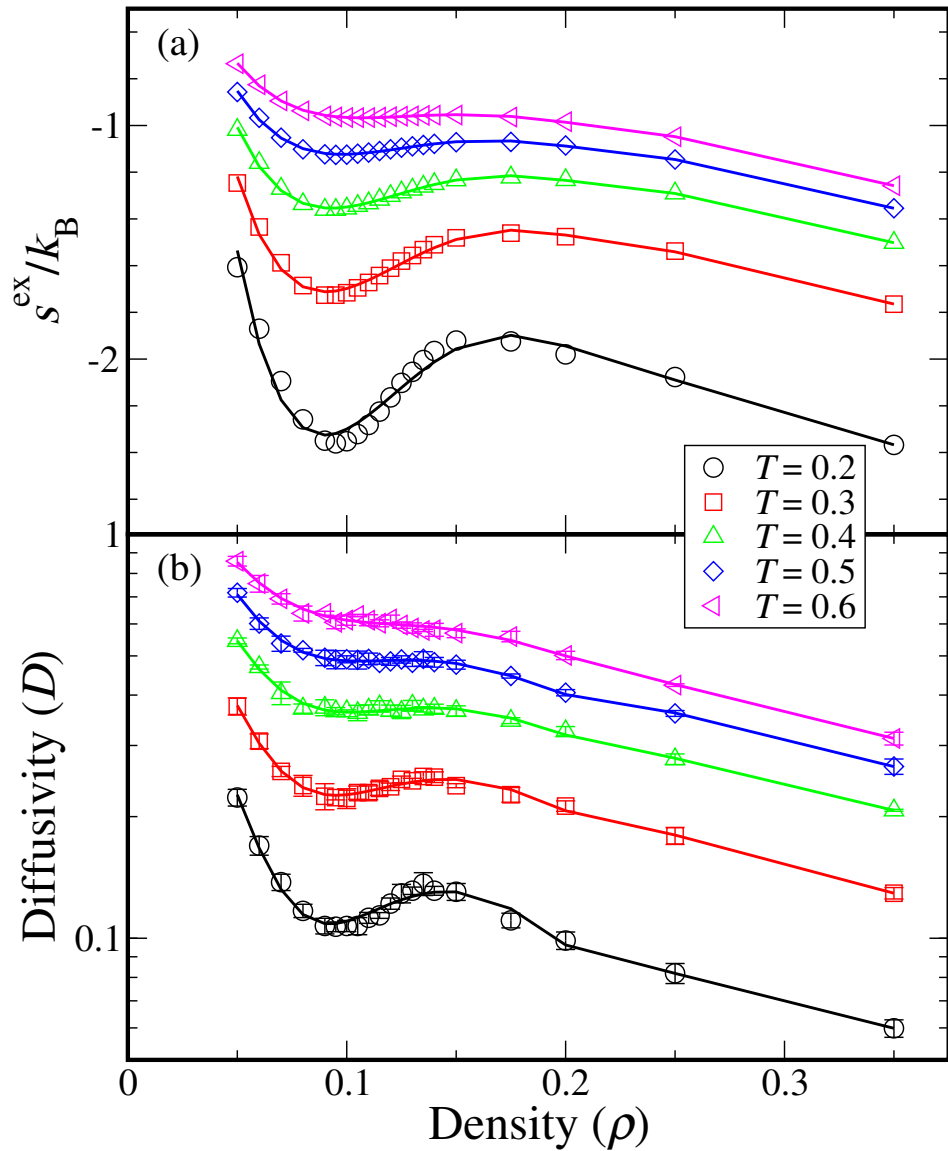


Figure 6.1: (a, b) Excess entropy and diffusivity versus density obtained from molecular dynamics simulations of 1000 particles interacting via a core-softened potential (i.e., a Lennard-Jones potential plus a Gaussian repulsion). Symbols are simulation data, and curves are guides to the eye.

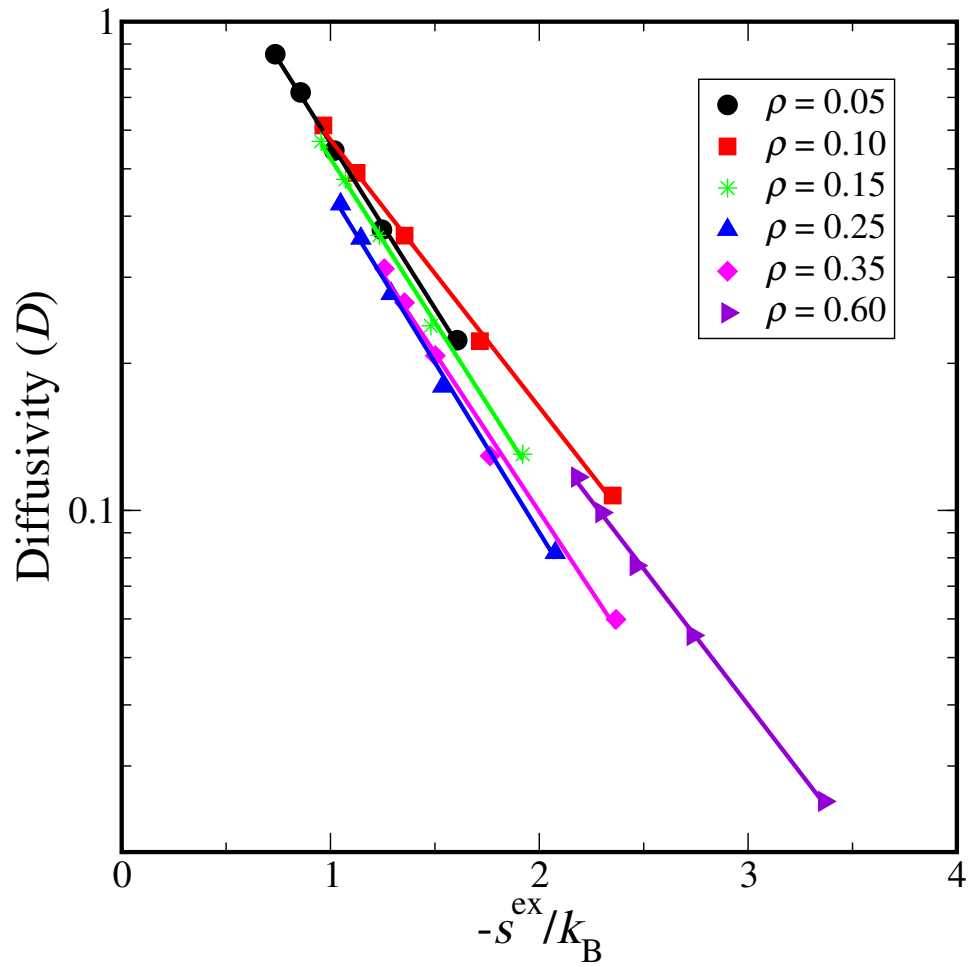


Figure 6.2: Diffusivity versus excess entropy for the data shown in Fig 6.1 along paths of constant density (symbols). Symbols are simulation data, and lines reflect the form.

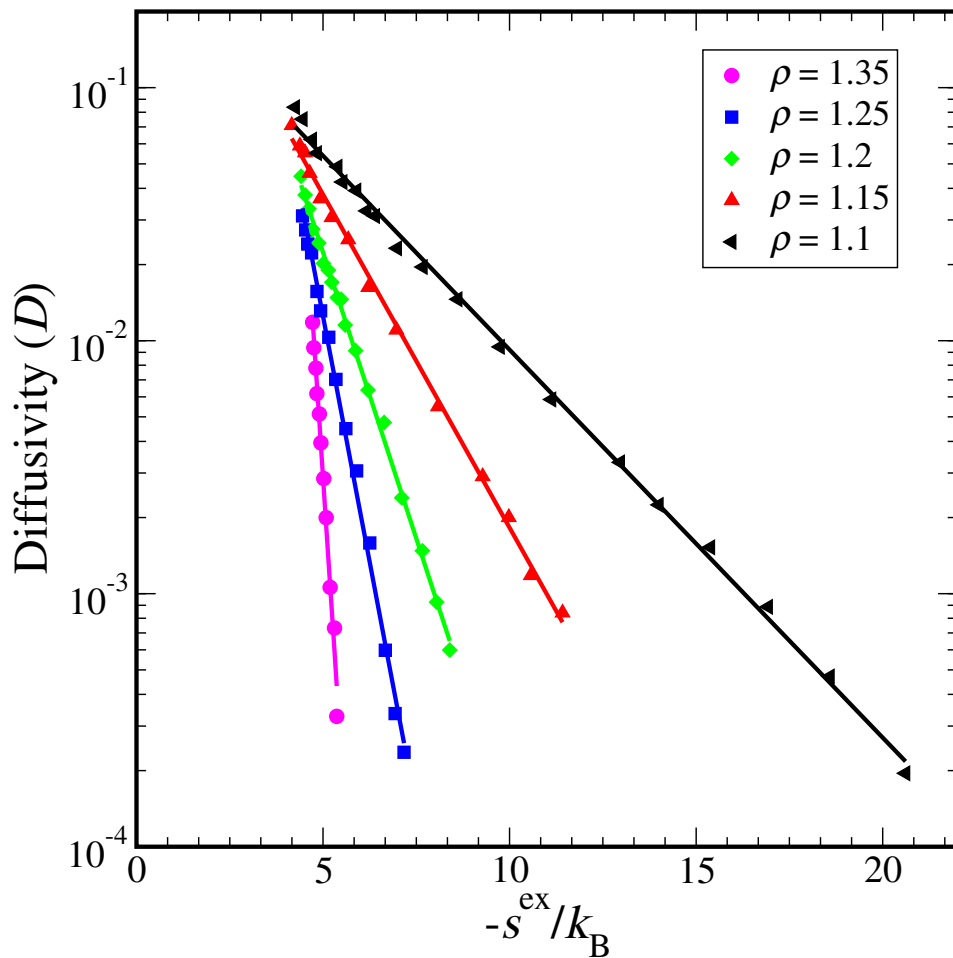


Figure 6.3: Diffusivity versus excess entropy for different density states of a binary Lennard-Jones alloy. Excess entropy has been obtained from the semi-empirical free energy expression reported in Ref. 18, and diffusivity has been extracted from the Figure 3 in Ref. 18. The lines reflect the form.

parameter. Since Adam-Gibbs relationship can adequately describe the diffusivity for many liquids near the glass transition, it is natural to ask whether and contain the same thermodynamic information about the supercooled fluid. Indeed, the Figure 6.4 demonstrates that these quantities are linearly related (at constant) for the binary alloy over all conditions for which data is available.

6.3 Relationship between static structure and dynamics

In order to make a quantitative link to static liquid structure, one can proceed to express s^{ex} as a sum of integrals over the N -body interparticle correlation functions $g^{(N)}$, [8, 69, 77, 78] which generally quantify *both* the translational and orientational interparticle correlations in the system. However, the translational correlations are believed to be of primary importance for D , and, for practical reasons, one is often interested in dealing with structure at the level of the pair correlation function $g(r)$. Working within these constraints, the natural structure-property relationship to test along isochores is $D \propto \exp[As_2]$, where A is again a density-dependent, but T -independent, parameter, and s_2 is the two-body, translational correlation contribution to the excess entropy, given by [8, 78]

$$s_2 = -\frac{k_B \rho}{2} \int d\mathbf{r} \{g(|\mathbf{r}|) \ln g(|\mathbf{r}|) - [g(|\mathbf{r}|) - 1]\}. \quad (6.1)$$

Here, k_B is the Boltzmann constant, $\rho = N/V$ is number density, N is number of particles, and V is volume. It is worth emphasizing that this type of relationship between D and s_2 has already been tested for simple equilibrium

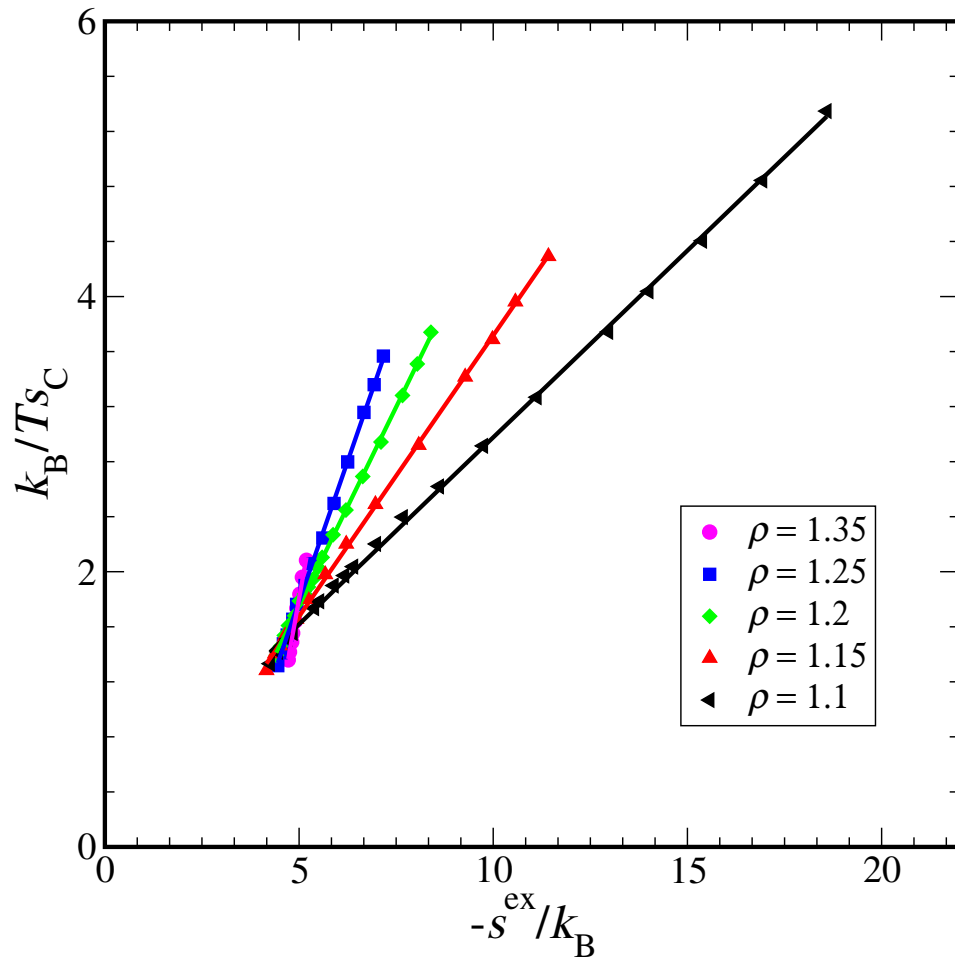


Figure 6.4: The plot shows the linear dependence between excess entropy and the inverse product of temperature and configurational entropy, the latter extracted from Figure 2 in Ref. 12 for the data used in Fig 6.3.

fluids *above their freezing points* [29, 89, 90] to explore the effectiveness of various proposed scaling laws for their transport coefficients. However, in this work, the goal is quite different. We want to put to a stringent numerical test the hypothesis, formulated based on previous section results, that this relationship provides a practical quantitative link between static structure and dynamics of supercooled fluids.

6.3.1 SPC/E water model

First, we examine the behavior of SPC/E water [12], which remains one of the most well-characterized models for liquid water in its supercooled state. It is able to qualitatively reproduce many of liquid water’s anomalous static structural, thermodynamic, and transport properties [34]. Of particular relevance in this work is the fact that the translational self-diffusivity of supercooled SPC/E water *increases* when the liquid is isothermally compressed over a wide range of pressures (see Fig. 1a). This anomalous volumetric response is related to the fact that the compressed liquid cannot support the same extent of low-coordinated, hydrogen-bond networks that serve to cooperatively impede molecular mobility in the liquid. In short, we are interested in whether the structure-property relationship, $D \propto \exp[As_2]$, is able to account for this unusual behavior.

To explore this issue, we performed canonical ensemble molecular dynamics of 500 SPC/E water molecules in a periodically-replicated cell using GROMACS [114]. We focused on temperatures from $T = 220$ K to $T = 300$

K and mass densities over the broad range 0.85 g/cm^3 to 1.3 g/cm^3 . Constant temperature conditions were imposed by Berendsen’s thermostat [13] with a coupling time constant of 0.1 ps. The particle mesh Ewald method was employed to account for the electrostatic interactions with a grid spacing of 0.12 nm, 4th order spline interpolation, and a cutoff distance of 1 nm. A time step of 2 fs was adopted for all the simulation runs. To calculate the mean square displacement and $g(r)$, each water molecule was taken to be “located” at the center of its oxygen atom.

Comparison of Fig. 6.5a and 6.5b reveals that the anomalous density-dependent trends in D for SPC/E water are directly reflected in s_2 over the entire range of conditions explored. In other words, the density dependence of the translational structural correlations in SPC/E water are sufficient to qualitatively explain its single-particle dynamics. In fact, it becomes apparent that this connection is quantitative when plotted along isochores, as in Fig. 6.6, where a structure-property relationship of the form $D \propto \exp[As_2]$ provides an excellent description of the simulation data. Of course, this structure-property relation examined here has a practical advantage over the Adam-Gibbs equation due to its dependence on s_2 rather than s_C . Unlike s_C , the quantity s_2 is trivially calculable from $g(r)$, a standard experimentally-accessible quantity.

6.3.2 Short-range attractive (SRA) colloid model

The second type of supercooled fluid that we examine is a simplified model suspension comprising colloidal particles of volume fraction ϕ_c and (im-

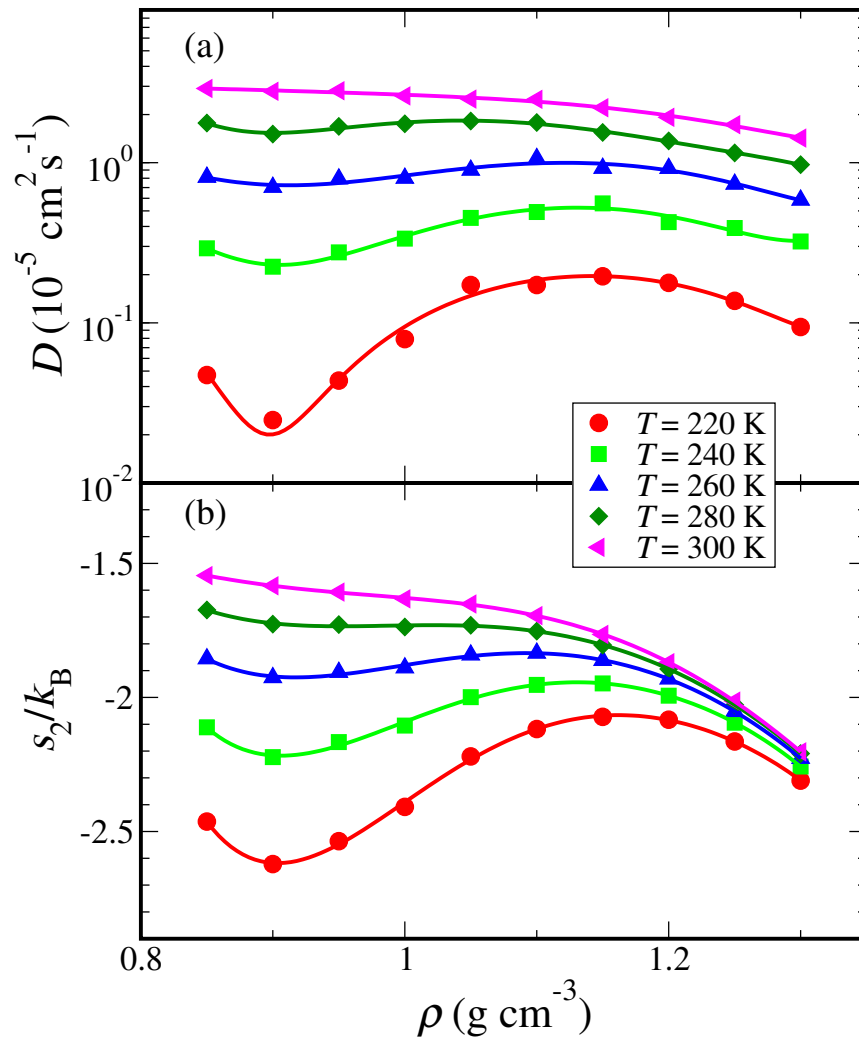


Figure 6.5: Diffusivity D and two-body entropy s_2 versus density ρ for SPC/E water. Symbols are simulation data, and curves are guides to the eye.

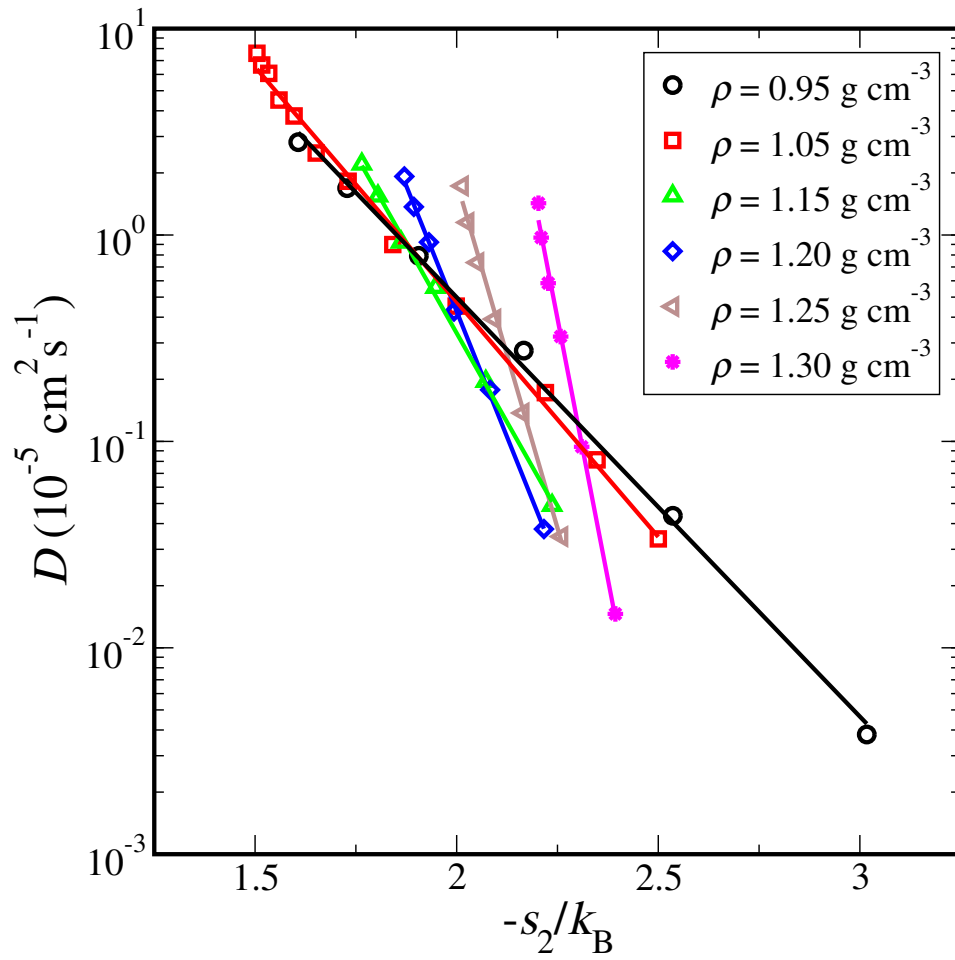


Figure 6.6: Diffusivity D versus two-body entropy s_2 for the data shown in Fig. 1 along paths of constant density ρ shown by symbols. Lines are fits to the data of the form $D \propto \exp[A(\rho)s_2]$.

implicit) non-adsorbing polymers of volume fraction ϕ_p [80, 81]. The effect of the implicit polymers in this model is to induce an entropic depletion attraction between the otherwise repulsively interacting colloids. The depletion interaction scales with $k_B T$, increases in strength with increasing ϕ_p , and is short-ranged compared to the colloidal particle diameter. We have considered this model fluid with short-ranged attractions (SRA) in this letter because, like water, it is known to exhibit the type of anomalous dynamical properties in its supercooled fluid state that can put our hypothesized structure-property relation, $D \propto \exp[As_2]$, to a stringent test.

The steeply repulsive interactions between the colloids in the SRA pair potential [80, 81] are of the virtually hard-sphere form. The depletion attraction $v_{AO}(r_{12})$ is modeled by the Asakura-Oosawa effective pair potential [6]. Here, r_{12} is the center-to-center distance between colloidal particles 1 and 2, and a_{12} is the effective exclusion radius. To prevent crystallization, the particle radii are taken to be polydisperse with uniform distribution of mean a and half-width $\Delta = a/10$. A longer-range soft repulsion is also added to the interparticle potential to prevent fluid-fluid phase separation. The details of this SRA potential and a comprehensive discussion of its physical significance can be found elsewhere [80, 81].

This model shows a maximum in D when plotted as a function of ϕ_p along lines of constant (and sufficiently high) ϕ_c (see Fig. 6.7a). To understand why this type of behavior is indeed anomalous, consider that it is analogous to a molecular fluid showing maxima in D as a function of T along isochores,

meaning that cooling the fluid would enhance its single-molecule dynamics under some conditions. This maximum in D is actually a more general characteristic displayed by other supercooled SRA fluids [103], and it is a reflection of the fact that they can form two different types of glasses: a repulsive glass at low ϕ_p (repulsive particles) and an attractive glass at high ϕ_p (attractive particles). Interestingly, mode-coupling theory, which incorporates the static structure of the fluid, can capture these unusual dynamical behaviors [14, 36]. Here, we are interested in whether $D \propto \exp[As_2]$ can also quantitatively predict these distinctive trends in single-particle dynamics.

To examine this issue, we have performed micro-canonical ensemble molecular dynamics simulations of 1500 SRA particles using periodic boundary conditions. The equations of motion were integrated using the velocity-Verlet scheme and a time step of 7.5×10^{-4} . In reporting our results, we have implicitly non-dimensionalized all quantities by the appropriate combinations of the characteristic length scale a and time scale $a\sqrt{4m/(3k_B T)}$ chosen in the original studies [80, 81]. We have focused on colloidal volume fractions of $\phi_c = 0.25, 0.30, 0.35, 0.40, 0.45, 0.50, 0.55$ and polymer volume fractions in the range $0 < \phi_p < 0.45$. In keeping with previous simulations using this potential [80, 81], we evaluate the system at an average thermal velocity of $\sqrt{4/3}$.

An examination of Fig. 6.7a and 6.7b shows that the ϕ_p dependence of s_2 qualitatively mirrors the trends observed by D of the SRA fluid for all conditions simulated, suggesting that the proposed structure-property relationship

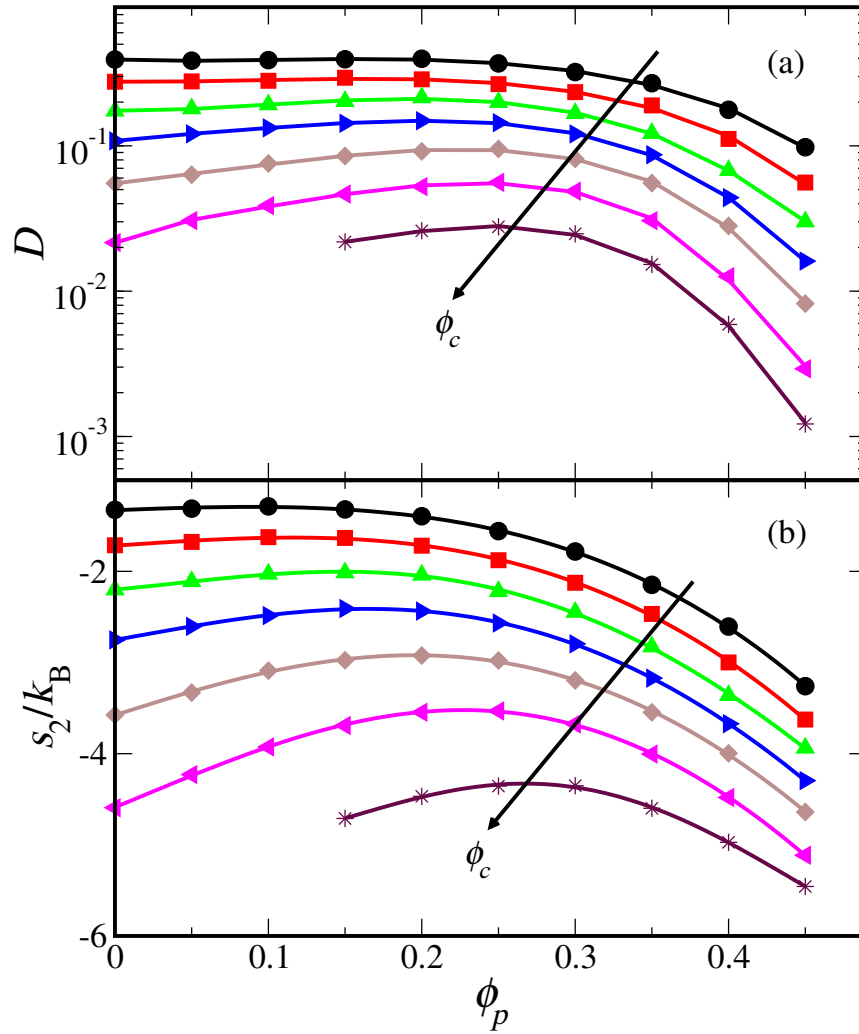


Figure 6.7: Diffusivity D and two-body entropy s_2 versus polymer fraction ϕ_p for the SRA model [80, 81]. Particle volume fractions of $\phi_c = 0.25, 0.30, 0.35, 0.40, 0.45, 0.50, 0.55$ from top to bottom are shown.

also captures the relevant physics for this system. In fact, Fig. 6.8 demonstrates that the functional form $D \propto \exp[As_2]$ again provides an accurate fit to the data, where A depends on ϕ_c but not ϕ_p . Here, we have separated the data into that of the “repulsive” fluid ($\phi_p < 0.25$, which forms a repulsive glass upon compression) and that of the “attractive” fluid ($\phi_p \geq 0.25$, which forms an attractive glass upon compression) [103]. Unlike the attractive fluid, the data for the repulsive fluid approximately collapses onto a single curve, as is also observed for simple equilibrium fluids away from their glass transition [29]. This is consistent with the fact that the attractive fluid is closer to its glass transition under these conditions than the repulsive fluid [80, 81].

6.3.3 Monatomic glass former “Dzugutov” model

The third type of supercooled fluid that we examine is a monatomic model glass former introduced by Dzugutov which promotes local icosahedral arrangement thereby preventing formation of crystallites at low temperatures. This is achieved by introducing a secondary minimum in the interaction potential at a distance larger than any stable crystalline arrangement’s periodic distance. In fact, the maximum in the potential between the two minimum is adjusted to be in line with the most favorable periodic arrangement distance which then avoids the formation of an arrangement at this particular distance.

To examine this model’s behavior, we have performed microcanonical ensemble molecular dynamics simulations of 3000 particles using periodic boundary conditions. The equations of motion were integrated using

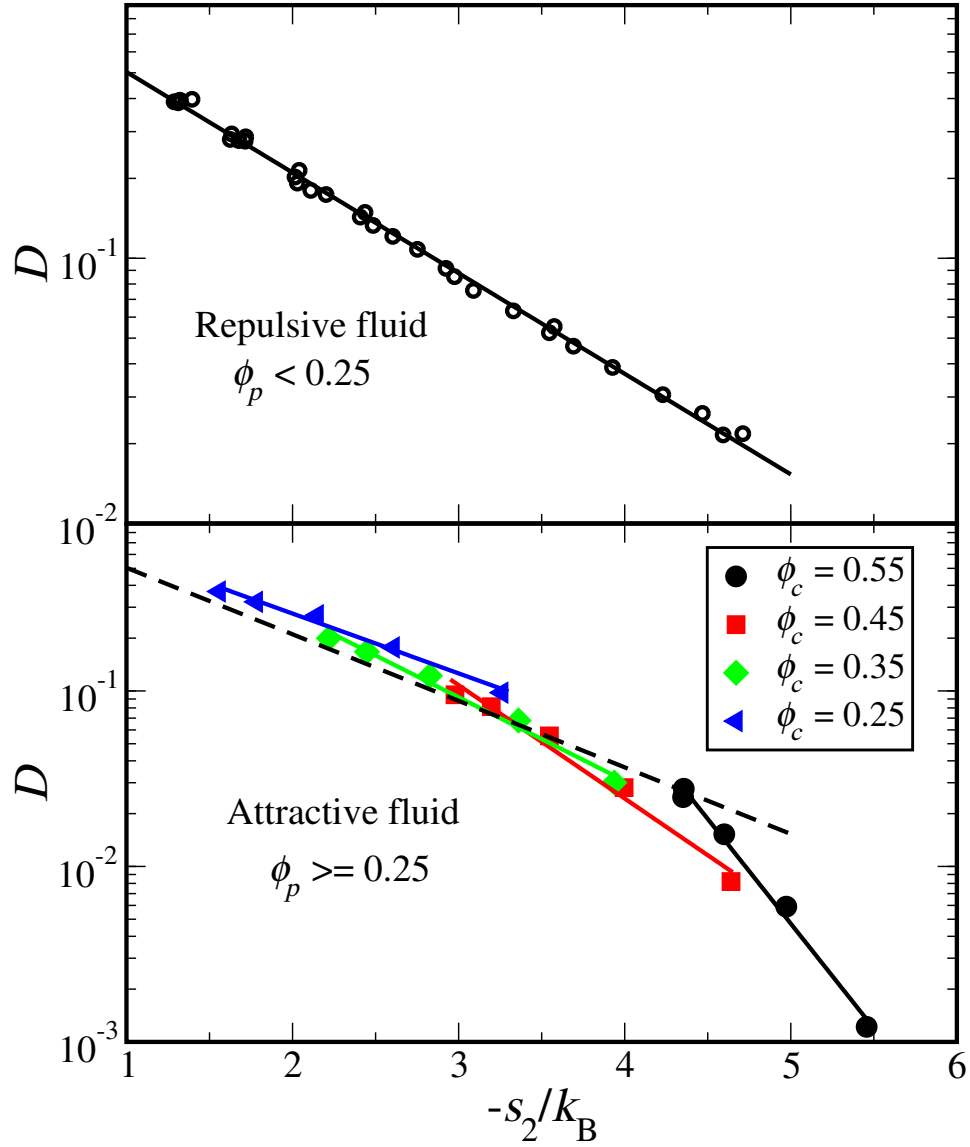


Figure 6.8: Diffusivity D versus two-body entropy s_2 for the data shown in Fig. 6.7 along paths of constant particle volume fraction ϕ_c for the “repulsive” (top panel, $\phi_p < 0.25$) and “attractive” fluid (bottom panel, $\phi_p \geq 0.25$). Lines are fits to the data of the form $D \propto \exp[A(\phi_c)s_2]$. The dashed line in the bottom panel shows the fit to “repulsive” fluid data ($\phi_p < 0.25$).

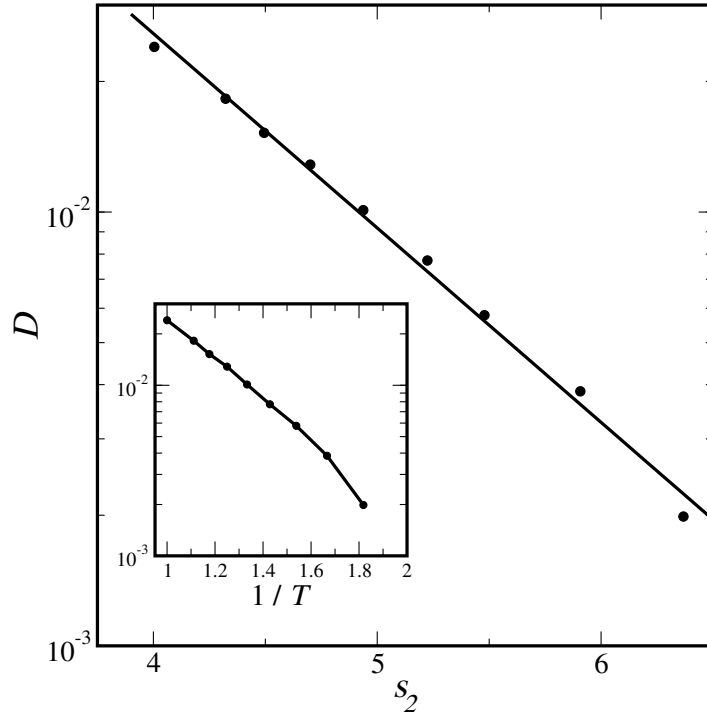


Figure 6.9: Diffusivity D versus two-body entropy s_2 along a constant particle density $\rho = 0.85$ for the “Dzugutov” fluid. Line is the fit to the data of the form $D \propto \exp[As_2]$. The inset also shows the diffusivity versus inverse temperature data for the same condition as the main plot.

the velocity-Verlet scheme and a time step of 3×10^{-3} . In reporting our results, we have implicitly non-dimensionalized all quantities by the appropriate combinations of the characteristic length scale a and time scale $a\sqrt{m/(k_B T)}$. We have simulated density of $\rho = 0.85$ over a temperature range $T = .55 - 1$. Figure 6.9 demonstrates that the functional form $D \propto \exp[As_2]$ again provides an accurate fit to the data.

6.4 Conclusions

In conclusion, the results presented here represent, to our knowledge, the first evidence that excess entropy, which provides a scaling for the diffusivity of simple equilibrium fluids, also captures supercooled liquid dynamics. We have also presented evidence that the supercooled fluid states of SPC/E water as well as the “repulsive” and “attractive” supercooled fluid states of a model for colloids with short-ranged attractions are characterized by the same type functional relationship between their self-diffusivity and the pair correlation function. The fact that this relationship is able to describe the nontrivial behaviors of these very different types of supercooled liquids suggests that its applicability may be far more general. At present, however, a general theory that can predict these observed relationships from first principles is lacking.

Bibliography

- [1] Gerold Adam and Julian H. Gibbs. The temperature dependence of cooperative relaxation properties in glass-forming liquids. *Journal of Chemical Physics*, 43:139–46, 1965.
- [2] M. Alcoutlabi and G. B. McKenna. Effects of confinement on material behaviour at the nanometre size scale. *J. Phys.: Condens. Matter*, 17:R461, 2005.
- [3] M. P. Allen and D. J. Tildesley. *Computer Simulation of Liquids*. Clarendon Press, Oxford, 1994.
- [4] P. W. Anderson. *Science*, 267:1615, 1995.
- [5] F. C. Andrews. A simple approach to the equilibrium statistical mechanics of two-dimensional fluids. *J. Chem. Phys.*, 64:1941, 1976.
- [6] Sho Asakura and Fumio Oosawa. Interaction between particles suspended in solutions of macromolecules. *Journal of Polymer Science*, 33:183–92, 1958.
- [7] S. Auer and D. Frenkel. Line tension controls wall-induced crystal nucleation in hard-sphere colloids. *Phys. Rev. Lett.*, 91:015703, 2003.

- [8] Andras Baranyai and Denis J. Evans. Direct entropy calculation from computer simulation of liquids. *Physical Review A*, 40:3817–22, 1989.
- [9] J. A. Barker and D. Henderson. Perturbation theory and equation of state for fluids. ii. a successful theory of liquids. *J. Chem. Phys.*, 47:4714, 1967.
- [10] S. Bastea. Transport properties of dense fluid argon. *Physical Review E*, 68:031204, 2003.
- [11] Dor Ben-Amotz and George Stell. Reformulation of weeks-chandler-andersen perturbation theory directly in terms of a hard-sphere reference system. *Journal of Physical Chemistry B*, 108:6877–6882, 2004.
- [12] H. J. C. Berendsen, J. R. Grigera, and T. P. Straatsma. The missing term in effective pair potentials. *Journal of Physical Chemistry*, 91:6269–71, 1987.
- [13] H. J. C. Berendsen, J. P. M. Postma, W. F. Van Gunsteren, A. DiNola, and J. R. Haak. Molecular dynamics with coupling to an external bath. *Journal of Chemical Physics*, 81:3684–90, 1984.
- [14] J. Bergenholtz and M. Fuchs. Nonergodicity transitions in colloidal suspensions with attractive interactions. *Physical Review E*, 59:5706–5715, 1999.

- [15] Jean-Louis Bretonnet. Self-diffusion coefficient of dense fluids from the pair correlation function. *Journal of Chemical Physics*, 117:9370–9373, 2002.
- [16] P. Bryk, R. Roth, K. R. Mecke, and S. Dietrich. Fluids in contact with curved walls. *Phys. Rev. E*, 68:031602, 2003.
- [17] A. Bunde and S. Havlin. *Fractals and Disordered Systems*. Springer, Berlin, 1991.
- [18] Norman F. Carnahan and Kenneth E. Starling. Equation of state for nonattracting rigid spheres. *Journal of Chemical Physics*, 51:635–6, 1969.
- [19] David Chandler, John D. Weeks, and Hans C. Andersen. Van der waals picture of liquids, solids, and phase transformations. *Science (Washington, DC, United States)*, 220:787–94, 1983.
- [20] Rakwoo Chang, Kamakshi Jagannathan, and Arun Yethiraj. Diffusion of hard sphere fluids in disordered media: a molecular dynamics simulation study. *Physical Review E*, 69:051101, 2004.
- [21] H. T. Davis. *Statistical Mechanics of Phases, Interfaces, and Thin Films*. VCH, 1996.
- [22] A. B. de Oliveira, P. A. Netz, T. Colla, and M. C. Barbosa. Thermodynamic and dynamic anomalies for a three-dimensional isotropic core-softened potential. *Journal of Chemical Physics*, 124:084505, 2006.

- [23] Pablo G. Debenedetti and Frank H. Stillinger. Supercooled liquids and the glass transition. *Nature (London, United Kingdom)*, 410:259–267, 2001.
- [24] Michael W. Deem and David Chandler. Classical diffusion in strong random-media. *Journal of Statistical Physics*, 76:911–927, 1994.
- [25] Marjolein Dijkstra. Capillary freezing or complete wetting of hard spheres in a planar hard slit? *Phys. Rev. Lett.*, 93:108303, 2004.
- [26] M. Dzugutov. A universal scaling law for atomic diffusion in condensed matter. *Nature*, 381:137, 1996.
- [27] M. Dzugutov. addendum: A universal scaling law for atomic diffusion in condensed matter. *Nature*, 411:720, 2001.
- [28] M. Dzugutov. Anomalous slowing down in the metastable liquid of hard spheres. *Phys. Rev. E*, 65:032501, 2002.
- [29] Mikhail Dzugutov. A universal scaling law for atomic diffusion in condensed matter. *Nature (London)*, 381:137–139, 1996.
- [30] J. R. Errington. Evaluating surface tension using grand canonical transition matrix monte carlo simulation and finite-size scaling. *Phys. Rev. E*, 67:012102, 2003.
- [31] J. R. Errington and V. K. Shen. Direct evaluation of multi-component phase equilibria using flat histogram methods. *J. Chem. Phys.*, 123:164103, 2005.

- [32] J. R. Errington, T. M. Truskett, and J. Mittal. Excess-entropy-based anomalies for a waterlike fluid. *J. Chem. Phys.*, 125:244502, 2006.
- [33] Jeffrey R. Errington. Direct calculation of liquid-vapor phase equilibria from transition matrix monte carlo simulation. *Journal of Chemical Physics*, 118:9915–9925, 2003.
- [34] Jeffrey R. Errington and Pablo G. Debenedetti. Relationship between structural order and the anomalies of liquid water. *Nature (London)*, 409:318–321, 2001.
- [35] Jeffrey R. Errington, Pablo G. Debenedetti, and Salvatore Torquato. Quantification of order in the lennard-jones system. *Journal of Chemical Physics*, 118:2256–2263, 2003.
- [36] L. Fabbian, W. Gotze, F. Sciortino, P. Tartaglia, and F. Thiery. Ideal glass-glass transitions and logarithmic decay of correlations in a simple system. *Physical Review E*, 59:R1347–R1350, 1999.
- [37] T. Fehr and H. Löwen. Glass transition in confined geometry. *Physical Review E*, 52:4016–25, 1995.
- [38] A. M. Ferrenberg and R. H. Swendsen. New monte carlo technique for studying phase transitions. *Phys. Rev. Lett.*, 61:2635, 1988.
- [39] I. Z. Fisher. *Statistical Theory of Liquids*. The University of Chicago Press, 1964.

- [40] Andrea Fortini and Marjolein Dijkstra. Phase behaviour of hard spheres confined between parallel hard plates: manipulation of colloidal crystal structures by confinement. *J. Phys.: Condens. Matter*, 18:L371, 2006.
- [41] G. H. Fredrickson and H. C. Andersen. Kinetic ising-model of the glass-transition. *Physical Review Letters*, 53:1244, 1984.
- [42] J. P. Garrahan and D. Chandler. Geometrical explanation and scaling of dynamical heterogeneities in glass forming systems. *Physical Review Letters*, 89:035704, 2002.
- [43] Yeshitila Gebremichael, Michael Vogel, Magnus N. J. Bergroth, Francis W. Starr, and Sharon C. Glotzer. Spatially heterogeneous dynamics and the adam-gibbs relation in the dzugutov liquid. *Journal of Physical Chemistry B*, 109:15068–15079, 2005.
- [44] W. Götze and L. Sjögren. *Transp. Theory Stat. Phys.*, 24:801, 1995.
- [45] J. P. Hansen and I. R. McDonald. *Theory of Simple Liquids*. Academic Press, 1986.
- [46] D. Henderson and M. Plischke. Pair correlation function in a fluid with density inhomogeneities: Parametrization for hard spheres near a hard wall. *Proc. R. Soc. Lond. A*, 400:163, 1985.
- [47] J. R. Henderson. Solvation of a solvophobic sphere. *J. Chem. Phys.*, 116:5039, 2002.

- [48] J. R. Henderson and F. van Swol. On the interface between a fluid and a planar wall: Theory and simulations of a hard sphere fluid at a hard wall. *Mol. Phys.*, 51:991, 1984.
- [49] M. Heni and H. Löwen. Interfacial free energy of hard-sphere fluids and solids near a hard wall. *Phys. Rev. E*, 60:7057, 1999.
- [50] D. M. Heyes. Transport coefficients of lennard-jones fluids: A molecular-dynamics and effective-hard-sphere treatment. *Phys. Rev. B*, 37:5677, 1988.
- [51] W. G. Hoover. *Molecular Dynamics: Lecture Notes in Physics*, volume 258. Springer, 1986.
- [52] J. J. Hoyt, M. Asta, and B. Sadigh. Test of the universal scaling law for the diffusion coefficient in liquid metals. *Phys. Rev. Lett.*, 85:594, 2000.
- [53] J. J. Hoyt, Mark Asta, and Babak Sadigh. Test of the universal scaling law for the diffusion coefficient in liquid metals. *Physical Review Letters*, 85:594–597, 2000.
- [54] C. S. Hsu, David Chandler, and L. J. Lowden. Applications of the rism equation to diatomic fluids: the liquids nitrogen, oxygen and bromine. *Chemical Physics*, 14:213–28, 1976.

- [55] G. Hummer, S. Garde, A. E. Garcia, M. E. Paulaitis, and L. R. Pratt. Hydrophobic effects on a molecular scale. *Journal of Physical Chemistry B*, 102:10469–10482, 1998.
- [56] R. A. L. Jones. The dynamics of thin polymer films. *Curr Opin Colloid Interface Sci*, 94:167, 1999.
- [57] H. S. Kang, C. S. Lee, T. Ree, and F. H. Ree. A perturbation theory of classical equilibrium fluids. *J. Chem. Phys.*, 82:414, 1985.
- [58] W. K. Kegel. Freezing of hard spheres in confinement. *J. Chem. Phys.*, 115:6538, 2001.
- [59] R. Kjellander and S. Sarman. Pair correlations of non-uniform hard-sphere fluids in narrow slits and the mechanism of oscillatory solvation forces. *J. Chem. Soc. Faradau Trans.*, 87:1869, 1991.
- [60] Walter Kob and Hans C. Andersen. Testing mode-coupling theory for a supercooled binary lennard-jones mixture: the van hove correlation function. *Physical Review E*, 51:4626–41, 1995.
- [61] V. Krakoviack. Liquid-glass transition of a fluid confined in a disordered porous matrix: a mode-coupling theory. *Physical Review Letters*, 94:065703., 2005.
- [62] J. Kushick and B. J. Berne. Role of attractive forces in self-diffusion in dense lennard-jones fluids. *J. Chem. Phys.*, 59:3732, 1973.

- [63] F. Lado. Choosing the reference system for liquid state perturbation theory. *Mol. Phys.*, 52:871, 1984.
- [64] G. X. Li, C. S. Liu, and Z. G. Zhu. Scaling law for diffusion coefficients in simple melts. *Phys. Rev. B*, 71:094209, 2005.
- [65] H. Liu, C. M. Silva, and E. A. Macedo. Unified approach to the self-diffusion coefficients of dense fluids over wide ranges of temperature and pressure-hard-sphere, square-well, lennard-jones and real substances - methane, ethane, propane, isobutane, and normal butane. *Chem. Eng. Sci.*, 53:2403, 1998.
- [66] W. G. Madden and E. D. Glandt. Distribution-functions for fluids in random-media. *Journal of Statistical Physics*, 51(3-4):537–558, 1988.
- [67] J. J. Magda, M. V. Tirrell, and H. T. Davis. Molecular dynamics of narrow, liquid-filled pores. *J. Chem. Phys.*, 83:1888, 1985.
- [68] G. A. Mansoori and F. B. Canfield. Variational approach to the equilibrium thermodynamic properties of simple liquids. i. *J. Chem. Phys.*, 51:4958, 1969.
- [69] Joseph E. Mayer. Contribution to statistical mechanics. *Journal of Chemical Physics*, 10:629–43, 1942.
- [70] John D. McCoy and John G. Curro. Conjectures on the glass transition of polymers in confined geometries. *Journal of Chemical Physics*, 116:9154–9157, 2002.

- [71] J. Mittal, J. R. Errington, and T. M. Truskett. Relationship between thermodynamics and dynamics of supercooled liquids. *Journal of Chemical Physics*, 125:076102, 2006.
- [72] J. Mittal, J. R. Errington, and T. M. Truskett. Thermodynamics predicts how confinement modifies the dynamics of the equilibrium hard-sphere fluid. *Physical Review Letters*, 96:177804, 2006.
- [73] J. Mittal, J. R. Errington, and T. M. Truskett. Thermodynamics predicts how confinement modifies the dynamics of the equilibrium hard-sphere fluid. *Phys. Rev. Lett.*, 96:177804, 2006.
- [74] J. Mittal, J. R. Errington, and T. M. Truskett. Using available volume to predict fluid diffusivity in random media. *Physical Review E*, 74:040102, 2006.
- [75] K. K. Mon, J. K. Percus, and J. Yan. Quasi one-dimensional non-passing self-diffusion. *Molecular Simulation*, 29:721–726, 2003.
- [76] Denis Morineau, Yongde Xia, and Christiane Alba-Simionesco. Finite-size and surface effects on the glass transition of liquid toluene confined in cylindrical mesopores. *Journal of Chemical Physics*, 117:8966–8972, 2002.
- [77] R. D. Mountain and H. Raveche. Entropy and molecular correlation functions in open systems: 2-body and 3-body correlations. *Journal of Chemical Physics*, 35:2250, 1971.

- [78] R. E. Nettleton and M. S. Green. Expression in terms of molecular distribution functions for the entropy density in an infinite system. *Journal of Chemical Physics*, 29:1365–70, 1958.
- [79] Athanassios Z. Panagiotopoulos. Monte carlo methods for phase equilibria of fluids. *Journal of Physics: Condensed Matter*, 12:R25–R52, 2000.
- [80] A. M. Puertas, M. Fuchs, and M. E. Cates. Comparative simulation study of colloidal gels and glasses. *Physical Review Letters*, 88:098301, 2002.
- [81] A. M. Puertas, M. Fuchs, and M. E. Cates. Simulation study of non-ergodicity transitions: Gelation in colloidal systems with short-range attractions. *Physical Review E*, 67:031406, 2003.
- [82] D. C. Rapaport. *The Art of Molecular Dynamics Simulation*. Cambridge University Press, 2nd edition, 2004.
- [83] H. Reiss, H. L. Frisch, and J. L. Lebowitz. Statistical mechanics of rigid spheres. *Journal of Chemical Physics*, 31:369–80, 1959.
- [84] Günter Reiter. Dewetting as a probe of polymer mobility in thin films. *Macromolecules*, 27:3046–52, 1994.
- [85] R. Richert and C. A. Angell. Dynamics of glass-forming liquids. v. on the link between molecular dynamics and configurational entropy. *Journal of Chemical Physics*, 108:9016–9026, 1998.

- [86] Y. Rosenfeld. Relation between the transport coefficients and the internal entropy of simple systems. *Phys. Rev. A*, 15:2545, 1977.
- [87] Y. Rosenfeld. A quasi-universal scaling law for atomic transport in simple fluids. *J. Phys.: Condens. Matter*, 11:5415, 1999.
- [88] Y. Rosenfeld. Excess-entropy and freezing-temperature scalings for transport coefficients: Self-diffusion in yukawa systems. *Phys. Rev. A*, 62:7524, 2000.
- [89] Yaakov Rosenfeld. Relation between transport-coefficients and internal entropy of simple systems. *Physical Review A*, 15:2545–2549, 1977.
- [90] Yaakov Rosenfeld. A quasi-universal scaling law for atomic transport in simple fluids. *Journal of Physics: Condensed Matter*, 11:5415–5427, 1999.
- [91] M. Ross. A high-density fluid-perturbation theory based on an inverse 12th-power hard-sphere reference system. *J. Chem. Phys.*, 71:1567, 1979.
- [92] M. Ross and P Schofield. Diffusion coefficients for the inverse twelfth power repulsive potentials. *J. Phys. C: Solid State Phys.*, 4:L305, 1971.
- [93] I. Saika-Voivod, P. H. Poole, and F. Sciortino. Fragile-to-strong transition and polyamorphism in the energy landscape of liquid silica. *Nature*, 412:514–7.

- [94] Alok Samanta, Sk. M. Ali, and S. K. Ghosh. New universal scaling laws of diffusion and kolmogorov-sinai entropy in simple liquids. *Physical Review Letters*, 92:145901, 2001.
- [95] Alok Samanta, Sk. M. Ali, and S. K. Ghosh. Universal scaling laws of diffusion in a binary fluid mixture. *Physical Review Letters*, 87:245901, 2001.
- [96] Srikanth Sastry. The relationship between fragility, configurational entropy and the potential energy landscape of glass-forming liquids. *Nature (London)*, 409:164–167, 2001.
- [97] Srikanth Sastry, David S. Corti, Pablo G. Debenedetti, and Frank H. Stillinger. Statistical geometry of particle packings. i. algorithm for exact determination of connectivity, volume, and surface areas of void space in monodisperse and polydisperse sphere packings. *Physical Review E*, 56:5524–5532, 1997.
- [98] Antonio Scala, Francis W. Starr, Emilia La Nave, Francesco Sciortino, and H. Eugene Stanley. Configurational entropy and diffusivity of supercooled water. *Nature (London)*, 406:166–169, 2000.
- [99] Peter Scheidler, Walter Kob, and Kurt Binder. The relaxation dynamics of a supercooled liquid confined by rough walls. *Journal of Physical Chemistry B*, 108:6673–6686, 2004.

- [100] M. Schmidt and H. Löwen. Freezing between two and three dimensions. *Phys. Rev. Lett.*, 76:4552, 1996.
- [101] M. Schmidt and H. Löwen. Phase diagram of hard spheres confined between two parallel plates. *Phys. Rev. E*, 55:7228, 1997.
- [102] Matthias Schmidt and Hartmut Löwen. Phase diagram of hard spheres confined between two parallel plates. *Physical Review E*, 55:7228–7241, 1997.
- [103] Francesco Sciortino. Disordered materials: One liquid, two glasses. *Nature Materials*, 1:145–146, 2002.
- [104] R. Sharma, S. N. Chakraborty, and C. Chakravarty. Entropy, diffusivity, and structural order in liquids with waterlike anomalies. *J. Chem. Phys.*, 125:204501, 2006.
- [105] P. Sollich. Predicting phase equilibria in polydisperse systems. *J. Phys.: Condens. Matter*, 14:R79, 2002.
- [106] R. J. Speedy, F. X. Prielmeier, T. Vardag, E. W. Lang, and H.-D. Ludemann. Diffusion in simple fluids. *Mol. Phys.*, 66:577, 1989.
- [107] Robin J. Speedy. Diffusion in the hard sphere fluid. *Molecular Physics*, 62:509–15, 1987.
- [108] Spotswood D. Stoddard and Joseph Ford. Numerical experiments on the stochastic behavior of a lennard-jones gas system. *Physical Review A*, 8:1504–12, 1973.

- [109] J. E. Straub. Analysis of the role of attractive forces in self-diffusion of a simple fluid. *Mol. Phys.*, 76:373, 1992.
- [110] P. A. Thompson, G. S. Grest, and M. O. Robbins. Phase transitions and universal dynamics in confined films. *Phys. Rev. Lett.*, 68:3448, 1992.
- [111] S. Torquato. *Random Heterogeneous Materials: Microstructure and Macroscopic Properties*. Springer-Verlag, New York, 2002.
- [112] S. Torquato, T. M. Truskett, and P. G. Debenedetti. Is random close packing of spheres well defined? *Phys. Rev. Lett.*, 84:2064, 2000.
- [113] T. M. Truskett, S. Torquato, and P. G. Debenedetti. Towards a quantification of disorder in materials: Distinguishing equilibrium and glassy sphere packings. *Phys. Rev. E*, 62:993, 2000.
- [114] David Van Der Spoel, Erik Lindahl, Berk Hess, Gerrit Groenhof, Alan E. Mark, and Herman J. C. Berendsen. Gromacs: Fast, flexible, and free. *Journal of Computational Chemistry*, 26:1701–1718, 2005.
- [115] Paul R. Van Tassel. Theoretical studies of the available volume for adsorption in a random quenched and depleted disordered medium. *Journal of Chemical Physics*, 107:9530–9534, 1997.
- [116] Paul R. Van Tassel, Julian Talbot, Pascal Viot, and Gilles Tarjus. Distribution function analysis of the structure of depleted particle configurations. *Physical Review E*, 56:R1299–R1301, 1997.

- [117] T. K. Vanderlick and H. T. Davis. Self-diffusion in fluids in microporous solids. *J. Chem. Phys.*, 87:1791, 1987.
- [118] J. D. Weeks, D. Chandler, and H. C. Anderson. Perturbation theory of the thermodynamic properties of simple liquids. *J. Chem. Phys.*, 55:5422, 1971.
- [119] T. Young and H. C. Andersen. Tests of an approximate scaling principle for dynamics of classical fluids. *J. Phys. Chem. B*, 109:2985, 2005.
- [120] Ronen Zangi and Stuart A. Rice. Phase transitions in a quasi-two-dimensional system. *Physical Review E*, 58:7529–7544, 1998.
- [121] R. Zwanzig. High-temperature equation of state by a perturbation method. i. nonpolar gases. *J. Chem. Phys.*, 22:1420, 1954.

Vita

Jeetain Mittal was born in Kapurthala, Punjab (India) on 14 June 1979, the son of Mr. Jugal Kishore and Veena. He received the Bachelor of Technology degree in Chemical Engineering from the Beant College of Engineering and Technology, Gurdaspur (India) and Master of Technology degree in Chemical Engineering from Indian Institute of Technology, Kanpur (India). He started his graduate studies in Chemical Engineering at the University of Texas at Austin in January 2003.

Permanent address: H. No. B-V/27
Sheran Wala Mohalla
Kapurthala 144601
Punjab (India)

This dissertation was typeset with L^AT_EX[†] by the author.

[†]L^AT_EX is a document preparation system developed by Leslie Lamport as a special version of Donald Knuth's T_EX Program.